ADDIS ABABA UNIVERSITY

ADDIS ABABA INSTITUTE OF TECHNOLOGY

SCHOOL OF CIVIL AND ENVIRONMENTAL ENGINEERING

THE EFFECT OF URBANIZATION AND ASSOCIATED CLIMATE CHANGE ON GNSS SIGNAL
(A Case Study in Addis Ababa City)

A Thesis in Geodesy and Geomatics (specialization in Geodesy)

By Ephson Kastro

September 2020

Addis Ababa

A Thesis

Submitted in Partial Fulfillment of the Requirements for the Degree of Master of Science

The undersigned have examined the thesis entitled 'The Effect of Urbanization and Associated Climate Change on GNSS signal, a case study in Addis Ababa City ' presented by Epheson Kastro Shanka, a candidate for the degree of Master of Science and hereby certify that it is worthy of acceptance.

Dr. Elias Lewi		
Advisor	Signature	Date
Dr. Shimeles Fisseha		
Internal Examiner	Signature	Date
Dr. Atalay Ayele		
External Examiner	Signature	Date
Chairperson	Signature	Date

UNDERTAKING

I certify that research work titled “The Effect of Urbanization and Associated Climate Change on GNSS signal, a case study in Addis Ababa City” is my own work. The work has not been presented elsewhere for assessment. Where material has been used from other sources it has been properly acknowledged / referred.

Ephson Kastro

ABSTRACT

Fast urbanization and the associated micro-climate change in the urban setting is a subject of interest, as it will affect the day to day life of contemporary urban dwellers in different parts of the world and the future generation. Since urban climate change affects the atmosphere and because the atmosphere acts as a medium through which the GNSS signal travels from the GNSS satellites to the receivers, it is logical to expect that urbanization has an impact on the propagation of GNSS signal. The assumption that urbanization can affect the accuracy of positioning was the basis for this research activity. The main objective of this study was therefore, to investigate the association between urbanization, change in the urban climate, and the long-term change on the propagation of GNSS signal through the atmosphere. The study was conducted in Addis Ababa city and used different data sources such as that from Landsat, MODIS Normalized Difference Vegetation Index, MODIS Land Surface Temperature, and GNSS data. The IGS station ADIS GNSS daily solutions were computed for the duration 2008-2019 to monitor possible residual change in the three-dimensional location of the station. Similarly, the Landsat built-up index, the Normalized Difference Vegetation Index, and the Land Surface Temperature were computed for the duration 2000-20019. Since the different data sets have different resolutions and are dominated by seasonal effects, long-term variations were computed using least squares curve fitting and these were compared using a linear correlation technique. The result showed that there is a very high correlation between the long-term changes in vertical location of the GNSS station and the built-up expansion, the vegetation coverage, and land surface temperature with correlation value amounting to -0.9227, 0.9489, and -0.9862 respectively. Even though, the level of impact is not quantified a conclusion is drawn that urbanization and its impact on climate change has an effect on the propagation of the GNSS signal.

Keywords: Urbanization, Land Cover Change, Climate Change, and GNSS.

ACKNOWLEDGEMENT

First of all, I would like to thank the almighty God of eternal mercy and love for his support and help in this thesis and my entire life.

Next, I would like to thank my advisor Dr. Elias Lewi for his continues support, guidance, and patience in the work. In addition, I would like to thank the staff members of IGSSA (Institute of Geophysics Space Science and Astronomy) especially those at the Unit of Geodesy, Geomatics, and Gravimetry.

I would like to thank my friends and classmate Endashaw Debru and Mekuanint Eresho for their encouragement and valuable discussions.

Last but not least I would like to thank my Family for all-rounded care, support, and love.

ACRONYM

C/A	Corse/Acquisition
Cs	Cesium
DOY	Day of Year
EMW	Electromagnetic wave
ERDAS	Earth Resources Data Analysis System
ESRI	Environmental Systems Research Institute
GLONASS	Global Navigation Satellite System
GNNS	Global Navigation Satellite System
GPS	Global Positioning System
HDF	Hierarchical Data Format
IEEE	Institute of Electrical and Electronics Engineers
IGS	International GNSS Service
IRNSS	Indian Regional Navigation Satellite System
IWV	Integrated Water Vapor
LC	Land Cover
LST	Land Surface Temperature
LUCC	Land Use Cover Change
MATLAB	Matrix Laboratory
MODIS	Moderate Resolution Imaging Spectroradiometer
NDBaI	Normalized Difference Bareness Index

NDBI	Normalized Difference Built-up Index
NDVI	Normalized Difference Vegetation Index
NDWI	Normalized Difference Water Index
P-code	Precision code
PNT	Position, Navigation, and Time
PRN	The pseudorandom noise
QZSS	Quasi-Zenith Satellite System
Rb	Rubidium
SVN	Space Vehicle Number
TIFF	Tagged Image File Format
UHI	Urban Heat Island
UN	United Nation
WGS84	World Geodetic System 1984
ZHD	Zenith Hydrostatic Delay
ZTD	Total Zenith Delay
ZWD	Zenith Wet Delay

TABLE OF CONTENTS

LIST OF TABLES

LIST OF FIGURES

CHAPTER 1 INTRODUCTION

1.1 Background

Urbanization is an activity that is ever increasing and it is taking place at an alarming rate in today's world. It is becoming an inevitable and dominant issue of our planet. The world's urbanization status shows these realities (UN, 2019). According to a United Nation report, since 2007 the world urban population exceeds the world's rural populations. In 1950 the population of urban dwellers was 30 percent and in 2018 the percentage increased to 55 percent. The residents of the world urban population are expected to reach 68 percent in 2055(UN, 2019). The growth rate of urbanization varies from country to country. As of UN, 2019 prediction in 2050, Latin America, the Caribbean, and Northern America will be 90 percent, Europe will be 85 percent, Asia will be 66 percent and Africa will be 59 percent. In general, the statistics so far shows that the current urbanization level is less in "developing" countries relative to "developed countries". However, the rate of urbanization is high in developing countries (Choudharyand Tripathi, 2018; Tahir, Muhammad, Mahmood, Ahmad, and Ullah, 2014). The experience of the last 20 years shows that there is a high growth of urbanization hot spots in the world (Cohen, 2006). Africa is one of the rapidly urbanizing continent with 1.1 percent growth of urbanization per year between 2015 and 2020 (UN, 2019). Even if Ethiopia is dominated by the rural population relative to other countries in sub-Saharan Africa, rapid urbanization was observed in the last few years (Study for Swiss Agency for Development and Cooperation, 2017). Addis Ababa, the capital city of Ethiopia is the fastest-growing city in Africa and 25 percent of the urban population of Ethiopia is living in Addis Ababa (World Bank Group, 2015). Thus, studying and understanding urban settings, the effect of urbanization and related issues is not a luxury but a critical factor for the safety of humanity.

Even though the driving forces of urbanization are many factors, population growth and economic developments are the major causes of urbanization. The three reasons for urbanization as described by United Nations are Natural increase, Migration, and Reclassification (UN, 2019). One characteristic of urban areas is the concentration of a high population in a small area (Tahir et al., 2014). This concentration or growth of the population in urban settings is consequential of birth and migration. From these, migration of people is the major source for urban population growth (Tahir et al., 2014). This is possible due to both rural to urban and urban to urban migration (Cohen, 2006; Study for Swiss Agency for

Development and Cooperation, 2017). Urban population growth occurs when the fertility and migration rate exceeds the mortality rate of urban dwellers (Cohen, 2006; UN, 2019). The economic growth of a city is also one of the factors that accelerate its urbanization rate. Economic development and industrial activities are connected with the growth of urban areas (Oliveira, Souza, Célia, and Guedes, 2016). This however well works vice versa. Reclassification increases urbanization by enlarging urban areas and population by incorporating near the rural area to urban settings (UN, 2019). Urban areas are center for social and economic growth, innovation and for employment (Cohen, 2006). Economic development and Population growth are not only driving forces for urbanization, but are also the consequence of urbanization. That means because of economic development and high level availability of facility and infrastructure, people migrate from rural and urban area to gain the benefit of urbanization. The main outcome of urbanization and economic prosperity is increase in number of population and occupation of large residence in urban land area.

An increase in population density and the need related to economic development in urban areas are mostly related to the utilization of urban space. One of the greatest challenges of urbanization is high consumptions of space and this is expressed by urban physical expansion. To fulfill the internal and external driving needs of urban dwellers, the urban area expands physically. The physical expansion of urban space is related to diversified issues and effects. One of the effects is urban land surface change. Urbanization is characterized by differencing land surface of urban areas from the rural area by converting land cover(Han, Baik, and Lee, 2013). The development of urban areas causes modification of urban land surface(K. Wang et al., 2007). The change in urban land cover is accomplished by human activities to achieve their needs (Tahir et al., 2014).

The change in land cover of urban settings with a built-up area is the common feature of urbanization. Most of the time agricultural land, Vegetated area, and barren surface are used for construction and affected by built-up area expansion. The conversion of vegetation cover in the urban area by an impervious surface is one of the consequences of urban growth (Odindi, Bangamwabo, and Mutanga, 2015). Towards this the normalized difference built-up index (NDBI) and normalized difference vegetation index (NDVI) are used to study the expansion and degree of change of urban landscape (Bhattiand Tripathi, 2014; Carlson and Arthur, 2000; Cui and Shi, 2012; Deng, Wang, Bai, Tian, and Wu, 2018; Potter, 2019; Sun, Wu, and Tan, 2012). One of the approaches to measure the expansion of urban land and built-up area and hence urbanization is measured by using satellite imagery (Fang and Quansheng,

2012). The physical expansion caused urban landscape changes have multidimensional effects from local up to global level.

Urbanization and associated land cover change is the main cause of urban climate change and it is one of today's concerns and central issues of research (Fang and Quansheng, 2012; Haishan and Ye, 2013; Zhang, Zhu, and Jiang, 2016). Studying the effect of the land cover change is commonly used to study the effect of urbanization on environmental change (Adeyeri, Akinsanola, and Ishola, 2017). Urbanization by itself is one of the anthropogenic forces of the planet (Cui and Shi, 2012). The land cover alteration which is resulting from the growth of urban areas is one of the main factors for local, regional, and global environmental change (Odindi et al., 2015). It affects microclimate (Lim, Cai, Kalnay, and Zhou, 2005; Naserikia, Shamsabadi, Rafieian, and Filho, 2019; Zhang et al., 2016). Urbanization related landscape changes affect the spatial distribution and amount of precipitation, atmospheric composition, near-surface humidity, energy balance, wind speed, and temperature (Choudhary and Tripathi, 2018; GALLO, OWEN, EASTERLING, and JAMASON, 1999; Han et al., 2013; Oliveira et al., 2016; Pathirana, Denekew, Veerbeek, Zevenbergen, and Banda, 2014; Tahir et al., 2014). Deng et al. (2018) stated that land use land cover is one of the major factors which affects land surface temperature and they also have a strong correlation (Rasuland Ibrahim, 2017). It also affects the trend of surface air temperature (Fang and Quansheng, 2012). The extent of urbanization effect on the environment varies with the size of the city. According to Gallo et al. (1996), the effect of dominant land cover on climate goes up to 10 kilometers radius. The main source of all this influence in urban areas is the land use/land cover change (Hoang, Linh, and Chuong, 2015; Odindi et al., 2015).

In general, the increment of the urban built-up area is directly related to a decrement in vegetation cover. These increments in the built-up area and decrement of vegetation cover affect the surface temperature of the region. The influence of the change in the urban built-up area on the atmosphere is observed through released particles, moisture, and heat (MOLDERS and OLSON, 2004; Odindi et al., 2015). These alter the composition of the atmosphere (Pielke et al., 2002). The change in temperature affects water vapor content in the atmosphere. According to Trenberth (2011) increase in temperature of 1 ^{o}C will increase the water vapor content by 7 percent. The cause of surface and lower atmospheric temperature change are not only greenhouse gases but also anthropogenic effects related to land cover

change (Laatand Maurellis, 2006). On the other hand, the propagation of the signal through the atmosphere will easily be affected by any change in the atmospheric composition.

Satellite-based positioning is one of today's world technology that has changed how things are being accomplished. It became a day to day lifestyle that no one is being able to escape. The application of satellite based positioning is instrumental for most aspect of our activities. For the last 20 years or more it was also used to understand the effect of the atmosphere on radio signals (Hordyniec, Kapłon, and Rohm, 2018). The basic working principle of satellite based positioning to determine the position of the end-user is mainly dependent on the tracking position of satellites. For this, the satellite broadcasts a radio signal to the user's receiver and this signal is propagating through the atmosphere. To gate precise and accurate positioning, it is necessary to study the effect of this propagation medium on the propagated signal. This Global Navigation Satellite System (GNSS) signal is available continuously but it is affected by variability in the atmosphere (Hordyniec et al., 2018).

The propagation of a signal from the satellite to the user's receiver is delayed by particles in the atmosphere. This is due to the atmosphere contain free electrons which is known as the ionosphere and neutral electrons which is known as the troposphere. The neutral atmosphere contains dry gas and water vapor. The delay due to the neutral atmosphere is called tropospheric delay and it causes the geometric lengthening of propagated signals (Jin, Park, Cho, and Park, 2007). The tropospheric delay plays a vital role in weather and climate and also the vertical motion of atmospheres (Hordyniec et al., 2018; Jin and Gleason, 2009; Jin et al., 2007; Jingyong, Peiyan, and Lee, 2005). The land surface temperature is directly or indirectly affects atmospheric composition. Vegetation cover and built-up area are related with land surface effects (Malik, Shukla, and Mishra, 2019) and they are interrelated. The transformation of landscape goes with changing local, regional, and global climate with diurnal, seasonal, and yearly scale and the practice of anthropogenic effect is one result of urbanization (Jingyong et al., 2005).

1.2 Statement of the Problem

In general, the effect of atmosphere on GNSS signal is known (Da Silva, Yamaguti, Kuga, & Celestino, 2012; Möller & Landskron, 2019) and the effect of urbanization on the atmosphere (Cao, Li, & Feng, 2020; Jin et al., 2007; X. X. Li, Koh, Panda, & Norford, 2016; Uttara, Bhuvandas, & Aggarwal, 2012) is well studied. However, if this change in the atmosphere due to urbanization has a direct effect on the positioning is not as such addressed yet. The degree of effect of urbanization on the atmosphere varies from one city to another (Choudharyand Tripathi, 2018) because the level of land cover compositions are different from city to city. To get precise and accurate information from GNSS signals, it is necessary to precisely model and remove the errors. One of the major sources of error in GNSS data processing is the error caused by the medium through which the signal is propagating.

In general, the particle on the atmosphere (electrically charged or neutral) affects the propagation of GNSS signal in the atmosphere and one of the things that affect the concentrations of atmospheric particles in urban settings is urbanization. Urbanization is associated with changes in urban landscape change due to urban physical expansion. The modification of the urban landscape affects the urban microclimate. The urban microclimate has its own role on the surface and above atmosphere change. The main goal of this thesis work is to check if this directly or indirectly affects the GNSS signal. Therefore in this study, an attempt will be made to answer the effect of urbanization and urban caused climate change on the GNSS signal.

The motivation that initiated this study is the long term change observed in the GNSS daily solution of the ADIS station.

1.3 Objective of the Study

General Objective:

- The general objective of the study is to analyze urbanization and the associated climate change effects on the GNSS signal.

Specific Objective:

- To measure the urban expansion of Addis Ababa city since 1989.
- To measure the change in vegetation cover in Addis Ababa city by making use of NDVI.
- To compute trends of the land surface temperature of Addis Ababa city.
- To generate a GNSS signal of the IGS station ADIS, located in Addis Ababa, within the premises of the Institute of Geophysics, Space Science, and Astronomy of Addis Ababa University.
- To analyze if there is any correlation between variables and arrive at an output that will enable us to conclude if the GNSS signal is affected by urbanization and urban-related climate change.

1.4 Scope of the Study

Urbanization and urban climate change effect is measured by different factors such as population density, number of cars, the increment of industry, building, built-up surface material, land use land cover change, and so on. Here this study considers land cover change due to urban expansion as a measure of urbanization and land surface temperature as a measure of climate change.

To study climate change it is common to make use of data measured for a long period of time. However, to assess microclimatic conditions, where changes are caused by specific parameters, such as urbanization, studies can be made on those periods, where these changes in the causative parameters are observed (Agnihotri, Ohri, & Mishra, 2018; Ali, Patnaik, & Madguni, 2017; Alshawaf et al., 2015; Greiser, Meineri, Luoto, Ehrlén, & Hylander, 2018; Tsoka, Tsikaloudaki, & Theodosiou, 2020; Y. Wang, Bakker, de Groot, Wortche, & Leemans, 2015) Moreover the long period change observed on the daily solution of the IGS site ADIS is observed during the given period 2008 - 2019.

1.5 Significance of the Study

The main goal of Geodesy is to provide accurate and precise information about the shape, orientation, and gravity field of the earth in time. It is applied in many fields to determine positions, navigation, and other purposes. For high precision GNSS positioning, the signal passes through different medium especially the ionosphere and troposphere that are also the basic sources of error in the determination of the 3D positions of points. Due to tropospheric delay, the resultant positioning solution obtained from the satellite positioning system is typically no longer precise. Hence, knowing the effect of urbanization and climate change, which causes a signal delay in the lower atmosphere, helps to improve the determination of positions, velocity, and time in geodesy. It is important to have good modeling of the delay in the neutral atmosphere in order to obtain the highest accuracy in the space geodetic results (e.g. station positions).

In addition to Navigation, position, and time, GNSS provides atmospheric information. The information obtained from the Global Navigation Satellite System is widely applied in meteorology and climatology. The Source of errors for GNSS from the atmosphere is used as a source of information about the water vapor content in the atmosphere. The quantification of water vapor content by making use of GNSS signal is relatively accurate than other methods (Jin, Cardellach, & Xie, 2014; Jin & Luo, 2009) Therefore, to improve already existing approaches that are being used to model the effect of the troposphere on GNSS signal, studying the impact of urbanization on GNSS signal will contribute towards GNSS data that will be generated in an urban setting. Apart from this, the research output can be used to understand the cause of the long term residual that is being observed at the station ADIS and remove it so that it cannot be interpreted as the effect of plate tectonics.

1.6 Study Area

The study area for this research work is the city of Addis Ababa, which is the capital city of Ethiopia. It is also an important city for the Africa Continent, as the headquarters of the African Union and United Nations Economic Commission for Africa are located in Addis Ababa. Addis Ababa serves as a social, economic, and political center for Ethiopia (Kasa, Zeleke, Alemu, and Hagos, 2011) and plays a dual role as the seat of the federal government and as a regional state (UN-Habitat, 2017). Addis Ababa city is located nearly in the center of Ethiopia with a longitude of (38°35’30” E, 38°57’030” E) and latitude of (8°46’00” N,

9°11'30" N), covering an area of about 527 km^2. The altitude of Addis Ababa is approximately between 2020m and 3000m above mean sea level. Addis Ababa is one of the fastest-growing cities in Africa. The city is divided into ten sub-cities. These are, Addis Ketema, Akaki Kaliity, Arada, Bole, Gulele, Lideta, Kirkos, Kolfe Keraniyo, Nifas Silk Lafto, and Yeka. According to the central statistical agency report of 2013, the official population of Addis Ababa city was about 3.1 million (CSA, 2013). The city continues to attract 90,000 to 120,000 new residents every year, mainly due to net immigration (UN-Habitat, 2007). As per the world bank 2015 report 58% of the average growth of the city, between 1995 and 2000, was attributed to migration (UN-Habitat, 2017). Figure 1 shows the study area map.

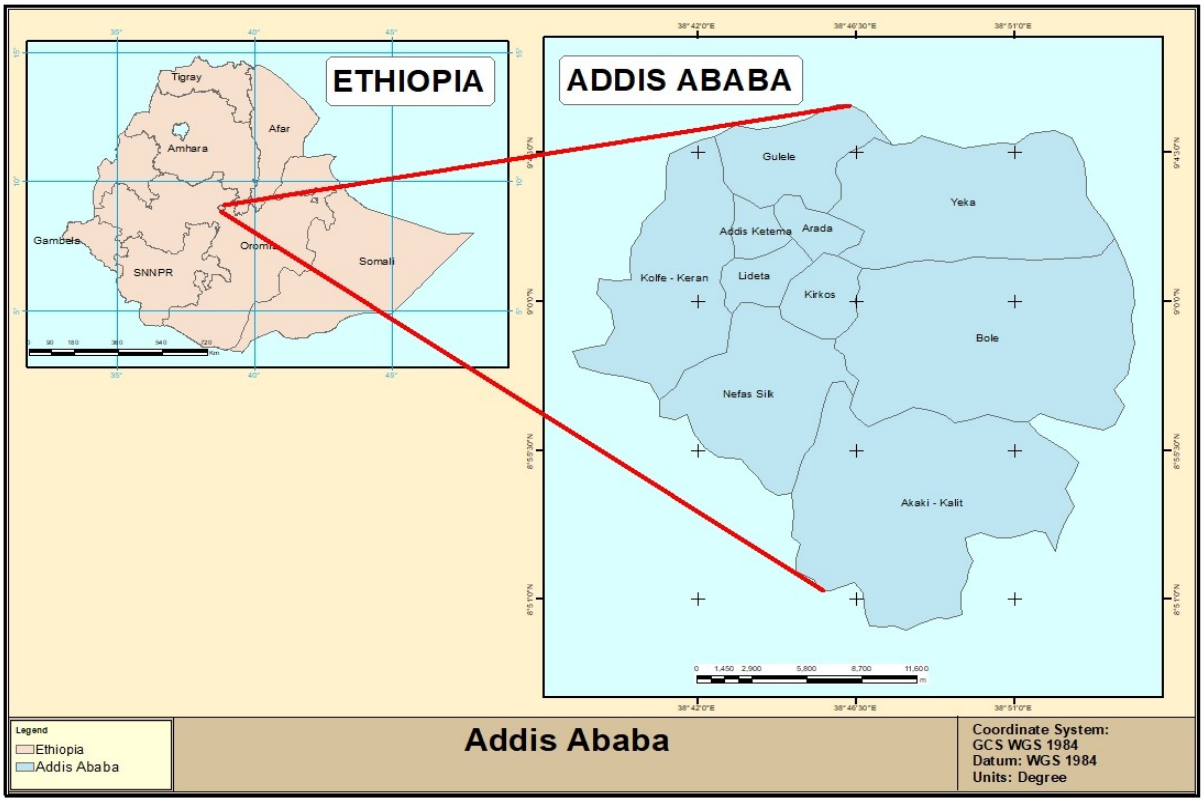

Figure 1 Location Map of the Study Area

1.7 Outline of the Thesis

The thesis contains six chapters. Chapter one discusses the introduction of the study. The general background of the study is included in this chapter. Objective, Scope, the significance of the study, the study area, and this subsection are all included in chapter one.

Chapter two covers theoretical bases about urbanization and urban climate change. In these chapter basics about urbanization such as definition, causes and measuring pattern of urbanization will be discussed. In addition, urbanization driving land cover change and way of measuring the changes will be included in this chapter. Urban related climate changes their effects are also discussed in chapter two.

Chapter three discusses about the theory and principles of GNSS. Specifically, it discusses how the signal propagates from the satellite to the receiver and the major source of error that affects the determination of positions from GNSS data.

Chapter four discusses about methods and materials. In this chapter, the processing steps, the data used, and the method implemented to analyze the data will be discussed. The general workflow of the study is also included in this chapter.

Chapter five covers results and discussion. The result obtained from the data analysis will be discussed in this chapter. In addition to that result will be discussed and interpreted in chapter five.

In Chapter six based on the results obtained and the discussion made in chapter five, a conclusion will be drawn and recommendations will be made.

CHAPTER 2 URBANIZATION AND CLIMATE CHANGE

2.1 Urbanization

Understanding urbanization and its impacts on microclimate changes would first demand the definition of what the term "urban" means. Because of the complex nature of parameters that define the urban setting, it is difficult to give a simple definition to the term "urban". The meaning encompasses parameters that are in natural and social sciences. In social science, the term "urban" is defined from a population density perspective. For example, according to the U.S. Bureau of the Census, the term "urban" is defined as an "area with more than 2500 people (> 620 individuals/km2)." According to the United Nation (1968), urban is defined by "Area with > 20,000 people". In the case of natural science (Ecologist) urban is defined from the perspective of dominant land cover. For example, Emlen, (1974) defines urban as "Area consisting of houses and lawns" and Odum, (1997) defines urban as from the perspective of energy consumption in such a way that "Area that uses at least 100,000 kcal/m^2/yr." Due to the complexity of urban definition, (MCINTYRE et al., 2001) suggest to include basic information of demography (such as population density, economic characteristic, etc.), physical geography (such as area, urban pattern, land cover, etc.), socioeconomic and cultural elements when defining urban. The urban ecosystem contains a "biotic and abiotic system". Biotic systems are biosphere (plant and animal) and anthroposphere (politics, economics, administration, civic participation, planning, and demography). Abiotic systems are atmosphere, hydrosphere, lithosphere, and soil/pedosphere (Uttara et al., 2012).

Different disciplines view urbanization from a different point of view. But we can categories those into three. The first one is the demographic point of view. Those are describing urbanization as an increase in population that contributes to the growth of the cities. This way UN describes urbanization as an increase in the number of people living in an urban area (UN, 2019). The International Organization for Migration (IOM), measures urbanization by the amount of total national population residing in the bounded area of an urban setting(IOM, 2015).

The second one is from an economic point of view. Those are describing urbanization from the perspective of the economic growth of a city. According to Pravitasari (2015), urbanization is associated with a high number of buildings and other urban land uses. On the

other hand Uttara et al. (2012), related urbanization with the development of urban areas because of industrialization and economic growth.

The third view is based on the physical expansion of the urban area. Urbanization is related to extent of cities and the amount of area occupies by urban residents (UN, 2019). Urbanization refers to an increase in the number and size of cities (Uttara et al., 2012; Carlson and Arthur, 2000).

Usually, urbanization has been a positive force for economic growth, poverty minimization, and human advancement. Cities are center for development, where closeness to economic movement, government, and transportation allows transferring useful information and knowledge within. As a result, urban residences will have a greater chance to education, better health, social and economic service (UN, 2019). Urbanization incorporates social, economic, and cultural parameters. Urban growth is mostly associated with social, economic, and environmental plans for sustainable development (UN, 2019).

2.1.1 World Status of Urbanization

Urbanization is an inevitable process of modern society. In this era, it is a global phenomenon that has the highest growth in every dimension. In the last centuries, urbanization increased drastically. According to a United Nations report (UN, 2019), the rate of urbanization is predictable to grow in all regions, but the increment with variable amounts. Latin America, the Caribbean, and North America are expected to be highly urbanized. It is projected that the percent of urbanization will rise from 80 percent in 2018 to 90 percent in 2050. In Europe, it is expected to reach 80 percent in 2040 and nearly 85 percent by 2050. In Oceania, it is expected to remain stable. The current 70 percent is expected to remain the same in 2050. The current 50 percent urbanization is projected to rise to 66 percent in 2050 in Asia. In Africa, different from the other region is projected to remain rural in 2050. It is 40 in 2018 and it is expected to be 59 percent in 2050. However, the rate of urbanization is higher in Asia and Africa than in other regions of the world. In Asia and Africa urbanization is growing at a rate of 1.3 and 1.1 percent yearly between 2015 and 2020 respectively but in the other region less than in 0.3 percent (UN, 2019).

2.1.2 Causes of Urbanization

Urbanization is an integrated socio-economic process that transforms the construction environment, to change rural to urban areas (UN, 2019). Many internal and external factors have driven urbanization in a different aspect. Population growth and economic development are the major consequences of urbanization. The populations of urban settlements are growing because of two factors. These are natural population growth and population growth due to migration (Alcoforado and Henrique Andrade, 2008). Even if rural to urban migration has a significant contribution to urbanization, the contribution of natural population growth is also significant (International Organization for Migration (IOM), 2015). The population growth of urban areas is the main indicator of this. Since 1950 the global population increases with rapid urbanization. In 1950 more than 70 percent of the world lived in a rural area. In 2007, the world urban population exceeded the world's rural population. Since 2007 the global urban population increases rapidly. The populations of urban areas were growing from 751 million in 1950 to 4.2 billion in 2018. At the end of a sustainable development plan in 2030, the urban population is expected to be 60 percent of the world population and in 2050 is expected to reach more than 68 percent (UN, 2019). For the next decades, Africa plays a significant role in the increase of the global urban population. Migration from rural to urban areas has its own role in the increment of the urban population. Urbanization is mainly the outcome of migration (International Organization for Migration (IOM), 2015). Migration from rural to urban areas will increase the number of cities (Makinde, 2012). Depending on the nature and pattern of migration, it has a strong or weak drive process on urbanization (Bhagat and Mohanty 2009). Migration from rural to an urban area is highly driven by population pressure and scarcity of a resource in the rural area (Pravitasari, 2015). There are pull and push factors that are causes of rural to urban migration. The pull factors are the expectation for a better life in the urban area and the main push factor is the living condition in the rural area (Jansen and Paelinck, 1981; Kaida, 1992).

Pravitasaric (2015) categorized the historical causes of urbanization into six factors. These are an industrial revolution, industrialization following the industrial revolution, emergence of large manufacturing centers, job opportunities, availability of easy transportation, and migration.

2.1.3 Effect of Urbanization

Urbanization has its own merit and demerits. Commonly urbanization has been a positive force for economic growth, poverty minimization, and human advancement (UN, 2019). Historically, urbanization has led to a cumulative transformation in economy, culture, and society, with dense living style (International Organization for Migration (IOM), 2015). Urban areas have much economic, political, and cultural advantages than rural areas (Pravitasari, 2015). Among many other things, the main benefits of urbanization are economic growth, improvement of commercial tasks, incorporation of social and cultural life, and service effectiveness (Pravitasari, 2015). The disadvantage of urbanization is the impact on public health due to pollution and other communicable diseases, a high number of unemployment, scarcity of housing, transportation problem, and social effects. The social effects are such as poverty, loss of opportunities, psychological difficulties, drunkenness, crime, violence, and other abnormal behaviors (Pravitasari, 2015). Fast urbanization, large population density, and high-level consumption of urban settlers have fueled many local and global socio-economic and environmental problems (Pravitasari, 2015).

In Uttara et al. (2015), the impact of urbanization is categorized into four areas. These are the impact on the atmosphere and climate (such as the creation of heat island, changes in air quality, and changes in patterns of precipitation), lithosphere and land resources (such as erosion, land quality change, and pollution), hydrosphere and water resources (such as high and fast flow of water into streams, loss water quality) and biosphere (modification and destruction of inherent habitats). The urban building material mainly affects the energy flux, circulation of water, and other factors of cities (Deng et al., 2014).

2.1.4 Pattern of Urbanization

It is the most crucial and significant factor to measurably describe and estimate the expansion of urban settings locally, regionally, or globally to assist urbanization forecasting and related issues, mainly for high urban growth expectation areas (Jiao, 2015). The measurement of urbanization is made using different factors in different disciplines. However, most of the disciplines are trying to study the rate of the growth of the urban area, in what extent, and how fast it moves. To answer such questions in urbanization, it needs spatial and non-spatial criteria. Different metric and statistical methods have been used to characterize urban growth and expansion (Tavernia and Reed, 2009; Wilson et al. 2003). The pattern of urbanization is

characterized by land-use patterns, transportation, water/sewer infrastructure, artificial drainage, and heat island (Grimm et al., 2008).

2.2 Land Cover Change

Gregorio and Jansen, (1998) defined Land Cover (LC) as "the observed biophysical cover of the Earth's surface." Land Cover may include vegetation cover, man-made feature as well as barn land and inland water surface. Mainly it is concerned about the physical and biotic characters of the Earth. Land cover is linked with soil, surface, and groundwater (Abtew and Melesse, 2016). The monitoring of land cover change is helping in monitoring the change in forest and rangeland, production of statistics for planning and investment, biodiversity, climate change, and desertification control. It is in general a cornerstone for many disciplines (Gregorio and Jansen, 1998). Land use and land cover are very significant for biogeochemical cycles, global climate, and seasonal changes (Kumar, Agrawal, and Krishnaveni, 2014). Recently a land cover study is used to know the past and to forecast future changes in our planet. Based on the level of application it can be implemented at various spatial and temporal scales. The spatial scale can be at a local, regional, and global level.

As many studies show, the role of studying land cover change is crucial. Hence, it needs advanced technology and scientific bases to measure, analyze, and report. Remote sensing plays a great role in land cover mapping. The advancement in remote sensing techniques is recently significantly used to measure global, regional, and local landscape change (Alcoforado and Henrique Andrade, 2008). Currently, satellite data are widely used to measure land-use changes (Torres-Vera et al. 2009; Muttttanon and Tripathi 2005). Remote sensing technology provides a different type of date for many applications. Information about land cover change, land surface temperature, and precipitation, that are extracted from remote sensing techniques, have shown great improvement and their role in studying the impact of urbanization on climate change is becoming more evident (Ke et al., 2014). Remote sensing data are primarily applied to control and identify continuously changing urban land cover, which is caused by urbanization (Karanamand Babuneela, 2017).

Urbanization is one of the anthropogenic factors for land cover change. The monitoring of changes observed in vegetation cover of urban settings is a significant factor as it indicates the change in urban land cover and their effect on the environment (Sharma and Joshi, 2015).

Currently, urban growth is a leading demographic trend and a significant part of the land change process, globally (Grimm et al., 2008). In addition to urbanization, population growth has also a high impact on land cover change. Population and economic growth are the driving factors for landscape change (Zhan et al., 2014). The change in the Earth's landscape by a human is significantly increasing. After the industrial revolution, the changed landscapes of the Earth by a human being are in the range of between 33 and 50 percent (Alcoforado and Henrique Andrade, 2008).

Land cover change is at an alarming level in today's world. It affects Earth's ecosystem at a local regional and global level. Land use land cover changes have a direct and indirect contribution on the world ecosystem (Sharma and Joshi, 2015). Land use land cover change is playing a great role in the global environment and it is the main scientific concern ever (Zhan et al., 2014). Changes in physical properties of the landscape such as albedo, long-wave radiation, surface roughness, and vegetation are mainly caused by a land-use change (Deng et al., 2014). The increase in population size and demands of resources for agriculture, industry, and urbanization transforms the Earth's surface. These lead to major biochemical changes (Alcoforado and Henrique Andrade, 2008).

To study land cover change various methods and techniques have been used in the scientific world. The method and techniques are basically depending on the area of application, spatial scale (global, regional, and local), temporal resolution (daily, weekly, monthly, annually, and so on), and data availability. Environmental quality is demarcated by four variables which are greenness, imperviousness, moisture intensity, and intensity of bareness. Normalized Difference Vegetation Index (NDVI) used to measure greenness, Normalized Difference Built-up Index (NDBI) is used to assess imperviousness, Normalized Difference Water Index (NDWI) is used to estimate moisture intensity, and the intensity of bareness is commonly measured by using Normalized Difference Bareness Index (NDBaI) (Sharma and Joshi, 2015). NDVI and NDBI are used to study the effect of urbanization on the city's land Surface Temperature (Sharma and Joshi, 2015). NDVI has a highly acceptable measurement capacity in remote sensing (Cracknell, 2001).

2.2.1 NDVI

Normalized difference vegetation index (NDVI) is the most widely applied index to study vegetation cover of land. NDVI is an approved method used to show vegetation cover of the world (Kundu, Denis, Patel, and Dutta, 2018). The NDVI is computed as a ratio of the difference of the Near Infrared and the Red bands(Molly E.B, 2008). Spectral vegetation indices are mostly derived from red and near-infrared reflectance (Tucker, 1979).

$$NDVI = \frac{(NIR - R)}{(NIR + R)}$$

Where NIR is the near-infrared band and R represents the red band of spectral reflectance.

The value of NDVI ranges from −1 to +1; negative NDVI values indicate open water bodies, and positive values show the areas covered by green vegetation. Vegetation has high spectral reflectance in NIR and low spectral reflectance in red. As a result, a high NDVI value indicates a vegetated area and on the other hand, low NDVI values show less vegetated area(Molly E.B, 2008). NDVI is used to measure the degree of vegetation cover. Dense vegetation has a value between 0.1 to 0.6 and on the other hand clouds, water, and snow have negative value but, rock and bare soil have nearly zero(Abtew and Melesse, 2016). NDVI mainly integrates with the photosynthetically active biomass, chlorophyll content, and energy received by plants (Myneni et al., 1995).

NDVI has many areas of applications such as land cover change detection, climate change, environmental monitoring, and more. NDVI value is also used to detect the density of vegetation and their well-being (Lo and Quattrochi 2003; Curran 1980). Globally NDVI is a widely accepted method for and measuring land cover changes and their characteristics. (Maselli et al. 2006; Dutta et al. 2013; Kundu et al. 2016). NDVI has been globally used to indicate vegetation dynamics for various regions (Tucker et al. 1986; Myneni et al. 1997; Nemani et al. 2003; Dutta et al. 2013, Kundu et al. 2016). NDVI is used to study land cover change at the global level by indicating the degree of photosynthetically active radiation absorbed by plants on the Earth (Molly E.B, 2008). According to Yengoh et al. (2015), NDVI is used to study land-use and land-cover changes, detect and investigate drought and drought early warning, identify and detect desertification, soil erosion, assesses soil salinization, identify and monitor vegetation fires, monitoring of biodiversity and conservation, and predict Soil Organic Carbon (SOC).

NDVI is commonly used together with other factors such as land surface temperature and rainfall data. An inverse relationship between NDVI and land surface temperature is used to show landscape change (Singh and Grover, 2015). NDVI is highly correlated with climate factors (temperature and precipitation)(Luo et al., 2015).

2.2.2 NDBI

Normalized Difference Built-up Index (NDBI) is used to automatically detects and map built-up areas. NDBI has been used for mapping urban built-up areas using Landsat Thematic Mapper (TM) data (Bhattiand Tripathi, 2014). The NDBI is computed as a ratio of the difference of the Near Infrared and the Medium Infrared bands.

$$NDBI = \frac{(\mathrm{MIR} - \mathrm{NIR})}{(MIR + NIR)}$$

Where MIR represent medium infrared band and NIR represent Near Infrared band

The value of NDBI ranges from −1 to +1; near to 0 values represent woodland and farmland, negative values for water bodies, and positive values for built-up pixels.

NDBI is firstly used by (Zha, 2003) to fill the gap of the long process to convert satellite imagery into a land-cover map using the existing methods of manual interpretation and parametric image classification by an automated process of mapping built-up areas. Normalized Difference Built-up Index (NDBI) has been used to extract built-up areas in an automated way (Ghoshand Siddique, 2018).

2.3 Urban Climate

Climate refers to the consistent condition of weather in a specific area (Palmate et al. 2017). Climate changes mostly manifest themselves through changes in temperature and precipitation levels that are highly impacting vegetation growth (Luo et al., 2015). The parameters that are used to measure climate variations include temperature, rainfall, humidity, sunshine hours, cloudiness, pressure, number of rainy days, wind velocity, etc. They are interrelated with each other and affect one another (Palmate, Pandey, Kumar, Pandey, and Mishra, 2017).

Climate change is quantified through changes in climate factors. Temperature and precipitation amount are the major factors that are commonly used to quantify climate

change. In general climate change is caused by natural and human driving factors. When it comes to urban climate change, it is driven by external and internal factors. The urban area climate is subjected to climate change from greenhouse gas and Urban Heat Islands (UHI) (Mccarthy, Best, and Betts, 2010). An artificial source of heat radiation and the reduction of green area coverage have a high role in the rise of land surface temperature (Deng et al., 2014).

The warming of urban areas relative to the surrounding is one indicator of local climate change. The local climate is different from the global climate by the level of intensities and extent. The urban climate is the climate difference between urban areas and the surrounding. The major characteristics of urban climate are greater surface and air temperature, alteration in radiation equilibrium, lesser humidity, and collection of polluted air in atmospheric from various sources. The effect is not only local and regional, but it has also a global impact (Kuttler, 2008). The urban climate is a result of regional and local spatial objects (Lowry, 1977).

2.3.1 Causes of Urban Climate Change

Solar energy is the primary energy source for the Earth's climate (Abtewand Melesse, 2016). The solar energy that reaches the surface of the Earth is mostly in the visible spectral domain. Depending on the type of surface, the Sun energy is either reflected or transmitted. The amount of radiation that will be reflected from the surface of the Earth is dependent on the surface reflectance. Because of this, urban areas absorb more and release less energy which induces urban surface and air UHI. At the Earth Surface, the expected incident energy from the Sun is 1350W/m^2 and from this 450W/m^2 is reflected by the atmosphere. The remaining solar energy not reflected from the surface is regulating Earth’s environment in a different direction. Therefore, the energy of the Earth depends on land surface characteristics, and this controls regional temperature, rainfall, and runoff (Abtew and Melesse, 2016).

The major sources for urban climate change, from urban built-up areas, are the change of natural surface by artificial surface, minimization of green area, a decrease of a long-wave releasing surface by different infrastructure, and emission of solid, liquid and gaseous particle in the atmosphere (Kuttler, 2008). Urban albedo affects local climate primarily, even if urban areas that cover 0.44 percent of the Earth's Surface (Spangmyr, 2010). The impact of land use on the climate system is not only through the change of the surface physical properties but

also through the amount of greenhouse emission (Deng et al., 2014). The human intervention in green cover and water flows mainly affect temperature distribution (Abtew and Melesse, 2016).

2.3.2 Africa

El Nin˜o/Southern Oscillation and land cover change are two main significant driving factors for the Africa climate alteration (Hulme et al. 2001). The main climate-related hazards in Africa are flooding, drought, desertification, heatwave, landslides, and sea-level rise. Flooding of the urban environment is not only caused by high rainfall, but also because of the expansion of the sealed surface of the urban canopy. Drought is mainly caused by weather variability of the urban environment, which is a result of highly built-up and land cover change. Desertification is mainly as a consequence of the degradation of natural land potential and the reduction of surface and groundwater capacity. These are caused by land cover changes such as deforestation, overgrazing, etc. The heatwave is characterized by high temperatures with a long duration. These affect human health as well as the environment. Sea level rise potentially affects urban areas that are near around the sea (Ruocco et al. 2015).

2.3.3 Urban Heat Island (UHI)

UHI is the main indicator of urban climate change. UHI is the difference between urban and rural temperatures. The period and amount of temperature difference related to geographical variation and urban land uses (Pickett et al., 2008). UHI is classified into Surface UHI, Canopy Layer UHI, and Boundary Layer UHI. Canopy Layer UHI and Boundary Layer UHI are related to atmospheric heat island (Singh and Grover, 2015). Canopy Layer UHI covers the height from the ground to below the tops of trees and roofs. Boundary-Layer UHI covers the height from the rooftop and treetop level and extends up to the point where urban landscapes no longer influence the atmosphere. UHI is expressed through surface, sub-surface, or air temperature. UHI is high at night time (Alcoforado and Henrique Andrade, 2008). Air temperature is maintained by evapotranspiration and vegetation play a great role in this process, by releasing water into the neighboring air and reducing ambient heat. Built materials are on the contrary releasing less water to the surrounding air and this causes a rise in surface and air temperature.

Factors that are related to UHI creation are vegetation cover, urban material, urban geometry, the heat emitted by human action (anthropogenic heat), weather, and geographical locations. They can be categorized in land cover, surface characteristics, and human activities. Urban heat is mainly affected by land-use, the structure of built-up, and the extent of urban areas (Kuttler, 2008).

2.4 Land Cover Change and Climate Change

Land cover change impacts climate change significantly and its effect cannot be neglected. Its impact on climate is both at a local and regional scale (Rees & Wackernagel, 2008), but with variable intensity (Hibbard et al. 2010). The land cover change increases surface heat and roughness. This change yields an increase in temperature and a decrease in precipitation at a regional scale (J. Shukla et al., 1990; V. Gornitz et al., 1997). Land use land cover change affects the climate of the Earth by altering land surface, which is a major source for atmospheric water vapor (Betts et al. 1996).

Changes in land surface properties highly disturb the interrelation between the atmosphere and land surface. Hence this leads to a change in the thermodynamic and dynamic characteristics of the atmosphere and this alteration affects climate form and pattern. Land cover changes that lead to noticeable climate change are deforestation, afforestation, and urbanization. These affect the energy budget, land surface temperature, distribution of precipitation water, runoff, and evapotranspiration (Phillips et al. 2009; Pielke et al. 2007; Arora and Montenegro 2011). Landscape change, mostly deforestation, is the source of 12.5 percent of the greenhouse gas emission (Herzog 2009). The highly impacting landscape changes in the atmosphere are the change in land surface and vegetation pattern (Brovkin et al. 1999).

The influence of LUCC on the local, regional, and global climate system is expressed through different biogeophysical and biogeochemical processes. Biogeophysical directly affects physical factors that control the absorption and transferring of land surface energy. Biogeochemical parameters indirectly affect the climate system by changing the chemical composition of the atmosphere (Dirmeyer and Shukla 1994; Arora and Montenegro 2011; Meiyappan and Jain 2012). The effect of the land cover change on regional climate depends on the physical, chemical, and biological characteristics of the landscape (Deng et al., 2014). Land-use change by human action has a high impact on the regional climate system

(temperature, evapotranspiration, precipitation, wind field, atmospheric pressure) but mainly affect temperature and precipitation (Pielke et al. 2007; Arora and Montenegro 2011; Degu et al. 2011; Woldemichael et al. 2012).

2.5 Urbanization and Climate Change

Urbanization is a major activity of human beings that changes the physical surface pattern and microclimate (Deng et al., 2014). The transformation of urban land cover caused the increase and densification of impervious surface (Singh and Grover, 2015). The positive correlation between the degree of UHI with urban area size, urbanization rate, and population size shows the inevitable contribution of urbanization on microclimate (Hung et al. 2006). The change in the urban landscape, because of land cover change is the source of surface temperature change (Singh and Grover, 2015). In the USA, the land's surface temperature is rising since 1950 and 50 percent of this is a consequence of urbanization (Stone 2009). Open water, wetland, and vegetation surface usually decrease local temperature but increase in the urban built-up area such as paved and dry surface increasing local temperature (Abtew and Melesse, 2016).

Urbanization is the most vital anthropogenic effect on the surface climate. Urbanization affects global, regional, and local climates by changing natural surface to artificial surface and heat emission from human action (Ke et al., 2014). There is a considerable indication that modern megacities are affected by climate and hydrological variations with the growth of city size and urbanization. The effect is observable at a regional scale (Berry, 2008). Urbanization causes UHI and this shows the impact of LUCC on regional climate (Deng et al., 2014). UHI and gases in precipitation that are caused by urbanization highly affect the local climate (Deng et al., 2014). The UHI causes climate change highly associated with the urban landscape and human energy consumption (OKE, 1995). In addition to the creation of heat islands, urban climate change that is associated with the growth of a city-size affects the content of cloud, fog, dust, precipitation, and humidity (Berry, 2008).

Urban atmospheric environment change can occur at three spatial scales. Local effects are mostly caused by the replacement of natural surfaces with artificial materials. This alters the nature of reflecting surface, heat exchange, and atmospheric roughness. Regional effects are caused by the level of artificial heat and change in the atmosphere composition through the release of pollutant particles. In addition to the effects of urbanization on regional atmospheric variability, urban activities have an impact on the global climate through CO_2

and fluorocarbons emission (Berry, 2008). The global effects from urban generated gas (such as sulfur, CO_2) are causes of the greenhouse effect, global warming, and increase of see-level (Berry, 2008). Even though urban area covers two percent of the Earth landscape, they contribute 78 percent of the greenhouse gases. These show the association of urbanization with a global event (Grimm et al., 2008).

The association between urban climate and global warming is an important topic for contemporary science. It is also hard to draw a boundary between them. There are different assumptions about the causal relationship between them, i.e. is urban climate change is the cause of global warming or vice versa. According to different literature, Alcoforado and Henrique Andrade (2008) conclude that urban heat exchange does not directly impact global warming because of small scale (less than 1%) coverage of urban areas relative to the size of the Earth. A unique feature of the urban ecosystem is a large amount of energy consumption per year per area, which is mainly caused by the burning of fossil fuel. Compared to the Earth's surface, urban areas occupy an insignificant portion, but they consume a high amount of energy (McIntyre et al., 2008). Urban climate change indirectly impacts global warming because urban is one of the sources of greenhouse gases. On the other hand, Global warming has a sizable impact on regional climate change. The influence of global warming can impact many factors such as human health, different ecosystem, the level of energy and water consumption may impact urban area. In general, the effects of urban climate change are not only limited to humanity and bio-climate but also on energy consumption, emissions of anthropogenic and biogenic hydrocarbons, and the formation of secondary pollutants (Kuttler, 2008).

CHAPTER 3 GLOBAL NAVIGATION SATELLITE SYSTEM

3.1 Introduction

GNSS is a satellite based navigation technique used to determine position, velocity, and time in space. According to Hofmann-Wellenhof et al. (2008) and other literature herein the Global Navigation Satellite System (GNSS) is defined as a space-based radio positioning system that includes one or more satellite constellations, augmented as necessary to support the intended operation, and that provides 24-hour three-dimensional position, velocity, and time information to suitably equipped users anywhere on, or near, the surface of the earth (and sometimes off earth). It is a passive ranging system in which a user determines their position by receiving the broadcasted signal from the satellite. Satellite broadcast precise orbital position and synchronized time information to the user. GNSS is a ranging system that makes use of the known position of the satellite, to determine positions on the Earth's surface, on water bodies, and space. GNSS is identified by the following characteristics (CERUZZI, 2018; Madry, 2015): availability of information at all times and in all weather conditions, accessibility of the service all over the world, relatively high accuracy of position in a short time, very small power consumption and simplified applicability.

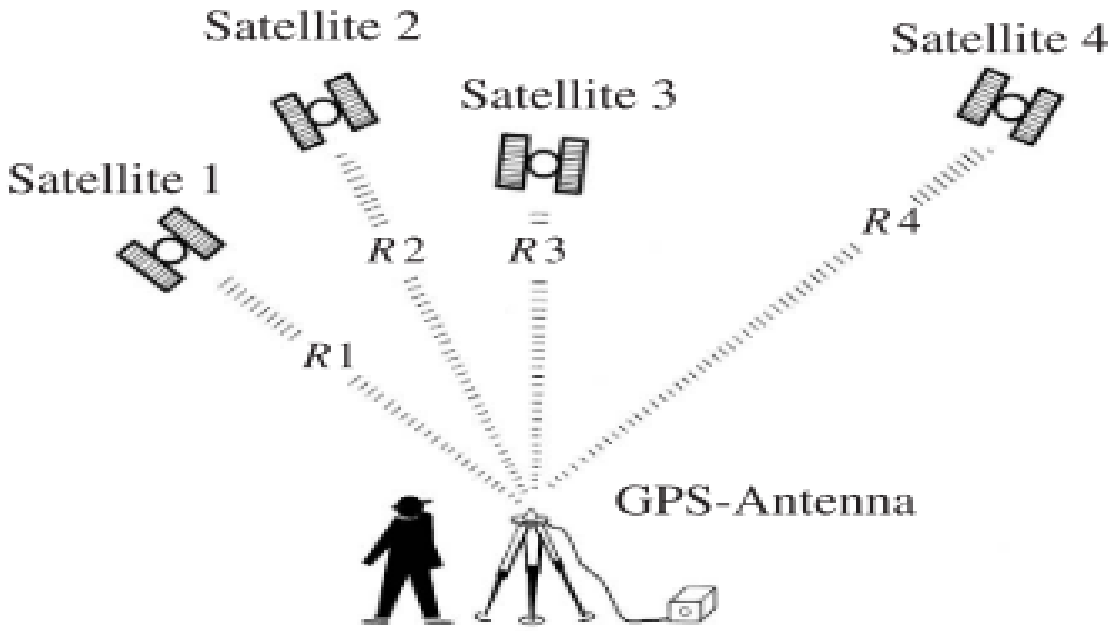

Figure 2 Basic principle of positioning with GPS (Seeber, 2003 page 211)

GNSS measurement uses a one-way ranging system from satellite to user in space. The incoming signal from the satellite to the receiver is correlated with the replica signal generated in the receiver. That determines the time it took for the signal to travel between the satellite and receiver. Using this time and the speed of light the pseudo-range from the receiver to a satellite is computed. By making use of this computed pseudo-range to different satellites, the 3D positions velocity and time will be computed. The detailed technique of positioning is discussed in many literature such as Hofmann-Wellenhof et al. (2008), Leick (2004), Kaplan and Hegarty (2006), and Subirana et al. (2013). In general, the computation of the position relies on elementary geometry principles. The receiver measures distances that are known as pseudo-ranges to a minimum of four satellites, with known position coordinate. These distances are used to compute the user's position that might be from several meters to centimeter-level precise, depending on the advancement of instrument and computation techniques.

The historical evolution of GNSS is based on the ancient navigation concept. In early times human beings use different signs to move from location to location. Fundamentally uses different landmarks and celestial bodies to determine their position. The ancient time navigation and mapmakers depends on heavenly body observations to determine both time and position on the earth (Misra and Enge, 2006). But these methods have their own deficiencies. Landmarks are prone to be removed and celestial bodies can be covered by cloud and other factors. These make their navigation and positioning difficult. To overcome the challenge various options were tested and through time artificial satellite-based navigation system was initiated. Satellite-based positioning is the process of identifying the location of observing sites on land, at sea, in the air, and in space through artificial satellites (Hofmann-Wellenhof, Lichtenegger, and Wasle, 2008).

The discovery of the radio navigation system was open new way for positioning. Radio beacons, VHF omnidirectional radios (VORs), long-range radio navigation (LORAN), and OMEGA were invented as a result of radios development (Parkinson, Jr., Axelrad, and Enge, 1996). For the first time, the Soviet Union launched the first satellite Sputnik, in 1957. Soon after this, the US military develops Transit System in 1959. This system uses the Doppler shift method to measure the distance between the signal source and the receiver. Later they have improved Transit and in 1964 Timation system concept was proposed and the Timation satellite was launched in 1967. Timation was using the satellite ranging system rather than the Doppler shift (Madry, 2015). The early systems have their limitations. Hofmann-

Wellenhof et al.,(2008) categorized these in two, the first one is the gap between two satellites pass. These make computation time long. And the second short come is less navigation accuracy. In addition to that Transit only provide two-dimensional information, not three-dimension (CERUZZI et al., 2018; Madry, 2015). The current, Satellite positioning systems shifted their working methodology from Doppler shift (Doppler based system) to Trilateration. Trilateration is method used to determine position by measuring distance to three or more known points.

GNSS is a generic name that is given to different satellite positioning systems such as GPS, GLONASS, Galileo, BeiDou and etc. In general, GNSS includes the US's Global Positioning System (GPS), Russia's GLONASS, European Union's Galileo, and Chinese BeiDou (also called COMPASS) as well as several regional navigation satellite navigation systems. GNSS can be characterized as a highly precise, continuous, all-weather, and near-real-time radio navigation system with signals in the microwave (L-band) frequency range propagating through the Earth's atmosphere (Jin et al., 2014). Currently, different GNSS systems are in use for Positioning, Navigation, and Timing Systems (PNT). These all are sharing comparable design and architecture (Madry, 2015) in such that they are in the medium-earth orbits, have atomic clocks, and spread-spectrum of coding (CERUZZI, 2018).

GPS is the most widely used and one of the GNSS, which is developed by the U.S. Department of Defense (DoD). Russia, the European Union, China, Japan, and India also develop positioning and navigation system (Madry, 2015). Russian, European Union's, Chinese, Indian, and Japanese positioning systems are called GLONASS, Galileo, BeiDou (originally called COMPASS), IRNSS, and QZSS respectively. GPS and GLONASS were developed for military purposes but later they were available for civilian use.

The application of satellite positioning systems grows rapidly and it is becoming part of our day to day activities. It has a very wide area of application that is from local to a global scale and used in military, science, surveying, recreational hiking, and boating (CERUZZI, 2018).

According to Misra and Enge (2006), the areas of application of the GNSS are categorized into three areas. These are for positioning (Aircraft, ship, tank, truck, solider, bomb), navigation (Car and truck driver, sailor, pilots, sportsmen, and outdoorsmen), and accurate timekeeping (Telecommunication, banking, power generation, and internet). On contrary, Parkinson et al. (1996) preferred to broadly categorize the application area into two, namely military and civilian uses. The military uses include minesweeping, aircraft landing, infantry

operations, etc. The civilian application includes primarily for accurate time transfer and survey. GNSS satellites deliver time information with the accuracy of atomic clocks, anywhere in space (Madry, 2015). Among others, the civilian application is in the area of utilities industry, forestry and natural resources, precision farming, civil engineering, monitoring structural deformations, open-pit mining, land seismic surveying, marine seismic surveying, airborne mapping, seafloor mapping, vehicle navigation, transit systems, the retail industry and cadastral surveying (El-Rabbany, 2002).

3.2 Component of GNSS

The global navigation satellite system consists of three segments, namely the space segment, control segment (ground segment), and user segment. The space segment includes the satellites and their constellation, the control segment is to control satellite associated issues and the user segment deals with receivers.

3.2.1 Space Segment

The orbital constellation of the satellite is designed in such a way that any receiver can see a minimum of four satellites from anywhere on the Earth surface or space. GNSS orbit constellation is Medium Earth Orbit (MEO) altitude from 19,000 – 30,000km by considering precise orbiting, launch cost, transmitted power, global coverage, and protection from enemy (Hofmann-Wellenhof et al., 2008; Jin et al., 2014; Madry, 2015).

The GPS Space constellation consists of a minimum of 24 satellites, which sometimes can reach up to 32 satellites, with elliptical orbit nearly circular. Satellites are arranged in six orbital planes and each orbit has four or more satellites. The inclination angle of the orbit from the equator is 55^{o} and the altitude of the satellites is approximately 20,000km. The satellite rotates around the earth with a speed of 3.874 km/sec, which means two complete rotations around the Earth per day. Each satellite has a space vehicle number (SVN) and specifically designed pseudorandom noise (PRN).

The GLONASS satellite constellation consists of 24 satellites with a nearly circular orbit. The inclination angle to the equator is 64.8^{0} with an altitude of approximately 19,100 km. The satellites are arranged in three orbital planes, with eight satellites in each equally spaced orbit. The period of revolution is 11 hours, 15 minutes, and 44 seconds.

The complete Galileo constellation is planned to consist 27 operational and 3 spare satellites with a nearly circular elliptical orbit. The satellites are arranged in three orbital planes with ten satellites in each. The inclination angle to the equator is 56^0 with an altitude of 23,222 km. The orbiting time around the Earth is 14 hours, 4 minutes, and 45 seconds.

The complete BeiDou space constellation is planned to consist 35 satellites. The constellation includes 5 geostationary (GEO) satellites with an altitude of 35,786 km, 27 satellite medium earth orbit (MEO) with inclination angle $55^{0,}$ and altitude of 21,528km, and 3 inclined geosynchronous orbits (IGSO) with inclination angle from the equator is 55^o and altitude of 35,786 km. Currently, it's under development in order to cover worldwide coverage. (https://www.glonass-iac.ru/en/guide/beidou.php).

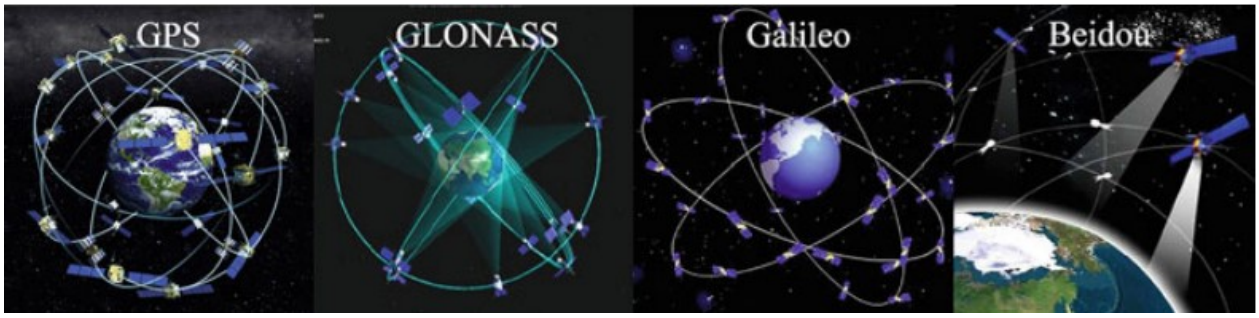

Figure 3 Global Navigation Satellite Systems (GNSS) satellite constellation from (Jin et al., 2014)

GNSS satellite generates and transmits a ranging signal to a receiver in order to determine the distance from the satellite to the receiver. The satellite also broadcast navigation message which contains information about satellite orbital position and clock correction. The satellite receives and stores signals that are coming from the monitor station that define the future position of satellite orbit and clock correction.

GNSS satellites consists atomic clocks, radio transceivers, computers, solar panels, a propulsion system for orbit adjustments and stability control, navigational payload, navigational antennas, altitude, and orbit determination and control (AODC), Tracking, Telemetry, and Command (TT and C) systems. Atomic clocks are used for precise timing (Hofmann-Wellenhof et al., 2008; Jin et al., 2014). Satellites are equipped with two cesium (Cs) and two rubidium (Rb) onboard atomic clocks. Primarily The cesium clock is used as a timing source to control the GPS signal (El-Rabbany, 2002). In addition to these, each satellite has a specific system identification number.

3.2.2 Control Segment

The basic functions of the control segment are frequently controlling and maintaining the status and configuration of the satellite constellation, forecast satellite ephemeris, and satellite clock status, determining and keeping the corresponding GNSS time system, and updating the navigation messages for each satellite continuously (Seeber, 2003; Subirana et al., 2013). It is also used to monitor additional data such as ionosphere parameters and encryption and preventing service from unauthorized users (Hofmann-Wellenhof et al., 2008).

The GPS control segment contains a Master control station (MCS), monitor station (MS), and ground antenna (GA). Figure 4 shows map of control segment of GPS. The master control station is located near Colorado Springs, USA. It is the main part of the control segment. "It is responsible for operating the system and providing command, control, and maintenance services to the space segment" (Seeber, 2003). MCS transmits the predict satellite navigation data, satellite positions as a function of time, satellite clock parameters, atmospheric data, and satellite almanac to the ground antenna. Monitor stations are unmanned operating stations that are located all over the world (in Ascension Island, Cape Canaveral, Diego Garcia, and Kwajalein, Colorado Springs, and Hawaii). MS receives a signal from the satellite and transmitted it into the master control station. MS is equipped with atomic clock standards and GPS receivers. The ground antenna receives a signal from the master control station and transmitted (uplink) to the satellite, via S-band radio signal. Signal uplink to satellite three times per day. GA is located in Ascension Island, Cape Canaveral, Diego Garcia, and Kwajalein, with master stations. The Master Control Station remotely control and operate the monitor stations and ground antennas (Seeber, 2003).

The function of the GLONASS control segment is tracking satellite, clock determination, and forecasting, uplink navigation message to satellites, synchronizing time between satellites, monitoring time offset between GLONASS and UTC (Hofmann-Wellenhof et al., 2008). The GLONASS control station consists System Control Centre (SCC), Command and Tracking Stations, and Central Synchronizer (CC-M). GLONASS ground segment composed of System Control Centre (SCC), Central Synchronizer (CC-M), Telemetry, Tracking and Control (TTandC) stations, Laser Station (LS), Monitoring Stations (MS). The SCC is responsible for all processes and functions at the system level. It processes data from TT and C, which is used to monitor the status of satellite clock and orbit, and to update navigation message (Subirana, Zornoza, and Hernández-Pajares, 2013). The tasks of GBCC are

determination and forecasting of satellite ephemeris, disseminating forecasted ephemeris, correction of clocks and almanac information, Synchronizing time between satellite clocks and GLONASS system, and calculating the offset between GLONASS system time and UTC (Kaplan and Hegarty, 2017).

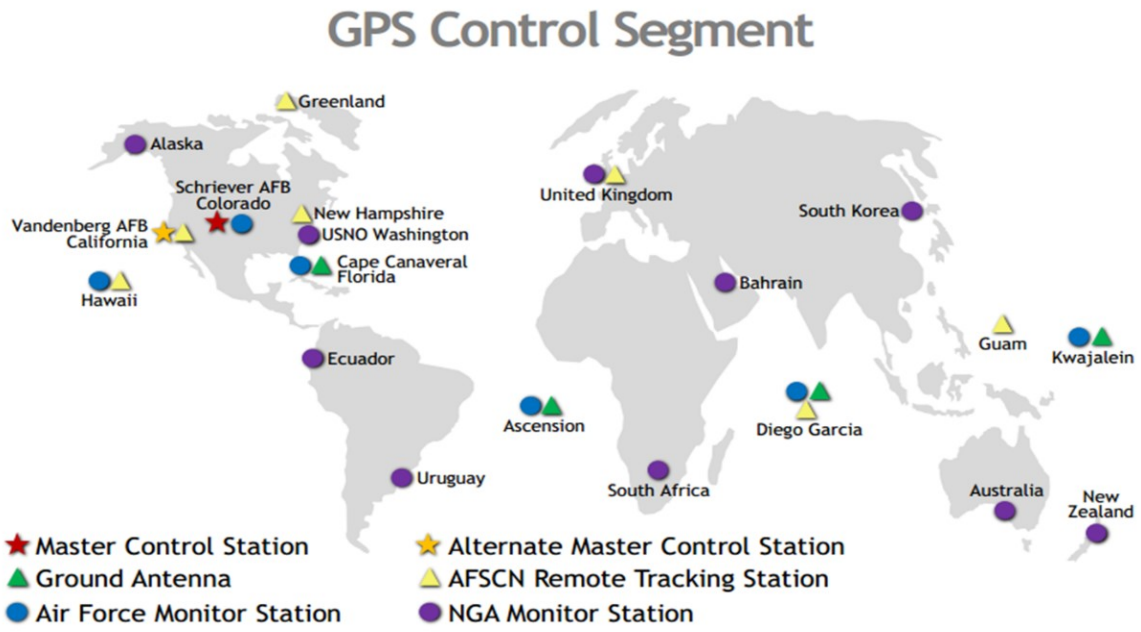

Figure 4 Map of GPS control segment (https://www.gps.gov/systems/gps/control/)

The Galileo control segment consists two parts. These are the Ground Mission Segment (GMS) and the Ground Control Segment (GCS). The ground control segment is composed of two ground control centers (GCC) with five telemetry, tracking, and control (TTandC) stations, nine C-band mission uplink stations (ULS), and about 40 Galileo sensor stations (GSS). GMS composed of Ground Control Centre (GCC), Telemetry, Tracking, and Control (TTandC) stations. GCS contains a worldwide network of Galileo Sensor Stations (GSS) and Mission Uplink Stations (ULS). GMS is responsible for all functions that are used to determine and upload the navigation message to satellite and synchronize information for the transfer of navigation and UTC. For these purposes, it uses globally distributed sensor stations, different facility services, and mission uplink stations (Kaplan and Hegarty, 2017; Subirana et al., 2013). The GCS is responsible for the functionality of each satellite and the sustainability of constellation geometry (Kaplan and Hegarty, 2017).

3.2.3 User Segment

The user segment contains receiver hardware and processing software. The user segment tracks signal downlink from satellite and determines pseudo-range. GNSS receivers track four or more satellites and determine the position, velocity, and time. The user's receiver tracks the broadcasted signal from these four or more satellites and determines the pseudo-range to each satellite and computes the three-dimensional position and time (Parkinson et al., 1996). According to Doberstein (2012), four main processes take place in GPS receiver. The first one is receiving a signal from the satellite. Next identifying the received signal, acquires lock on the signal, and stores the data. Thirdly measure the range from receiver to each tracked satellite. The final step is computing the position of the user from the acquired information. The common functionality of any receiver is tracking visible satellite, computing range from user to satellite, and making Triangulation (Jin et al., 2014).

Currently, a large number of GNSS receiver types, models, and brands are available in the market. The variety of receivers depends on purpose (military or civilian use), cost (from expensive up to cheap), precision (ultra-high precision, high precise or low) and etc. It ranges from inexpensive smartphones and handheld to high expensive ultra-precise surveying receivers. It is also from simple navigation applications up to sophisticated scientific applications. The design of the receiver is taking into consideration, cost, portability, ease in operability, and precision for all users over the globe. The implementation of this was possible because, all the high cost and sophisticated parts such as atomic clock standards are taken care by the control segment or space segment (Madry, 2015).

Generally, all receivers have an antenna with a preamplifier, a radio frequency, a microprocessor, signal tracker and correlating section, oscillator, a feeding source, power supply, memory, data storage, and user interface (Seeber, 2003; Subirana et al., 2013)

3.3 Source of Error

When realizing the general principle of determining position from satellite navigation, it faces various problems. Different studies classified the effects into three groups: those associated with satellite errors, those associated with signal propagation errors, and those associated with receiver errors (El-Rabbany, 2002; Hofmann-Wellenhof et al., 2008; Seeber, 2003). But seeber (2003) reclassified as distance-dependent errors and station dependent errors. In general, the signals in practice propagate through a medium and not through a

vacuum. Moreover, even the atomic clocks in the satellite are drifting through time and the satellite orbits are perturbed by many factors. On the receiver side, there are errors such as problems with the variation in the antenna phase center and clocks are not accurate and they are drifting. In order to get accurate information, it is necessary to model all these errors.

The error related to satellite contains ephemeris or orbital errors and satellite clock errors. The errors related to signal propagation are mainly ionospheric delay and tropospheric delay. The main errors related to the receiver are the receiver's clock errors, multipath error, receiver noise, and antenna phase center variations(El-Rabbany, 2002). The observations are affected by random and systematic errors. "Some errors can be removed, others can be reduced, and others are just neglected" (Strang and Borre, 1997). Identifying and mitigating errors in pseudo-range measurement is crucial for precise positioning both in code and phase measurement. This section will address the main error sources which affect the GNSS measurement.

3.3.1 Clock Error

Time is major information in satellite navigation. The range from satellite to receiver is computed from the measured time. The basic challenge of GPS is to measure time not to measure range, as a result, the entire process and function depend on solving the issue of time (Doberstein, 2012). The precision of time is determined by the stability and accuracy of the clock. Thus the behavior of the clock determines the information derived from it. The failure in synchronizing satellite and receivers clocks enormously affects the measured propagation time of signals (Hern´andez-Pajares, Zornoza, and Subirana, 2005). The primary mission of meaningful GNSS observation is the synchronization of the clock between satellites and a receiver (Xu and Xu, 2016). But both satellite clock and receiver clocks have their own limitations. The modeled behaviors of clocks differ from their behavior during operation. Moreover, both satellite and receiver clock are affected by the relativistic effect.

- **Satellite**

GNSS satellites are equipped with atomic clocks from cesium, rubidium, and hydrogen. Atomic standard clocks are highly stable but not perfect. The GPS satellite clock frequency stability is at 10^{-12} s per day (Strang and Borre, 1997). Thus Satellite clocks are more stable and accurate but they drift slightly. The effect is recognizable on range measurement even if it looks small. For example, 1ns drift of clock results in approximately 30cm error in range

measurements. Satellite clocks are also affected by the relativistic effect, Satellite clock errors are monitored by the GNSS ground segment. The ground control station calculates the amount of drift and uplinks the clock correction to the satellite. The corrections are broadcasted to receivers together with navigation message.

- **Receiver**

To reduce cost and ease of portability, the GNSS receiver uses a quartz crystal clock. But it is less stable than the atomic clock and the accuracy is between 10^{-5} and 10^{-7} (Strang and Borre, 1997), which is smaller than satellite clock accuracy. The instability of the quartz clock unlike the atomic clocks is mostly due to temperature variation, shock, and vibrations (Sickle, 2015). Theoretically, the effect of the receiver clock error can be reduced by either replacing the quartz crystal clocks with atomic clocks or eliminate by putting the receiver clock offset as a fourth unknown parameter in the adjustment of data, in addition to the three-position unknowns. The second method is usually used as the first is not cost-effective and makes the receiver bulky to transport.

3.3.2 Ephemeris

One of the fundamental parameters in GNSS is a satellite location that is orbital information of the satellite. The satellite provides its orbital position to the user through the navigation message. This is important because to determine the user position, it is very important to precisely known the position of the satellite. The orbital information is predicted from previously measured data. The orbital positions of the satellite are tracked and determined by the ground control station. The predicted position is periodically (usually 4 hours) uploaded from the control station and this information is broadcasted to the receiver through a navigation message. The navigation message actually provides the Keplerian parameters of orbit and the receiver uses these Keplerian parameters to derive the location of the satellite.

But the forecasted orbit of satellite location fluctuates with time from the actual position of the satellite as a result of different factors. The error is small at the time of upload and gradually increases until the next upload. The main perturbing forces are earth gravity variation, the attraction of the sun and the moon, and solar radiation pressure (Sickle, 2015). This causes errors in the user's observables.

3.3.3 Atmospheric

An electromagnetic wave passing through a medium can be reflected, diffracted, dispersed, or refracted. Refraction is a directional change of propagated wave when passes from one medium to the other (Hofmann-Wellenhof et al., 2008). Atmospheric refraction is the deviation of electromagnetic propagation within the atmosphere due to the difference in air mass and density (Jin et al., 2014). Electromagnetic waves transmitted in vacuum travel at the speed of light but in actual cases, the medium is not vacuum and it causes the delay or advance in the speed.

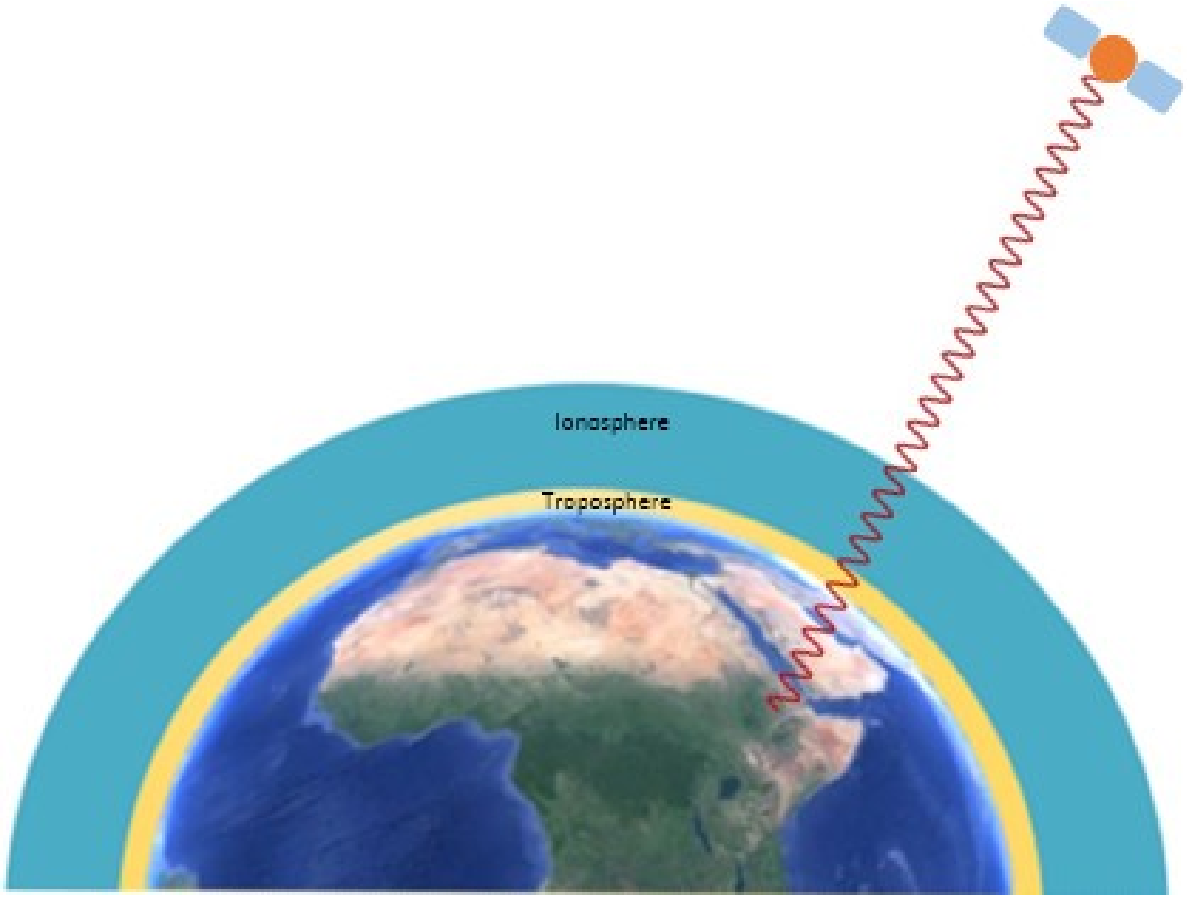

Figure 5 GNSS signal propagation through the Earth's Atmosphere (drawn not to scale)

The broadcasted signal from the satellite is transmitted through a different medium. One of the mediums is the Earth's atmosphere. When a signal travels through the atmosphere it is delayed by the atmosphere and the range measured from satellite to the receiver using the transmitted signal became longer than it usually be if the medium was a vacuum. The amount of delay is dependent on the atmospheric condition, which is spatially, temporally and the

signal traversed elevation angle (Parkinson et al., 1996). Atmospheric error is the delay due to the effect of the medium through which the signal is transmitted.

The Earth's atmosphere is composed of different layers. There are different types of classification of the atmosphere, depending on the study to be conducted. Here the classification based on the electromagnetic structure is used and the atmosphere is classified into the neutral atmosphere (it is composed of troposphere and stratosphere) and ionosphere (Hofmann-Wellenhof et al., 2008). Figure 5 shows the GNSS signal propagation through the atmosphere. The delay of the GNSS signal due to the atmosphere is divided into the ionospheric and tropospheric delay.

- **Ionosphere**

The ionosphere is the region of ionized gases that covers an area from 50km to 1000km or more, above the Earth surface. It is a dispersive medium or the behavior of a propagated signal is frequency-dependent. Hence, the broadcasted signal from the satellite is delayed in case of code measurement and resulted in a false satellite to receiver distance, and computed geometric distance will not be valid. In the case of phase measurement, the transmitted signal from the satellite is advanced and the results distance from the satellite to the receiver is shorter than the true geometric distance.

The magnitude of delay is dependent on the amount of electron content in the atmosphere along the signal passed path. The free electron in the ionosphere affects the propagation of the electromagnetic wave. The delay varies with the function of time and geographical location. El-Rabbany (2002) made four major variability observations. First, in the time of the day, it reaches higher in the early afternoon and a minimum around midnight. Second, in time of the year maxima is observed in winter than summer. Third, in the 11-year solar cycle, electron density levels reach a peak in the solar flare activities known as the solar cycle. Fourthly, with respect to the geographical locations total electron content is minimum in mid-latitude regions and highly irregular in polar and equatorial regions. Solar activity and the geomagnetic field is the main source of fluctuation in the ionospheric effect (Seeber, 2003).

The error of GNSS measurement due to the ionospheric effect ranges from a few meters up to more than 20m (Xu& Xu, 2016). It can also reach 150m under a different condition such as extreme solar activities, at midday, and near the horizon (El-Rabbany, 2002). This effect is easily mitigated by using multiple frequency receivers or by using different modeling processes. Because the ionosphere is dispersive, the delay of the L1 signal is different from

L2 or L5 and L2 is different from L5. In the case of a short baseline, we can also remove error duo to ionospheric effect by using differential GPS method. This is based on the assumption that within a small area the behavior ionosphere is not that much variable.

- **Troposphere**

The troposphere is the lower part of the atmosphere up to 50km from the surface of the Earth. For frequencies up to 30 GHz, the troposphere is a non-dispersive medium (Hofmann-Wellenhof et al., 2008) and we cannot remove the error due to the troposphere using multiple frequency receivers. Both code and carrier phase measurements are delayed by tropospheric effects. The error from tropospheric delay is mitigated through the usage of different models. In order to get a high accuracy position and time, one needs to model and remove the effect of a tropospheric delay from observables.

The effect depends on the temperature, pressure, and humidity of the atmosphere. The tropospheric delay can be divided into a dry and wet component. The dry component contributes 90% of the error and it depends on temperature and pressure. The wet component contributes about 10% of the error the tropospheric delay error budget, and it mainly depends on the water vapor distribution in the atmosphere. The amount of error due to the troposphere is 2.3m in the zenith direction and more than 20 m at elevation angles below 10 deg. The delay of signal is minimum when the satellite at the zenith and it reaches a maximum when the satellite near to the horizon. At an elevation angle of 90° and at sea level, the delay will be about 2.4 m, but it increases up to 9.3 m at 75° and reaches 20 m at a 10° elevation angle(Sickle, 2015).

3.3.4 Multipath

Multipath occurs when the antenna receives the same signal in a different path and at a different time in addition to direct signal from the satellite. This is the effect due to reflecting surface either artificial (building, vehicle, fence, road) or natural (water body, soil, tree) nearby the antenna. Since the reflected signal travels in a different direction from the true signal, the range is longer than the geometric distance from the satellite to receivers. The effect of multipath differs based on the location of the receiver relative to the reflecting surface, satellite elevation angle, the receiver's software, antenna gain pattern, and signal properties (Kaplan & Hegarty, 2017).

It affects both code and phase measurement but the magnitude of influence is different because the multipath effect is frequency-dependent (Hofmann-Wellenhof et al., 2008). The effect is different in magnitude in P-code and Corse Acquisition (C/A) code. The error of multipath might reach 15cm in p-code and 150m in C /A code measurements (Xu& Xu, 2016). Multipath is one of the major sources of error in GNSS observable and it needs to be eliminated in order to get a higher level of accuracy. The multipath effect can be reduced by observing for a long period of time (Seeber, 2003) of using a high-end geodetic antenna. A few Solutions to reduce the multipath effects are:

- Antenna selection

The architecture of the receiver antenna plays a great role in detecting or overcoming the multipath effects. For example, the usage of a chock ring antenna reduces the effect of multipath by attenuating the reflected signal from a low elevation angle. In addition, multipath can be eliminated by using an antenna with signal polarization, because the signal from GNSS is right-handed polarized but the signal from the reflected object is left-handed polarized(Hofmann-Wellenhof et al., 2008). But the disadvantage of this antenna is when the signal is reflected twice from a different surface (El-Rabbany, 2002).

- Site selection

Multipath is a local effect because it depends only on the surrounding situation of the receivers (Xu& Xu, 2016). Thus, to avoid the influence of multipath one needs to select a site, with great attention and placing the antenna away from any reflective surfaces.

- Elevation angle restriction

Most of the time the signal exposed to multipath is from low elevation angles. The most applicable solution is the usage of a cutoff or masking angle of 15° (Sickle, 2015).

- Phase measurement

Because the carrier phase measurement is less affected relative to the code measurement, Xu and Xu, (2016) recommended the usage of phase measurement only, as one of the reducing methods for the multipath effect.

In addition to major sources of error, others such as receiver measurement noise, earth tide (which is due to the gravitational attracting force of the moon and the sun) and oceanic loading, antenna phase center, relativistic effect, and satellite geometry contribute to the reduction of the accuracy of positioning using GNSS. In GNSS measurement the quality of

the range measurements and the quality of the satellite geometry are the two main factors for positional accuracy (Kaplan & Hegarty, 2017).

3.4 Principle of GNSS

The determination of position, velocity, and time needs the understanding of GNSS signal and range measurement principles. As discussed in the previous sections the main tasks of GNSS are providing position, time, and velocity information. In order to get these observables, GNSS uses trilateration principles. The user's unknown position is determined by measuring the distance to the Satellite which has a known position. The user segment uses either code or phase to measure the distance from the receiver to the satellite. By using autocorrelation between the signal generated from the satellite and the replica signal generated in receive the time delay is computed. From the time delay, the pseudo-range between the user's receiver and the satellite is determined. To do this one needs a minimum of four satellites, three for position coordinate, and one for the determination of the receiver clock offset. The satellite ephemeris and time information are broadcasted by each satellite through with the navigation message. In addition, other necessary information is incorporated into the navigation message.

3.5 GNSS Signal

GNSS carrier signals have dual functions. It serves as a means to determine ranges to satellites and as an information carrier. The information from the satellite to the user is transmitted using the GNSS carrier signals.

Pseudorandom Code

Basically, PNR codes transmitted from satellites are two, which are Corse Acquisition (C/A) code and Precision (P) code. They are differ in precision, cheap rate, wavelength, sequence, repeating time, accessibility, and position service. Each code contains bits or chips that are binary digits (zeros and ones).

- ***C/A code***

The C/A code is 1,023 binary digits long and it repeats every millisecond. The chip rate is 1.023 MHz. Each satellite has a unique C/A-code that is used by the receiver to easily identify the satellite.

- ***P-code***

P-code is ten times faster than the C/A- code. That means the chipping rate is 10.23MHz. It repeats itself after 266 days. The length of the sequence is seven days. The 266-day long code is divided into 38 segments result 1 week long and 32 segments are assigned to the different GPS satellites the remaining six segments are kept for other purposes (El-Rabbany, 2002). Every satellite is assigned one weak segment of P-code which is re-initialized each weak Saturday/Sunday midnight (Kleusberg & Teunissen, 1996). P-code is more precise than C/A-code.

- ***Navigation Message***

In addition to C/A- code and P-code satellite also transmit navigation message to the receiver. The information packed on navigation message includes the health of the satellite, orbital parameters, correction parameters of satellite clock, ionospheric corrections, satellite almanac, and time transfer to Coordinated Universal Time (UTC). The information is arranged in five sub-frames and transmitted at a rate of 50 bps. As discussed by Benedetto et al. (2007) navigation message sub-frame 1 contain satellite clock and health data, Sub-frames 2 and 3 contain the satellite ephemeris data, and Sub-frames 4 and 5 contain almanac data. In addition sub-frames 4 and 5 include various data such as; UTC parameters, health indicators, and ionospheric parameters.

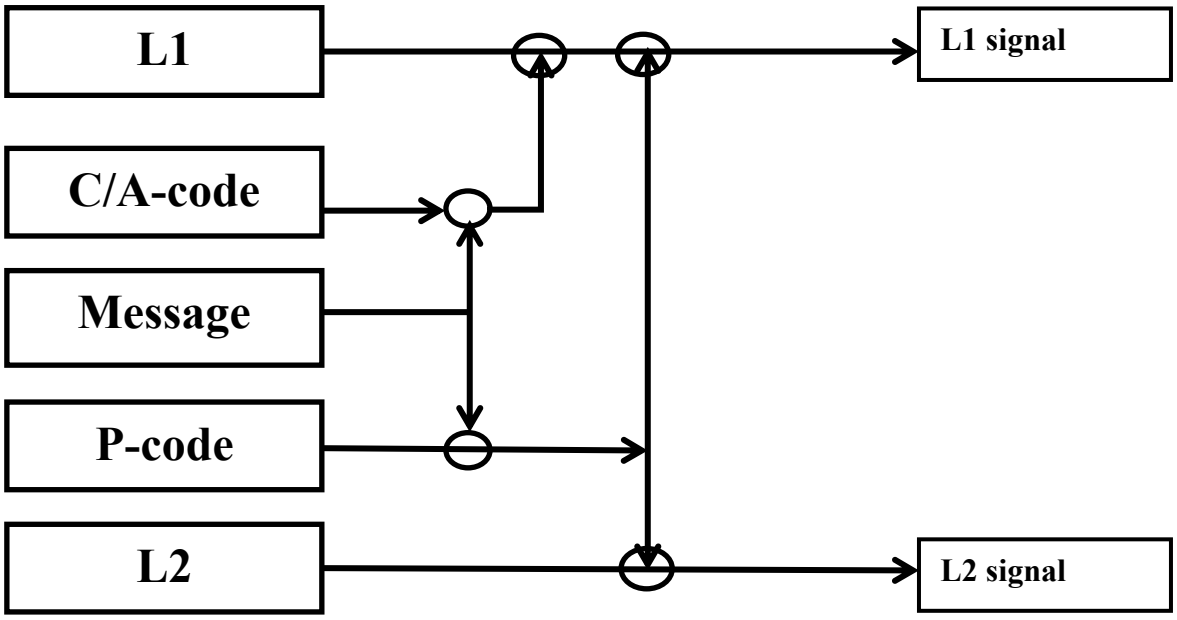

Figure 6 GPS Signal Structure

According to Kaplan and Hegarty (2017), almost all GNSS signals currently use carrier frequencies in the L-band in the range 1 to 2 GHz. The fundamental frequency generated from precise atomic clocks, onboard the GPS satellites, L-band frequency are generated (Awange, 2018). The fundamental frequency is 10.23MHz and all the other signals are generated by multiplying or dividing these frequency. L1 which has a frequency of 1,575.42 MHz is generated by multiplying the fundamental frequency by and has a wavelength of 19cm. Similarly, the L2 frequency which is 1127.60 MHz is derived by multiplying the fundamental frequency by 120 and it has a wavelength of 24.4cm. The L5 signal with a frequency of 1176.45 MHz is derived by multiplying the fundamental frequency by 115. GPS satellite broadcast PRN code and navigation message, they are modulated with the carrier signal. Figure 6 shows the signal structure. The phase modulation is used to modulate the codes and messages with the carrier signal. In L1 carrier frequency, both C/A-code and P-code are modulated. In the case of L2 carrier frequency, only P-code is modulated.

3.6 Observables

Observation of range between satellite and receiver is computed from either code or carrier phase measurement. From the basic physics principle, distance is the product of velocity and time.

$$D = v \cdot t \tag{3.1}$$

Then the general observation equation to determine position of user (X_r, Y_r, Z_r) from the known position of the satellite(X, Y, Z), will be as follow:

$$R = c * \tau + \varepsilon \tag{3.2}$$

$$R = \rho + c * d\tau + \varepsilon \tag{3.3}$$

$$\rho_1 = \sqrt{(X_1 + X_r)^2 + (Y_1 - Y_r)^2 + (Z_1 - Z_r)^2}$$

$$\rho_2 = \sqrt{(X_2 + X_r)^2 + (Y_2 - Y_r)^2 + (Z_2 - Z_r)^2}$$

$$\rho_3 = \sqrt{(X_3 + X_r)^2 + (Y_3 - Y_r)^2 + (Z_3 - Z_r)^2}$$

$$\rho_4 = \sqrt{(X_4 + X_r)^2 + (Y_4 - Y_r)^2 + (Z_4 - Z_r)^2}$$

Where

R = the pseudo-range, which is the measured distance between the satellite and the receiver which is the function of many errors.

c = the speed of light

τ = the time it takes for the signal to travel from the satellite to the receiver

ρ = the true distance between the satellite and the receiver

$d\tau$ = mainly the receiver clock error

ε = All other sources of errors such as ionospheric, tropospheric, multipath, satellite clock error and etc.

The aim then will be to determine ρ from the measured R by removing all errors. In this, there are four unknowns, namely X_r, Y_r, Z_r, and $d\tau$ that need to be determined, and a minimum of four equations are needed and hence four pseudo-ranges to four satellites. This is true if we assume that the other sources of errors are already removed. To get information about R there are two approaches that are used in GPS data processing. These are the code and phase measurement.

- ***Code Measurement***

In the code measurement, the user segment uses either the C/A code or P-code to determine the time it takes for the signal to travel between the satellite and the receiver. Though it is straight forward, the code measurement delivers low accurate pseudo-range, but absolute or unambiguous. The pseudo-range equation can be written as follows:

$$P_r^s = \rho_r^s + C * \delta^s + C * \delta_r + I_r^s + T_r^s + M_r^S \quad (3.4)$$

Where P_r^s: Pseudorange due to code measurement

ρ_r^s: Geometrics Distance

C : Speed of light

δ^s : Satellite Clock Error

δ_r : Receiver Clock Error

I_r^s : Ionospheric Error

T_r^s : Tropospheric Error

M_r^S: Multiphase Error

- ***Phase Measurement***

In case of phase measurement, the user segment determines their positions by computing the phase difference between signals generated from the satellite and the replica signal generated in the receiver. Phase measurement uses L1, L2, or L5 signals in GPS. This method is more precise than code measurement; we can get up to millimeter level accuracy. The major challenge of phase measurement is ambiguity.

$$\varphi = \rho_r^s * \frac{1}{f} + f * \delta^s + f * \delta_r + I_r^s + T_r^s + M_r^S + N_r^s \quad (3.5)$$

Where φ: Pseudorange due to phase measurement

ρ_r^s: Geometrics Distance

f : Carrier Frequency

δ^s : Satellite Clock Error

δ_r : Receiver Clock Error

I_r^s : Ionospheric Error

T_r^s : Tropospheric Error

M_r^S: Multiphase Error

N_r^s : Integer Ambiguity

3.7 Atmospheric delay

As discussed above GNSS signal travel from the satellite to the user through the atmosphere. The atmospheric medium affects the GNSS signal either by advancing or by delaying signal traveling time. Majorly, the effects are divided into the ionospheric and tropospheric delay.

As the current research topic is focused on events that are primarily and directly affecting the troposphere and as a consequence the propagation of GNSS signal in the troposphere, the focus is given to this part of the atmosphere in this section. Tropospheric delay is a delay of the GNSS signal as it passes through the neutral atmosphere. Atmospheric pressure, temperature, humidity, and moisture content are the main factors that are used to define changes in the neutral atmosphere. The delay due to the atmospheric refractivity is lengthening the geometric path of the propagated signal (Liu et al. 2019). The refractive index of an electromagnetic wave can be expressed as (Jin et al. 2007):

$$n = \frac{c}{v} \quad (3.6)$$

Where n: index of a refractive substance,

c: speed of an electromagnetic wave in vacuum

v : speed electromagnetic wave in atmosphere medium.

When electromagnetic waves travel in a vacuum the speed of an electromagnetic wave is c and in the atmosphere, the speed changed in to$v$. Instead of n tropospheric refractivity is mostly expressed by using N (Böhm& Schuh, 2013):

$$N = 10^6 (n - 1) \quad (3.7)$$

N is tropospheric index and it can be divided in wet and dry:

$$N = N_w + N_d$$

Due to atmospheric pressure variation, the Zenith Tropospheric Delay (ZTD) decreases with the increase in altitude.

The ZTD is the integrated refractivity along a vertical path through the neutral atmosphere (Jin, 2012) and it can be expressed using:

$$ZTD = c * \tau_T$$

$$ZTD = \int_0^\infty N(s)\, ds \quad (3.8)$$

Where, τ_T is the time delay in the troposphere. N is mainly related to meteorological variables as stated in Liu et al. (2019) and other literature therein (Davis et al. 1985) and it can be determined from:

$$N = k_1\rho + k_2 \frac{P_w}{Z_w T} + k_3 \frac{P_w}{Z_w T^2} \quad (3.9)$$

where k_i (i=1, 2, 3) are constants, ρ is the total mass density of the atmosphere, $P_w$is the partial pressure of water vapor, $Z_w$is a compressibility factor near unity accounting for the small departures of moist air from an ideal gas, and T is the temperature in degrees Kelvin.

Refractivity N can be divided in to dry and wet components:

$$N_d = k_1\rho \quad (3.10)$$

$$N_w = k_2 \frac{P_w}{Z_w T} + k_3 \frac{P_w}{Z_w T^2} \quad (3.11)$$

The dry component only depends on the total density of air and the wet component depends on the partial pressure of water vapor and the temperature. From the above equation, ZTD can be expressed in ZHD and ZWD:

$$ZTD = ZHD + ZWD \quad (3.12)$$

$$ZHD = \int_0^\infty (k_1 \rho) ds \quad (3.13)$$

$$ZWD = \int_0^\infty \left(k_2 \frac{P_w}{Z_w T} + k_3 \frac{P_w}{Z_w T^2} \right) ds \quad (3.14)$$

By using mapping function GNSS is widely used to determine the ZTD (Jin et al., 2014). Therefore, the ZTD in the direction of zenith can be derived from the mapping function related to the satellite zenith angle E (Jin et al., 2014):

$$ZTD = ZHD \cdot m_h(E) + ZWD \cdot m_w(E) \quad (3.15)$$

where E is satellite elevation angle, $m_h$is hydrostatic mapping function and m_w is a wet (non-hydrostatic) mapping function.

According to Jin et al. (2014), a number of mapping functions have been developed by geodesists and meteorologists for the past 30 years or more. Herring Mapping Function developed by Marini and Herring, Niell Mapping Function developed by Niell, Vienna Mapping Functions 1 (VMF1) and Global Mapping Function are some of those functions listed by Jin et al., Niell Mapping Function is commonly used one (LEICK, RAPOPORT, and TATARNIKOV, 2015).

CHAPTER 4 METHOD AND MATERIALS

The methods used to assess the impact of urbanization on GNSS signal propagation is mainly making use of correlation analysis of remotely sensed data from different sources and GNSS data from the IGS station ADIS. In this chapter, the data used in the study, and the respective method of data processing and analysis will be discussed.

4.1 Data

In order to achieve the objective of the study, different data was used for this study. The Landsat, MODIS, and IGS data are the main sources of information for this research. Landsat data were used to study the urban expansion of Addis Ababa city. Two sets of information were taken from MODIS to study vegetation cover change and land surface temperature. IGS data were used to compute positional information of the ADIS station. These sources of data are discussed in the next subsections.

4.1.1 Landsat Data

Landsat, the former Earth Resource Satellite Technology (ERST) is designed to study the Earth's surface. Since 1972 Landsat satellite continuously provides information about the changes occurring on the Earth's surface in a multispectral image (USGS, 2019b). It delivers moderate-resolution multispectral data of the Earth's surface at a global scale. The system is run by NASA, NOAA, and the US Geological Survey. Landsat satellite uses circular, near-polar sun-synchronized, orbit with an altitude of 920km for Landsat 1, 2, and 3. Other Landsat have an altitude of 705 km. Through time Landsat uses different sensors, such as Multispectral Scanner System (MSS) for Landsat 1-5, the Thematic Mapper (TM) for Landsat 4 and 5, the Enhanced Thematic Mapper Plus (ETM+) for Landsat 7, and Operational Land Imager (OLI)/ Thermal Infrared Sensor(TIRS) for Landsat 8. Landsat 5, 7, and 8 passes the same point on Earth every 16 days. But Landsat 1, 2, and 3 passes the same point on Earth every 18 days. Landsat have a wide range of applications such as global change research, agriculture, forestry, geology, land cover mapping, resource management, water, and coastal studies, deforestation research, volcanic flow studies, and understanding the effects of natural disasters, oil spills, and monitoring mine waste pollution(USGS, 2019b). Information emanating from these satellites is widely used by different stakeholders such as agribusiness, global change researchers, academia, state and local governments, commercial

users, national security agencies, the international community, decision-makers, and the wider public (USGS, 2019a).

Landsat 5 satellite is launched in 1984 and used for collecting information about the Earth's surface. It uses a Multispectral Scanner System (MSS) and Thematic Mapper (TM) sensor. Multispectral Scanner System (MSS) sensor has four bands with a spatial resolution of 79m. Thematic Mapper sensor uses seven bands. Visible, near-infrared, and shortwave infrared bands have 30m spatial resolution, and the remaining thermal infrared band with a spatial resolution of 120 m.

Landsat 7 satellite is launched in 1999 and the primary mission was to provide timely and high-quality, visible, infrared, and thermal-wavelength data of all land and near-coastal areas on Earth (USGS, 2019a). It uses Enhanced Thematic Mapper Plus (ETM+) sensor for data acquisition. ETM+ has eight bands which include visible, near-infrared, and shortwave infrared, thermal and panchromatic bands. The spatial resolutions of visible, near-infrared, and shortwave infrared are 30m. Thermal and panchromatic bands are 60m and 15m spatial resolution respectively.

Landsat 8 satellite was launched in 2003. The mission of Landsat 8 is primarily to provide a timely high-quality visible and infrared images of all landmass and near-coastal areas on the Earth, by continually refreshing an existing Landsat database(USGS, 2019b). Landsat satellite Operational Land Imager (OLI) and the Thermal Infrared Sensor (TIRS) sensor are used to achieve the goal of the mission. Operational Land Imager uses nine bands that are visible, near-infrared, and shortwave infrared bands with 30m spatial resolution and panchromatic bands with 15m spatial resolution. Thermal Infrared Sensor uses two thermal bands with a spatial resolution of 100m.

In this study, Landsat 5 TM, Landsat 7 ETM+, and Landsat 8 OLI product were used to study the urban physical expansion of Addis Ababa city, from 1989 to 2019. In addition to the automatic extraction of vegetation index, the built-up index is also generated from Landsat image since 2000.

4.1.2 MODIS Data

Landsat has a good spatial resolution to measure land cover change. However, it has a limitation on temporal resolution and highly affected by clouds. Moderate Resolution Imaging Spectroradiometer (MODIS) sensors enable measuring of surface change by providing daily worldwide observation (Weng, 2011). One of the qualities of the MODIS sensor is a consideration of the former earth observing satellite essential properties. A different important characteristic of CZCS, AVHRR, HIRS, and Landsat Thematic mapper was incorporated in the MODIS sensors (Qu et al., 2006).

Moderate Resolution Imaging Spectroradiometer has two missions, which are Terra and Aqua missions. Formerly Terra and Aqua satellites were named as EOS AM-1 and EOS PM-1. The difference between Terra and Aqua is the orbiting direction and Equator passing time. They are also different launching time. According to this, Terra goes from north to south and passes the equator in the morning. On the other hand, Aqua satellite follows south to north direction and passes over the equator in the afternoon (https://modis.gsfc.nasa.gov). Terra satellite was launched in December 1999 and the aqua satellite was launched, following the Terra satellite in May 2002. The data acquisition of Terra and Aqua began in February 2000 and July 2002 respectively (https://pubs.usgs.gov).

The MODIS sensors orbit the Earth at an altitude of about 705km with swath dimensions in cross-track 2330 km and in along-track 10 km at nadir. It provides global data with a high temporal resolution, which covers the whole Earth in 1 to 2 days. The spatial resolution covers the range from 250m to 1000m with 34 spectral bands. Band 1 and 2 have 250m spatial resolution, band 3 to 7 contain 500m spatial resolution, and band 8 to 36 have 1000m spatial resolution. The whole bandwidth covers the range from 0.4µm to 14.4µm wavelength.

MODIS data will improve our insight about the Earth's surface variability at a larger scale and process global changes, such as in oceanography, biology, and the atmosphere(Gao, 2009). The application area of MODIS is multidisciplinary, relative to other Earth observation satellites. It ranges from the study of the Earth's surface to the atmosphere globally, regionally, and locally (Gao, 2009). From those vast application areas and data sources of MODIS, in this study vegetation index and land surface temperature were used to study urban vegetation cover and land surface temperature of Addis Ababa city, from 2000 to 2019.

4.1.2.1 Vegetation Data

The vegetation index is one of the MODIS data, which is used to study vegetation covers. It empirically measures vegetation coverage at the land surface. The knowledge of how vegetation is distributed globally, in terms of biophysical and structural characteristics as well as spatial and temporal variation helps to understand the role of vegetation on how the Earth functions as a system (Solano et al., 2010). The vegetation index is computed from the atmosphere corrected bidirectional surface reflectance of the earth. In this study, the Terra Moderate Resolution Imaging Spectroradiometer (MODIS) Vegetation Indices (MOD13Q1) was used. Terra vegetation index has two vegetation indexes. These are the Normalized Difference Vegetation Index (NDVI) and Enhanced Vegetation Index (EVI). Both are generated from atmospherically corrected blue, red, and near-infrared bands (https://lpdaac.usgs.gov). The Terra vegetation indexes (used in this study) fly over the same track every 16 days with a spatial resolution of 250m in the Hierarchical Data Format (HDF). The scientific data set of the HDF file contains different bands. The detail information are described in Table (4.1). The MOD13Q1 data used in this study include those since 2000 for Addis Ababa, Ethiopia.

4.1.2.2 Land Surface Temperature Data

The other MODIS data used in this study is land surface temperate. Land surface temperature is one important measure of surface energy (Assiri, 2017). It measures how hot the surface of the Earth is at a particular location. MODIS provides land surface temperature daily in global coverage. "MODIS LST is derived from the thermal infrared signal, received by the sensor, that is a combination of radiant temperature of the land surface and the prevailing atmosphere" (Assiri, 2017).

In this study, MODIS land surface temperature and emissivity MOD11A1 Version 6 product was used. MOD11A1 provides a daily product with a 1 km spatial resolution. The data uses the Hierarchical Data Format (HDF). The HDF file contains different bands and some of the detail descriptions of the bands are shown in Table (4.2). The MOD11A1 data used in this study include those from 2000 to 2019 for Addis Ababa, Ethiopia.

Table 4-1 Different bands of NDVI data set (https://lpdaac.usgs.gov)

SDS Name	Description	Units	Data Type	Fill Value	Valid Range	Scale Factor
250m 16 days NDVI	16 day NDVI	NDVI	16-bit signed integer	-3000	-2000 to 10000	0.0001
250m 16 days EVI	16 day EVI	EVI	16-bit signed integer	-3000	-2000 to 10000	0.0001
250m 16 days VI Quality	VI quality indicators	Bit Field	16-bit unsigned integer	65535	0 to 65534	N/A
250m 16 days red reflectance	Surface Reflectance Band 1	N/A	16-bit signed integer	-1000	0 to 10000	0.0001
250m 16 days NIR reflectance	Surface Reflectance Band 2	N/A	16-bit signed integer	-1000	0 to 10000	0.0001
250m 16 days blue reflectance	Surface Reflectance Band 3	N/A	16-bit signed integer	-1000	0 to 10000	0.0001
250m 16 days MIR reflectance	Surface Reflectance Band 7	N/A	16-bit signed integer	-1000	0 to 10000	0.0001
250m 16 days view zenith angle	View zenith angle of VI Pixel	Degree	16-bit signed integer	-10000	0 to 18000	0.01
250m 16 days sun zenith angle	Sun zenith angle of VI pixel	Degree	16-bit signed integer	-10000	0 to 18000	0.01
250m 16 days relative azimuth angle	Relative azimuth angle of VI pixel	Degree	16-bit signed integer	-4000	-18000 to 18000	0.01
250m 16 days composite day of the year	Day of year VI pixel	Julian day	16-bit signed integer	-1	1 to 366	N/A
250m 16 days pixel reliability	Quality reliability of VI pixel	Rank	8-bit signed integer	-1	0 to 3	N/A

Table 4-2 Different bands of LST data set (https://lpdaac.usgs.gov)

SDS[1] Name	Description	Units	Data Type	Fill Value	Valid Range	Scale Factor	Additional Offset
LST_Day_1km	Daytime Land Surface Temperature	Kelvin	16-bit unsigned integer	0	7500 to 65535	0.02	N/A
QC_Day	Daytime LST Quality Indicators	Bit Field	8-bit unsigned integer	N/A	0 to 255	N/A	N/A
Day_view_time	Local time of day observation	Hours	8-bit unsigned integer	255	0 to 240	0.1	N/A
Day_view_angl	View zenith angle of day observation	Degree	8-bit unsigned integer	255	0 to 130	N/A	-65
Emis_31	Band 31 emissivity	N/A	8-bit unsigned integer	0	1 to 255	0.002	0.49
Emis_32	Band 32 emissivity	N/A	8-bit unsigned integer	0	1 to 255	0.002	0.49
Clear_day_cov	Day clear-sky coverage	N/A	16-bit unsigned integer	0	1 to 65535	0.0005	N/A

4.1.3 GNSS Data

GNSS is not only about position determination. Currently, it has a wide area of application starting from those that utilize low navigation accuracy to those in the scientific world, with demand for higher accuracy. In those areas of application that demand very high accuracy, it is common to use a differential approach in the data processing. This on the other hand demands the availability of reference stations. The quality of data processed using a differential approach, demands for an accurate data from the reference station. The International GNSS Service is one of the pioneering organizations, which stands to fulfill this mission of quality reference data.

[1] Scientific data sets

Table 4-3 Description of IGS stations

Sites	Network (s)	Latitude	Longitude	Height (m)	Satellite System
ADIS00ETH	IGS	9.035134	38.766301	2439.154	GPS+GLO
HERS00GBR	IGS	50.8673	0.3362	76.5	GPS+GLO+GAL+BDS +QZSS+ IRNSS+SBAS
HYDE00IND	IGS	17.417256	78.550867	441.68	GPS+GLO
MAL200KEN	IGS	-2.996	40.194	-20.4	GPS+GLO+GAL+BDS+ SBAS
MAS100ESP	IGS	27.7637	-15.6333	197.3	GPS+GLO+GAL+BDS+ SBAS
MBAR00UGA	IGS	-0.601469	30.737876	1337.653	GPS+GLO+GAL+BDS+ IRNSS
NKLG00GAB	IGS	0.353908	9.672126	31.496	GPS+GLO+GAL+BDS+ SBAS
NOT100ITA	IGS	36.876108	14.989808	126.2	GPS+GLO+GAL+BDS+ SBAS
RAMO00ISR	IGS	30.597758	34.763139	893.1	GPS+GLO
REUN00REU	IGS	-21.208333	55.571667	1558.4	GPS+GLO+GAL+BDS+ SBAS
TEHN00IRN	IGS	35.697281	51.334092	1194.57	GPS+GLO
YIBL00OMN	IGS	22.186458	56.112333	95.1	GPS

International GNSS Service (IGS) is established in 1992, with the mission to openly deliver the highest-quality GNSS data, products, and services in support of the terrestrial reference frame, Earth observation, and research (http://www.igs.org/about). Since its establishment, IGS provides globally high-quality data for education, community service as well as commercial uses. IGS is committed to supporting science and society by delivering high precision GNSS data (Johnston, Riddell, & Hausler, 2017). The objective of IGS is to helps

"advance scientific understanding of the Earth system components and their interactions, as well as to facilitate other applications benefiting society" (Dow & Neilan, 1994).

ADIS is one member station of the IGS network, which is run by the Institute of Geophysics, Space Science and Astronomy of Addis Ababa University. Since 2007 ADIS station played its role by providing continuous data with 30 second temporal resolution. It is located in Addis Ababa, Ethiopia. In this work, the data from ADIS is used to analyze the effect of urbanization and the associated climate change on the GNSS signal. In addition to ADIS other 11 IGS stations (HERS, HYDE, MAL2, MAS1, NKLG, NOT1, RAMO, REUN, TEHN, and YIBL) data were used during the processing according to the requirement of processing software. The detail information of IGS stations that were used in this study is discussed in Table (4.3). Even though GNSS data for ADIS is available from July 2007 onward, the data from 2008 to 2019 is used in this research to avoid any interference from monument settlement, which is common to see at an early stage of any station. This precaution is made as the final change in station coordinate is expected to be in millimeters. In total 11 IGS stations are used as a reference to compute the daily solution for ADIS. All the required information for data analysis was downloaded from the IGS sites.

4.2 Material

To process and analyses the data, different software were used. The main programs that were used for data processing were GAMIT/GLOBK, ERDAS IMAGINE, ArcGIS, and Python (in addition to other python modulus PyModis was used for MODIS data analysis).

GAMIT/GLOBK

GAMIT/ GLOBK software was used to analyze GNSS data. This program is developed by members of the Massachusetts Institute of Technology(MIT), the Harvard-Smithsonian Center for Astrophysics (CfA), and the Scripps Institution of Oceanography (SIO) (Herring et al., 2010). GAMIT determines three-dimensional relative position and velocity of ground stations and satellite orbit, atmospheric delay, and Earth orientation parameters by using the GNSS broadcast carrier phase and pseudo-range observables (T. Herring et al., 2010). In addition to that GAMIT output, which is the station velocity can also be used to study post-seismic deformation. The software is mainly designed to run under any UNIX operating system but currently, it also supports other operating systems. In order to compute these parameters, GAMIT applies a weighted least squares algorithm(Herring et al., 2010). It

incorporates varies packages, such as those that can be used to prepare the data for processing (makexp and makex), generating reference orbit and rotation values for the satellites (arc, yawtab), interpolating time and location specific values of atmospheric and loading models (grdtab), computing residual observations (O-C's), partial derivatives from a geometrical model (model), detecting outliers or breaks in the data (autcln), performing the least-squares analysis (solve), for modeling, editing, and estimation(fixdrv) and etc. (T. Herring et al., 2010). These packages are run either separately or through batch files or shell scripts.

GLOBK, a program which among others uses the Kalman filter has a basic purpose of combining various geodetic solutions such as GNSS, VLBI, and SLR experiments. It estimates the covariance matrices for station coordinates, earth-orientation parameters, orbital parameters, and source positions generated from the analysis of the primary observations by using data, or "quasi-observations" (http://geoweb.mit.edu/gg/).

The processed data by using GAMIT is transferred into GLOBK to estimate station positions, velocities, orbital and Earth-rotation parameters that are beyond one year duration. The output of GAMIT which is H-file is used as input for GLOBK. The basic tasks of GLOBK are generating reference orbits for the satellites, computing residual observations and partial derivatives from a geometrical model, detecting outliers or breaks in the data, and performing a least-squares analysis (Herring et al., 2010). In general, GLOBK can be used for the following purposes (Herring et al., 2010):

- To combine individual sessions of observations to obtain the average estimate of station coordinates.
- To combine the estimated mean station coordinates from a different experiment, using different methods from several years of observations, to estimate station velocities.
- To independently calculate coordinates from individual sessions to generate time series of locations with their precision over days and years.

Both GAMIT and GLOBK have program packages and the different program packages can be run separately or by making use of batch files.

The whole workflow of GAMIT and GLOBK can be accomplished using sh_gamit and sh_glred (T. Herring et al., 2010), which are shell scripts used to run many other programs of the package. Sh_gamit uses raw data (RINEX) and estimates coordinates for each day with sky plots and generates H-file which is input for sh_glred. Sh_glred is used to determine time

series and station velocity, which can then be plotted and examined for outliers and the appropriate scaling to obtain reasonable uncertainties (Herring et al., 2015).

Other Software

In addition to GAMIT/GLOBK software different software are used in this study. GAMIT/GLOBK is mainly used to generate a daily solution of stations for the period 2008 to 2019. Urbanization and related issues are analyzed using ArcGIS, ERDAS IMAGINE, and python. MATLAB was used to carry out the correlation analysis of the outputs generated from the other software. In this sub-section, a short discussion will be made on how ArcGIS, python, ERDAS IMAGINE, and MATLAB are used for the purpose.

ArcGIS is GIS software developed by ESRI (Environmental Systems Research Institute) which is used to create process, analyze and share spatial data. It supports both vector and raster data. ERDAS IMAGINE is a software package that is used to analyze images that support users to process geospatial based and other rasters as well as vector data. It can also use to process different data from different sources such as hyperspectral imagery and LiDAR data from various sensors (https://www.dataone.org/software-tools/erdas-imagine). Python is “an interpreted, object-oriented, high-level programming language with dynamic semantics” (https://www.python.org). It supports modules and packages. In this study, Python is used in two modes. One is as an extension of ArcGIS which is an arcpy module and independently used for the time-series data processing. pyMODIS module of python is used specifically for MODIS data. pyModis is a Free and Open Source Python-based library to work with MODIS data. It offers bulk-download for user-selected time ranges, mosaicking of MODIS tiles, and the reprojection from Sinusoidal to other projections, convert HDF format to other formats, and the extraction of data quality information (Delucchi, 2017). Matrix Laboratory (MATLAB) is a high-performance language software package. In MATLAB computation, visualization, and programming working environments are integrated into one for data processing, analysis, and visualization. The summary of all software used in this study with their functions is given in Table (3.4).

Table 4-4 software used for the processing and analysis of data

Software	**Function**
GAMIT/GLOBK	To Process GPS data
ERDAS IMAGIN	To generate Land cover change
ArcGIS	To process MODIS data
Python	To process MODIS data
MATLAB	To analyses the results

4.3 Methods

General Work Flow of the Study

To study urbanization and associate climate change effects on the Global Navigation Satellite System signal different data and data analysis tools were used. The urban expansion is measured using information derived from the Landsat image. The NDVI and LST information are generated from MODIS data. GPS time series data for ADIS station is derived from IGS data. Data emanating from these sources are then processed using the software in section (4.2) and the relational analysis of the four outputs is computed. In order to achieve the objective of the study the following general workflow was used. The flow chart shows the general workflow of the study.

Data Processing

The main goal of the GNSS data processing in this study is to determine the average daily position of the station ADIS. To achieve this first the raw observation and broadcast ephemeris data that are in RINEX format are downloaded and archived in the experiment directory. Then the precise ephemeris data are also downloaded and archived in the same directory. Then after the required information for data processing is gathered and fed to the different control files and saved in the respective subdirectories of the experiment directory. In addition to that editing of site information, computation environment, instrument specification, and appropriate analysis option were made the GNSS data downloaded from the IGS site were then processed using GAMIT/ GLOBK 10.7, as described in the GAMIT/GLOBK manual. The first shell script used during the processing is sh-gamit and the daily solution for ADIS and the other reference stations as well the respective root mean

square error were obtained. In addition to this information such as sky plots and quality of the data processing in the form of histogram were produced. After a thorough control of the first processing stage, a yearly time series results were generated using sh_glred. After generating the time series solution outlier results were removed by using tsview, which is a MATLAB based software for data editing. Then after, GLOBK was used to combine the yearly solution to generate the time series between 2008 and 2019.

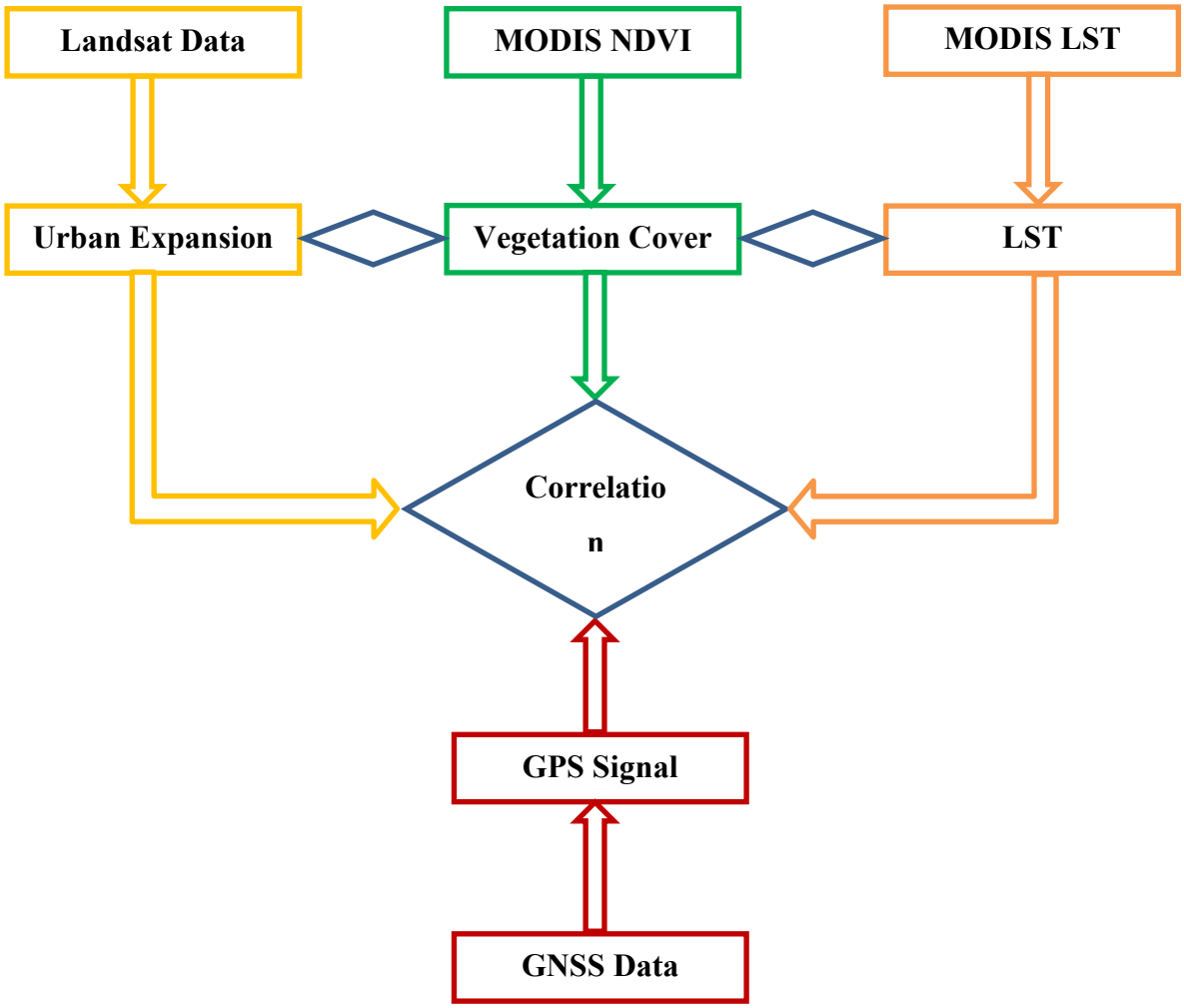

Figure 7 General Workflow of the study

The urbanization in this study is measured using urban physical expansion as a parameter. The physical expansion of Addis Ababa city was on the other hand measured from Landsat images. Landsat image is one of the dominantly applied Earth-observing satellite system in studying land cover changes. In order to process Landsat images, EARDAS IMAGINE software was used. Landsat images from 1989 up to 2019 were used with a decadal and an annual interval. To overcome the problem of cloud cover and check the expansion by making

use of data from the same season of the year, the images used were from the month of January. In very few cases it was necessary to look for data from December to April, to get cloud-free images. From the Landsat images, urban buildup area and vegetation cover information were generated. The built-up cover of the study area was generated by using two methods. The first is using feature extraction based on the supervised method and the second is using an automatic generation built-up index. The information about the vegetation cover is generated using the automatic generation of NDVI.

Data that are downloaded from the US Geological Survey had different bands and from these bands, those that are applicable for the study of land cover change are selected and layers staking were used for each year. After layer staking, the images are clipped, by making use of the boundary of Addis Ababa city. Supervised classification and automatic indices generation were applied to the clipped images of the study area. The supervised classification method classifies the given data in a number of classes based on the training sample. In this study based on training sample urban built-up area and non-built up area, classes were generated. Based on the supervised classification method, four years of images were classified. These are the 1989, 1999, 2009, and 2019 images. For the rest of the study period, the automatic built-up index method was used to generate an urban built-up area. Depending on the quality of the generated classes, the recoding of features was applied based on the supervised classification method. Recoding is one of the corrective methods to convert the wrong class to the appropriate class.

The vegetation cover of Addis Ababa city is extracted from MODIS and Landsat data. The MODIS data is used because it has high temporal resolution but the less temporal resolution in comparison to Landsat images.

The NDVI that is used in this study has 16 days of temporal resolution and 250m by 250m spatial resolutions. The time range covered in the study is from 2000 to 2019. The data was downloaded from the MODIS site with the tile gird of h21/v08 in HDF format. The software pyModis was to prepare the data for analysis. After downloading the 16 day interval MOD13Q1 NDVI data from the NASA FTP server, they are re-projected to the WGS84 reference system and converted to TIFF format, by using pyModis. The re-projected and converted NDVI data were then further analyzed using ArcGIS software and a python script for automation. One advantage of the ArcGIS software is it has a python scripting extension. The development of the script played an important role in the analysis of the time-series data.

It would have been very difficult, time-consuming, and error-prone to use the manual method to process such data. In the end, the NDVI data ware clipped to the boundaries of the study area and processed. Finally, all generated information about the built-up area and vegetation cover were converted to tabular data. Tabular data was used as input for the next analysis stage.

The MODIS data with the good spatial and temporal resolution was used to generate information about land surface temperature. MODIS has daily LST data with a 1km spatial resolution. However, missing data were encountered, in some images. The MOD11A1 product LST data was downloaded from NASA's FTP server with a tile of h21/v08. The data analyzed over the time range from 2000 up to 2019. Because the downloaded data have HDF format with sinusoidal projection, pyMODIS software is used to re-project it to WGS84 and convert it to the TIFF file format. Later the data is clipped using Addis Ababa city boundary using python in ArcGIS. To generate zonal statistics from the extracted images ArcGIS zonal statistic tools are used. Using this tool the minimum, maximum, mean, and median of LST were generated for daily data. The daily statistic information of the study area was converted to tabular data for the next correlation analysis.

To study the effect of urbanization and associated climate change on GNSS signal, the inter-relation between different parameters were first visually analyzed. In this study physical urban expansion, vegetation coverage, land surface temperature, and daily GNSS data for ADIS were used. The built-up area from 2000 to 2019, NDVI from 2000 to 2019, LST from 2000 to 2019, and GNSS data from 2008 to 2019 were taken and the long term changes were modeled using regression, least-squares curve fitting method. For this, the second-degree polynomial was used in the analysis. The parameters obtained from the least-squares fits are then used to generate the long-term trends in the NDVI, built-up area, LST, and GNSS data, between 2008 and 2019 and are checked for any correlation using Pearson's correlation method.

CHAPTER 5 RESULT AND DISCUSSION

The results from the Landsat data, MODIS NDVI, MODIS LST, and GPS data processing are presented in this chapter. The result of the correlation between any two pairs of the four parameters will also be presented in this chapter.

5.1 Urban Expansion

The urbanization as measured by the physical expansion of Addis Ababa city, generated from Landsat image using supervised classification method for 1989, 1999, 2009, and 2019, is shown in Figure 8. As can be seen from the figure, the expansion of the city during the period 1989 to 2019 can be clearly observed visually.

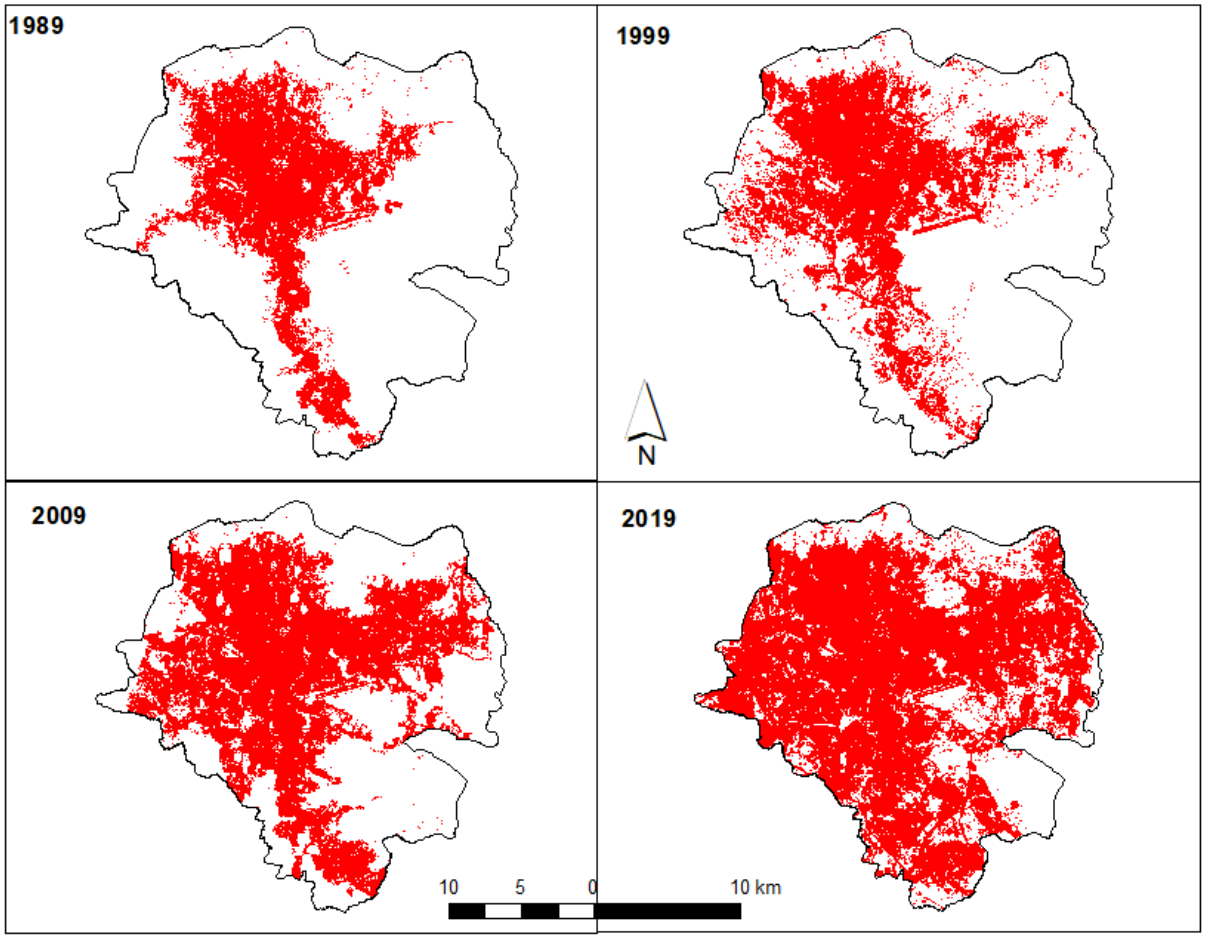

Figure 8 Built-up area of the Addis Ababa City, as derived from Landsat satellite imagery with ten years interval

The total built-up area coverage grown from 89484300m^2 in 1989, to 107241300m^2 in 1999, 188745300m^2 in 2009 and 278686800m^2 in 2019. The percentage of built-up coverage from the total area was 17.22% in 1989, 20.62% in 1999, 36.32% in 2009 and 53.63% in 2019.

The yearly built-up coverage of the study area, that was generated from the built-up index of Landsat images are shown in Figure 9. Because of high cloud coverage, some years of data were missed and data for the years 2000, 2001, 2002, 2005, 2011, 2014, 2015, 2016, 2017, and 2018 are presented in the Figure. Based on supervised classification and built-up index, the generated built-up area coverage of the study area is graphically presented in Figure 10.

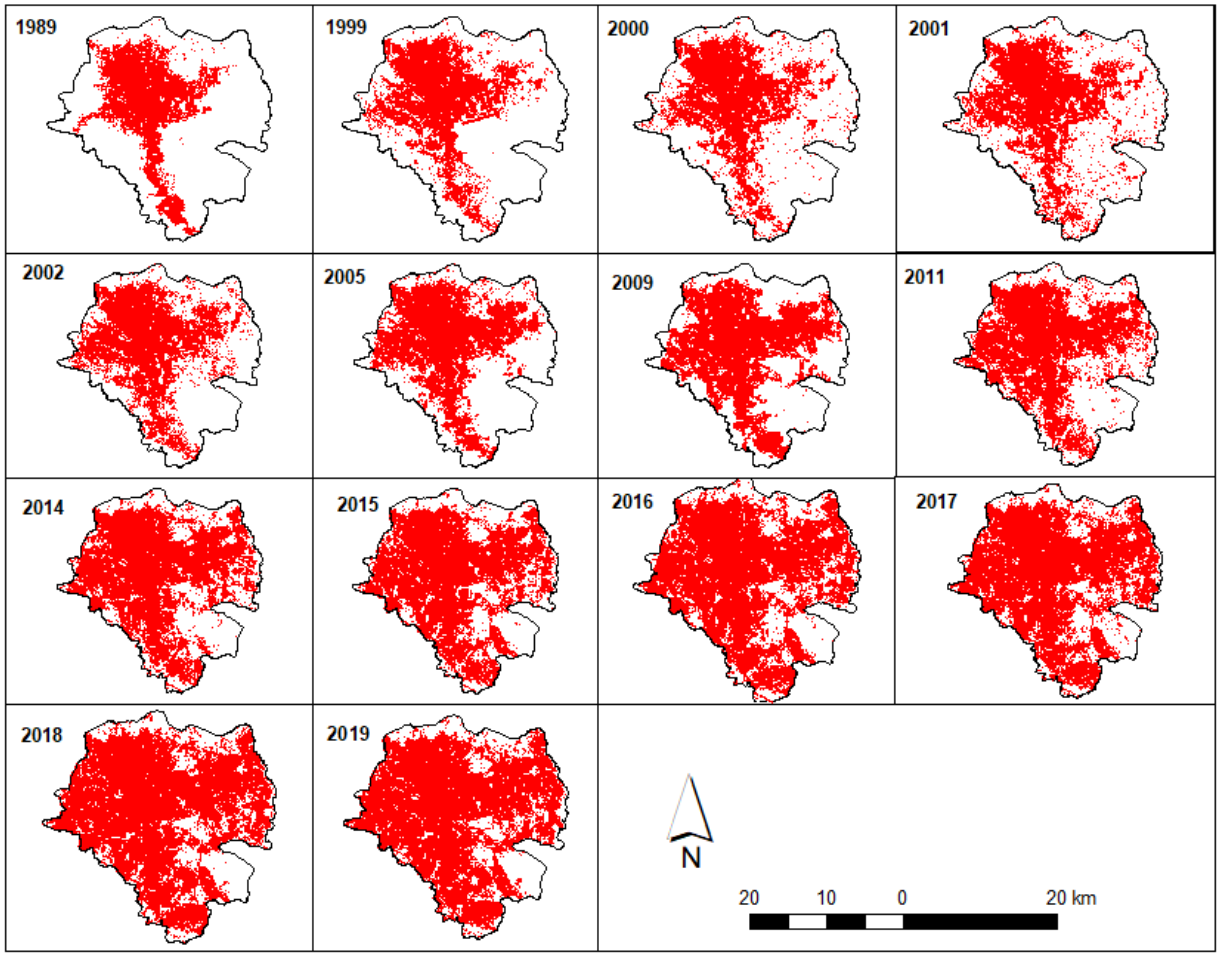

Figure 9 Built-up area of the Addis Ababa City, as derived from Landsat satellite imagery in a yearly interval.

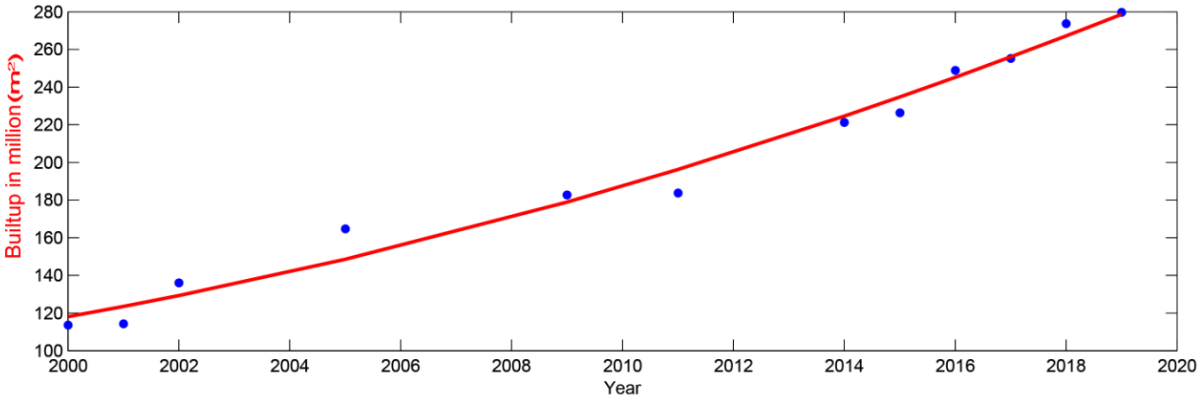

Figure 10 The dotes show, the total built-up area and the red line is the result of the curve fitting, using a second-degree polynomial and least-squares approach, to discern the long-term trend in the expansion of the city.

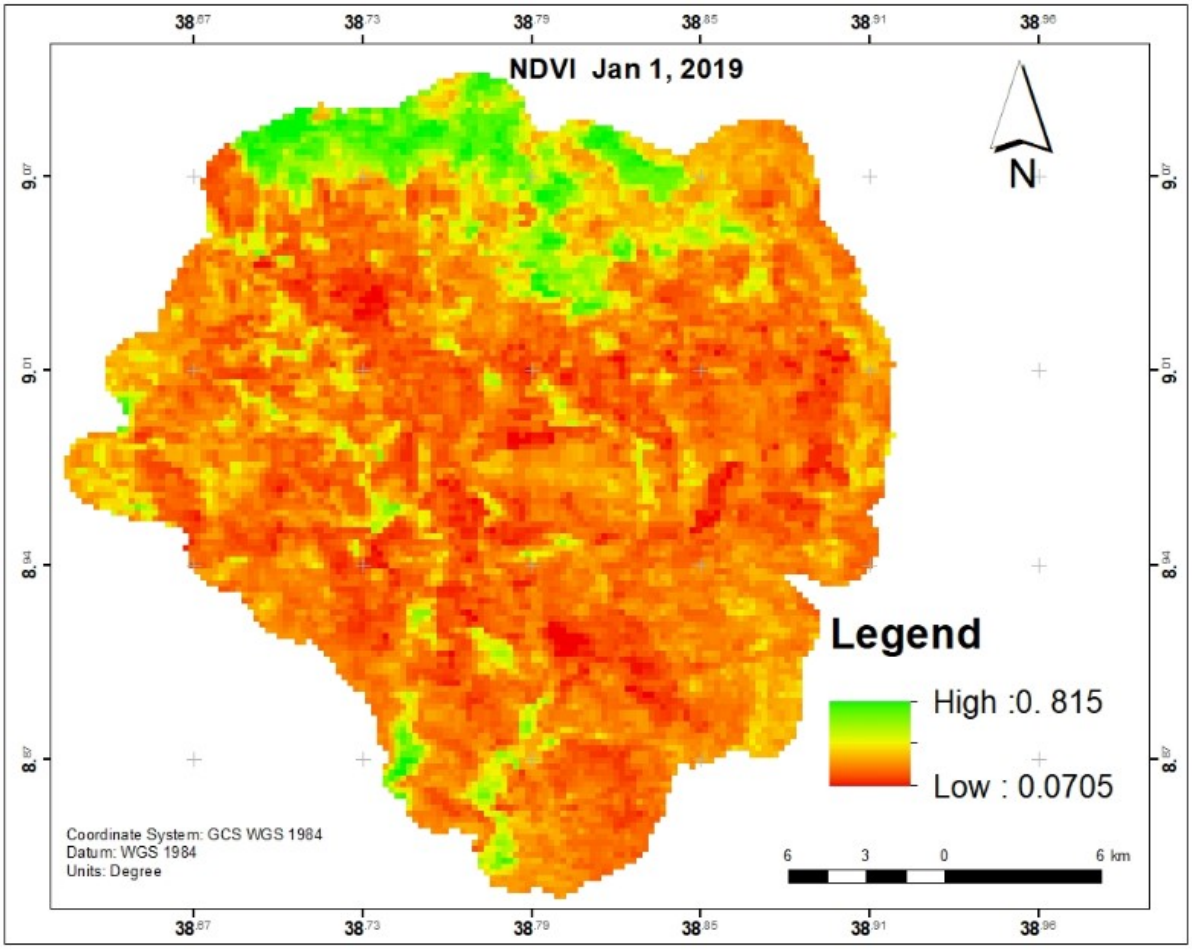

Figure 11 Map of NDVI for January 1, 2019

5.2 Vegetation Cover Change

The vegetation cover of the study area is derived from the MODIS MOD13Q1 data for 19 years period. To demonstrate the type of map generated, the NDVI for the first day of 2019 is shown in Figure 11. By making use of the 16 days interval processed NDVI data, the total vegetation coverage is computed and tabulated. Then the tabulated total vegetation coverage is plotted as shown in Figure 12. The graph also shows the curve fitted by making use of the least-squares approach to the 19 years of 16 days interval data. The main aim of fitting a quadratic to the data is to remove the seasonal effects and be able to analyze the long term trend.

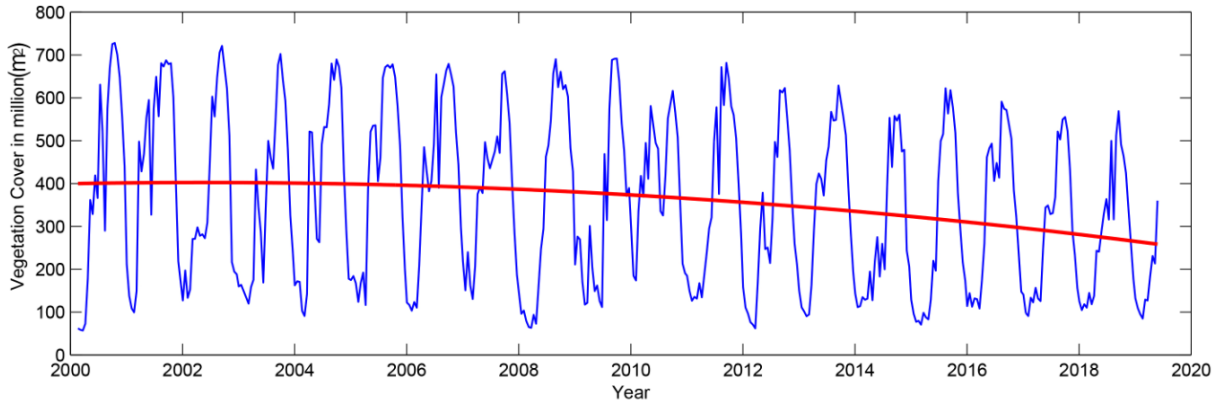

Figure 12 The blue line represents the total vegetation coverage, derived from the NDVI maps, while the red line represents the curve fitted to this data using second-degree polynomial, with the help of the least-squares curve fitting approach, to see the long term trend of the vegetation coverage.

5.3 Land Surface Temperature Change

Land surface temperature for the study area is analyzed from the MODISMOD11A1 data. The LST is computed for 19 year period and the result obtained from the analyses is generated in the map and tabular format. For the purpose of demonstration the LST map for January 1, 2019, is shown in Figure 13. The daily tabular data LST is graphically described in Figure 14. Like NDVI, LST data have also seasonal effects. The weekly and monthly effect was removed and only long-term effect is used for relational analysis. The graph Figure 14 shows the daily LST value and the curve fit of the data. The curve fit is represented by red color.

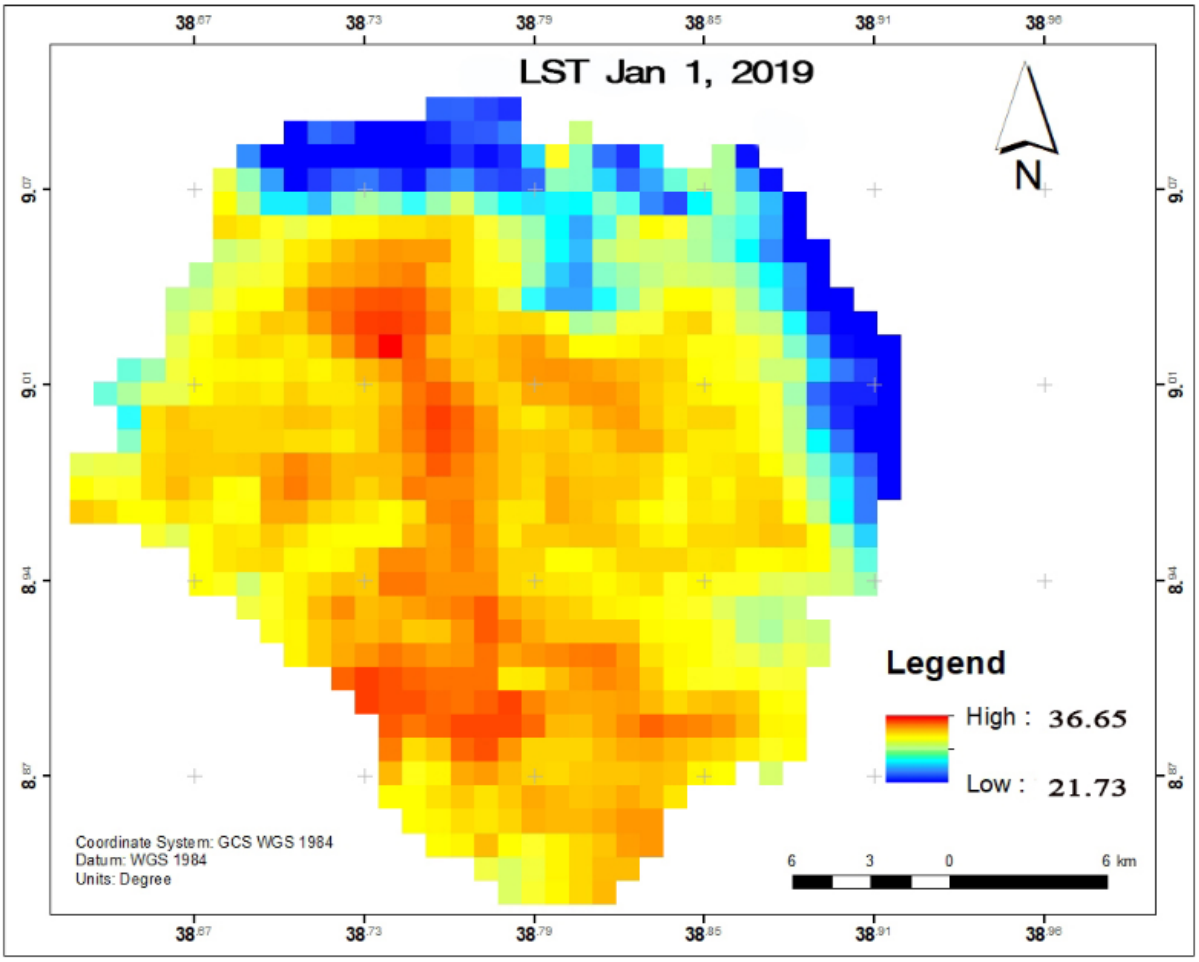

Figure 13 Map of LST in Jan. 1, 2019

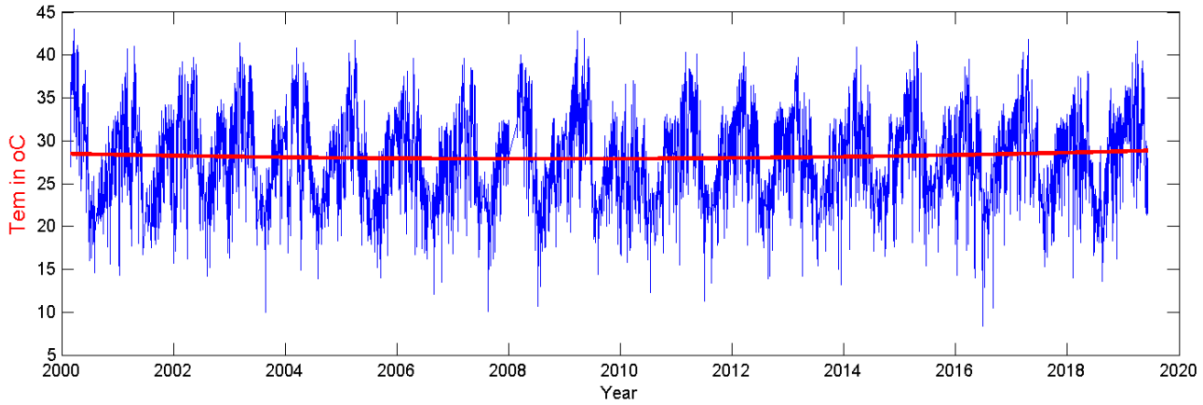

Figure 14 The blue line shows the dailly mean LST of the survey area, for 19 years period and the red line is a curve fitted to this data by making use of a second degree polynomial and least-squares method with an aim to study the long term trend in LST.

5.4 GNSS signal

The daily solution for the IGS station ADIS and other 11 IGS stations (HERS, HYDE, MAL2, MAS1, NKLG, NOT1, RAMO, REUN, TEHN, and YIBL) was first computed using GAMIT software. The daily solution generates a summary file for each day, in the DoY directories which among others include Postfit RMS (Root-mean-square) and Postfit nrms (normalized RMS), ambiguity resolution, and adjusted coordinates. In addition, sky plots and phase versus elevation plots can also be optionally generated, for each day, to understand possible sources of errors in the observation. Sky plot is usually used to indicate positive and negative residual, look at the multipath effect, and the existence of water vapor. As a demonstration, Figure 15 shows a sky plot of ADIS for DoY 5 in 2019.

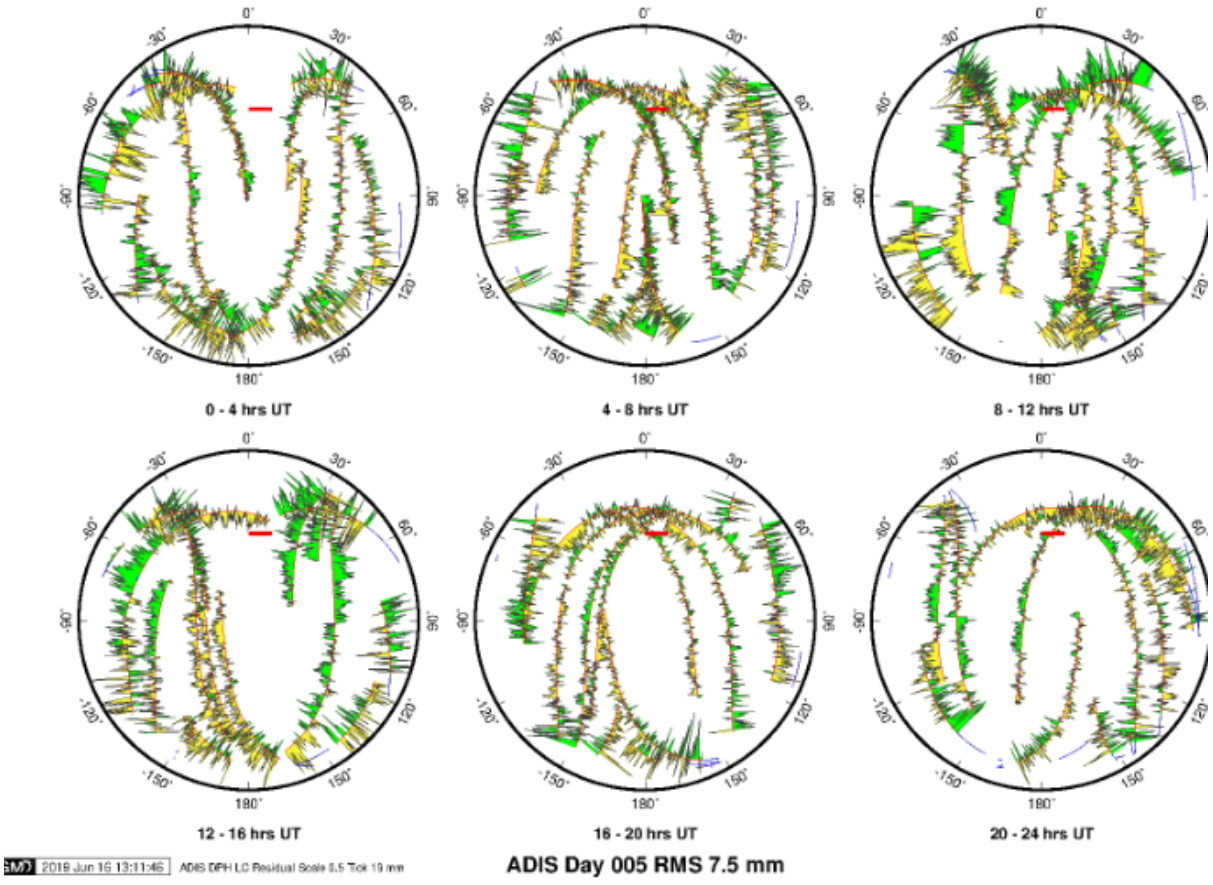

Figure 15 Sky plots of ADIS for DoY 5, 2019

Residual versus elevation plots are also used to visualize the quality of raw and processed data. Figure 16 shows such a plot for the station ADIS. Depending on the distribution of the points shown on the graph relative to the ideal curves indicated, one can clearly see if the

cause of higher nrms is multipath, water vapor, or/and a problem with the antenna path center.

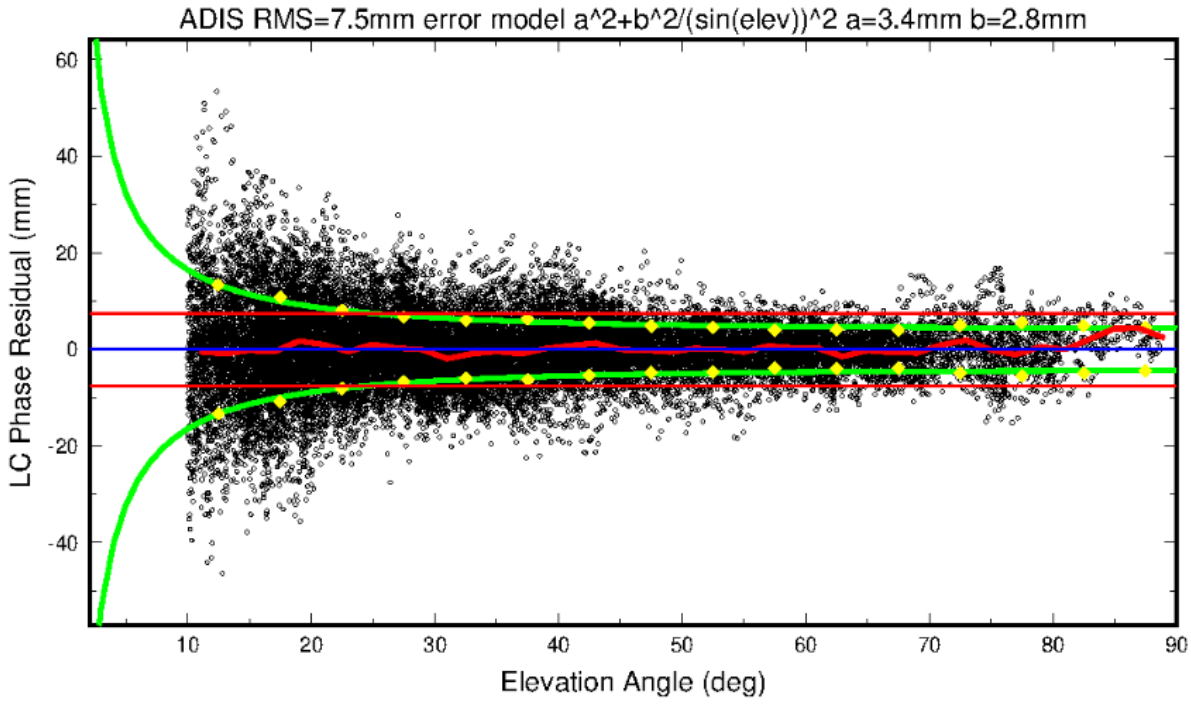

Figure 16 Elevation plot of ADIS station for the DoY 5 in 2019

Time Series

The daily solutions for 12 years (2008 up to 2019) were generated for each year using sh_gamit and sh_glred is used to generate the time series on a yearly basis. For each IGS station in the analysis, a yearly time series plot was generated, and each time series plot has included the three dimensional (North, East, and Up) daily position of the station in time. Figure 17 shows the time series result for ADIS station in 2016.

This time serious solution in the year directories, for ADIS and the other 11 IGS stations were later combined using sh_glred, to get a single time serious with three components for the whole period of 12 years. 11 IGS station that used in the analysis presented in annex.

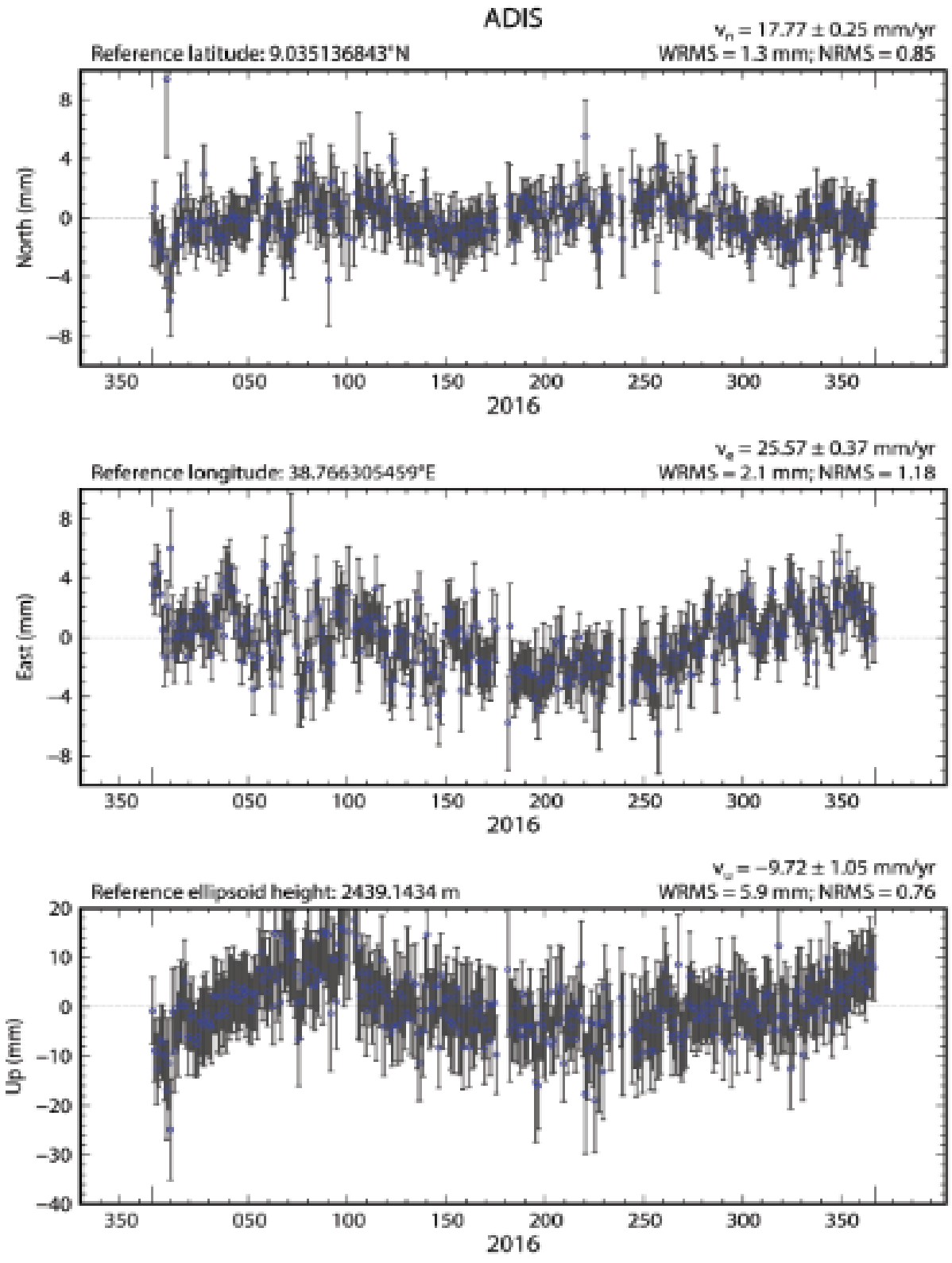

Figure 17 Time serious result of ADIS year 2016

The time series result generated using the above steps resulted some outliers. These outliers were removed using the MATLAB based software tsview. The whole process starting from sh_gamit is run after removing the outliers and the final result was obtained with acceptable residuals. Figure 18 shows the final time series plot for the station ADIS, with graphs for the North, East, and Up directions.

The 12 years' time series plot of ADIS IGS station after removing outliers the following result obtained.

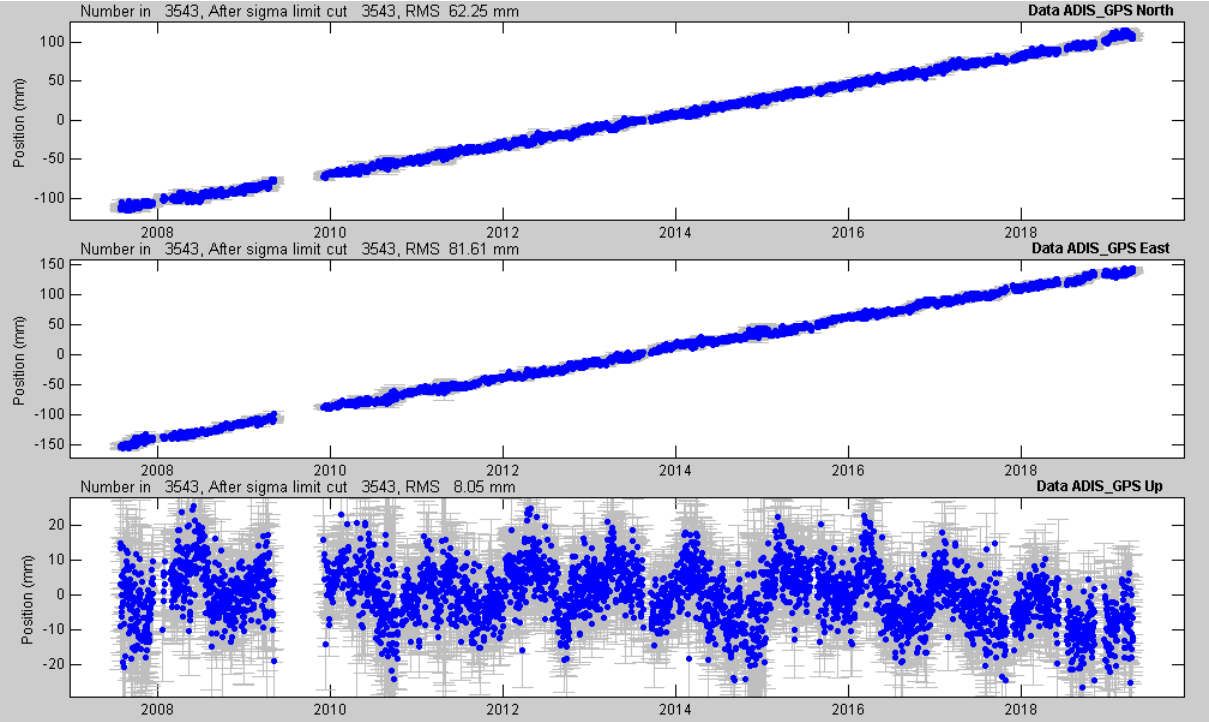

Figure 18 The time serious result of ADIS for the years 2008- 2019. The top part of the figure shows the position of the station in the north direction, the middle the East direction, and the bottom part in the vertical direction between 2008 and 2019.

The final time series result for the up direction was then extracted from the GAMIT/GLOBK output and imported to the MATLAB software for the final correlational analysis Figure 19 shows the final plot of the residual for the UP direction and a trend in red, which is fitted to the UP direction data using a second-degree polynomial and least-squares approach. This long term trend is meant to study the effect of urbanization and associated climate change on GNSS signal propagation.

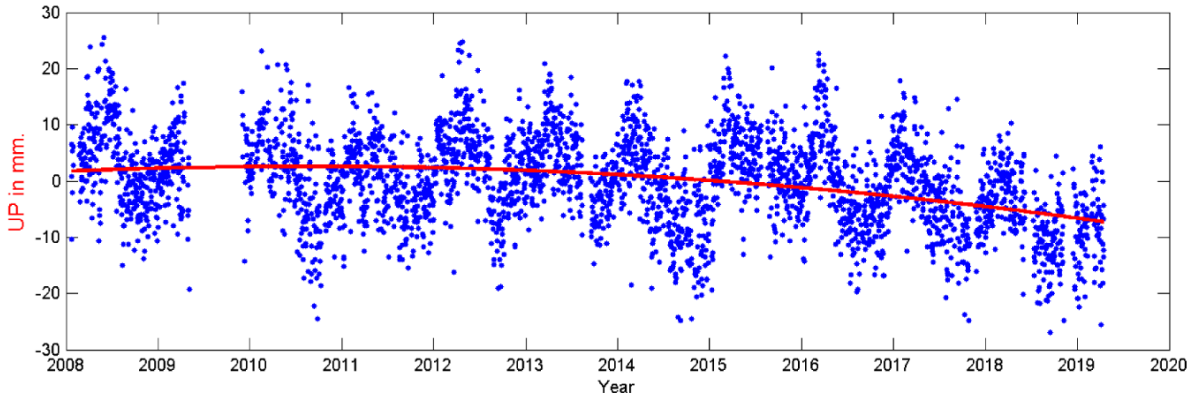

Figure 19 The blue dotes show the daily solution of positions for the UP direction of the station ADIS and the red line shows the curve fitted to this data using a second-degree polynomial and the least-squares approach.

Table 5-1 The correlation coefficient between the different data pairs

No.	Data Source		Pearson's Correlation coefficient
1	Built-up	Vegetation cover	-0.9972
2	Built-up	GNSS, UP direction	-0.9227
3	Vegetation cover	LST	-0.9881
5	Vegetation cover	GNSS, UP direction	+0.9489
6	LST	GNSS, UP direction	-0.9861
7	LST	Built-up	+0.9738

5.5 Correlation

Even though visual interpretation already shows that all long-term trends from the four data sources show some association, in order to quantify this association a correlation analysis has been made. Figure 20 shows the long term trend of the Built-up cover, vegetation cover, LST, and UP direction of the ADIS, for the years 2008 until 2019. The Pearson correlation coefficient between the different data sets is presented in Table (5.1).

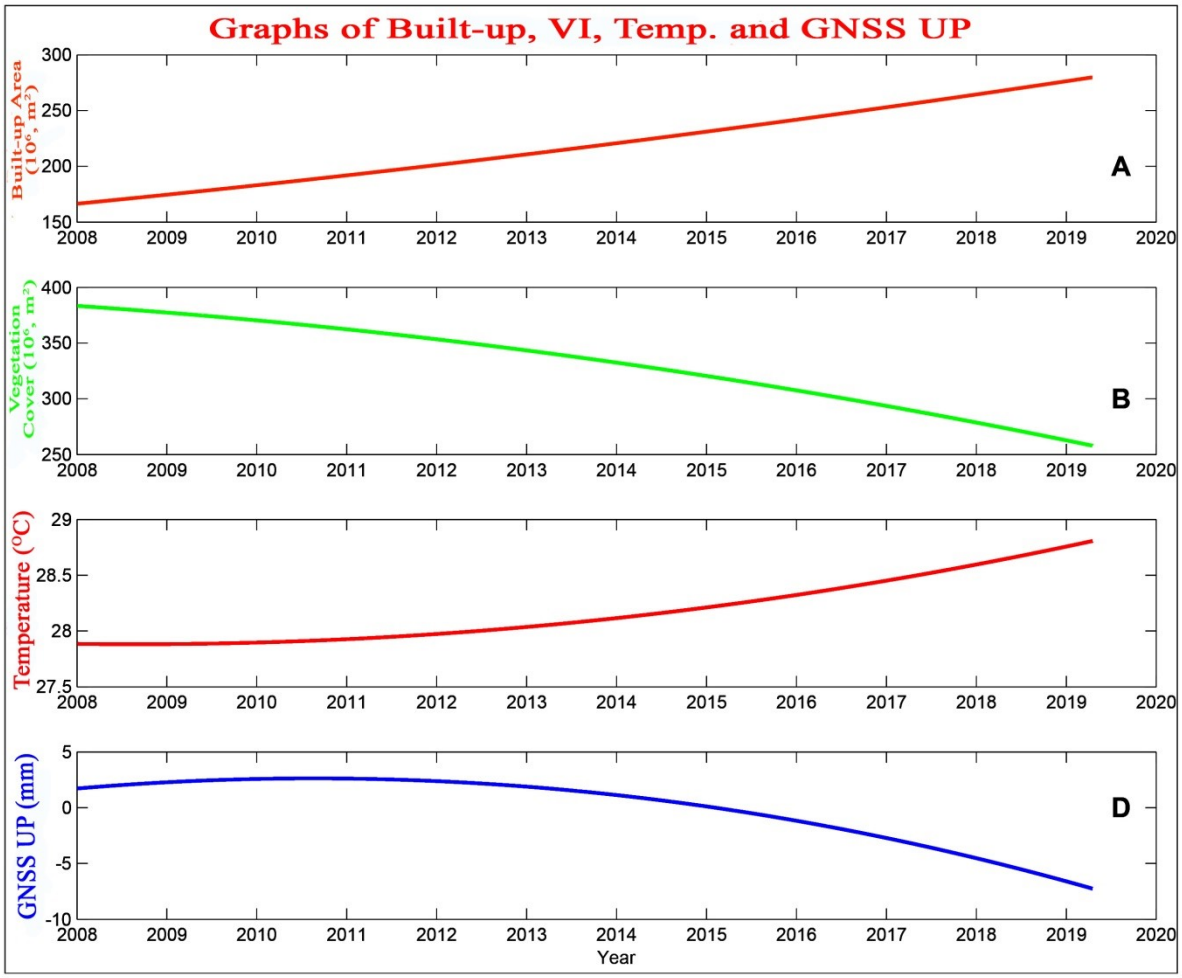

Figure 20 The long term trend in the different parameters where (A) shows the built-up area (B) the total vegetation coverage (C) the LST and (D) the UP direction of the Station ADIS.

5.6 Discussion

The urban physical expansion which is derived from satellite image data is one of the parameters used to measure urbanization (Fang and Quansheng, 2012). In this study, the physical expansion of the study area was generated from 1989 to 2019, using the Landsat image of Multi Spectral Scanner (MSS), Enhanced Thematic Mapper Plus (ETM+), and Operational Land Imager (OPI) sensor data. The result showed that there is a significant increment in the built-up area, which caused a physical expansion of the Addis Ababa City. The expansion took place both in a planned and unplanned manner (Study for Swiss Agency for Development and Cooperation, 2017). The result indicates that the Addis Ababa city experienced a high rate of expansion in the last three decades. From these three decades, the highest rate of expansion was observed in the last ten years. This statement will be clearer,

when one looks at the expansion of the city, for the years between 2008 and 2019 in Figure 20, where we have GNSS data (2008-2019) showed that major expansion is taking place.

The other effect of urbanization in Addis Ababa is the transformation of the landscape. Agricultural land, barren land, and forest are replaced by a built-up area due to urbanization. This is also the case internationally (Cui & Shi, 2012). As a result, vegetation covers in the current urbanized areas are affected by the expansion of the built-up area. As one can see from the red color curve in Figure 12, there is a significant depletion of vegetation cover in the last two decades. Similarly, a high rate of change took place in the last ten years.

The expansion of urban built-up and the decline of vegetation cover affect the urban land surface temperature (Adeyeri et al., 2017). Even though, unlike the other parameters, there was a slight drop in temperature at the beginning of the millennium, the trend of the LST also followed the pattern of other parameters beginning 2009 onwards. Even though the trend is similar, the increment on the land surface temperature of the city is about 0.93^0C in 10 year time.

From the result of GNSS data for ADIS station Figure 18, the three-dimensional position of ADIS is continuously changing in time, with the North and East component almost following a linear trend with a rate almost similar, but not exactly the same, to that of the Nubian plate movement. However, the UP component shows, both seasonal and a non-linear but low-frequency movement. It is optically obvious that the station on an average was not showing any low-frequency movement until 2013, but subsided noticeably after 2013 until 2019.

Both NDBI and NDVI results were studied as a measure of the physical expansion of Addis Ababa City and association with the change in the UP direction was obvious from the visual compassion. However, as both cannot directly affect the change in the location of the station, it was necessary to study urban climate change through the LST. NDBI, which is used to study built-up expansion, and NDVI, which is used to study vegetation cover contribute to urban climate change (Jamei et al., 2019).

In this study, the NDBI and NDVI were used to study urban expansion and the LST to study the urban climate of Addis Ababa. The individual results and the very strong correlation (Table, 5.1) between built-up and vegetation cover that amounts to -0.9972, clearly indicate that the city is indeed expanding. The strong negative correlation shows that as the city is expanding, the vegetation coverage is decreasing at the same rate. There is also a strong

relation between LST and the two parameters (built-up and vegetation cover) that are used to measure the city expansion (Table 5.1). The correlation between the built-up area and LST is 0.9738, and this shows that as the built-up area is increasing the temperature of the city is increasing and the -0.9881 correlation between the NDVI and LST shows that as the vegetation coverage is decreasing the temperature of the city is increasing. The result is agreeing with different scholars findings. A strong negative correlation between LST and NDVI is also seen in shanghai, China (J. Li et al., 2011). The study of (Fang & Quansheng, 2012) also indicates that the effect of urbanization on climate changes with respect to temperature trends varies by city size (small and large cities), at a local and regional level, and also by season. According to Hoang et al. (2015) the decrease of NDVI in Danang city, Vietnam is correlated with the high value of LST. The study of (Rasul and Ibrahim, 2017) also shows that there is a negative relation between LST and NDVI in Dohuk City, Iraq. The relation between LST and NDVI shows a significant negative correlation in Yinjiang, China(Deng et al., 2018).

The correlation between the UP direction of GNSS data taken from the station ADIS and LST over Addis Ababa, also showed a correlation that amounts to -0.9861 (Table 5.1). This also shows that as the temperature is increasing the speed of the signal in the atmosphere is decreasing to increase the computed pseudo-range between the satellites and the receiver antenna. This on the other hand will lead to the impression that the station is subsiding. Dodo et al. (2015), stated that the computation of the UP direction of station position is relatively affected by changes in the lower atmosphere and the current result, which showed that there is a very good correlation between LST and the UP direction will be in good agreement with their statement. According to Trenberth (2011), the increment of temperature by $1^{o}C$ has a significant effect on the propagation of signals in the lower atmosphere.

The very good correlation between built-up area and vegetation cover with the UP direction of GNSS that amount to -0.9226 and 0.9489 respectively clearly shows that the long term subsidence observed in the Up direction of the station ADIS is clearly related to the expansion of the city. The correlation of the LST signal with the other data sets during the same period shows that the expansion of the urban built-up area and the associated depletion of vegetation cover affect the LST of the study area. However, further investigation is needed to check if urbanization only is the cause of the change in the LST. Similarly, further studies need to be made to investigate other possible causes of the long-term change in the up direction of the daily GNSS solution.

CHAPTER 6 CONCLUSION AND RECOMMENDATION

6.1 Conclusion

The research work was conducted to study the effect of urbanization and urban climate change on the GNSS signal, by correlating the GNSS signal from the IGS station ADIS with the urban built-up expansion, vegetation cover, and land surface temperature for the city of Addis Ababa. The result clearly showed that there is a strong correlation between urbanization, climate change, and the change in the vertical position of the station ADIS. From the findings one can conclude the followings:

- By using geospatial technology we can measure the urban physical expansion from satellite images. The measured result shows the urban built-up area of Addis Ababa city clearly expands in the last three decades. The rate of expansion was fastest in the last ten years.
- Because of the expansion of the urban built-up area, the reduction of vegetation cover in Addis Ababa city was observed in the last twenty years. Visual observation clearly showed that, because of the fast expansion in built-up areas in the last ten years, vegetation cover is highly depleted accordingly.
- A notable change in the LST was also observed in Addis Ababa city in the last twenty years. The correlation of this change with vegetation cover and built-up area showed that the urban expansion and associated depletion of vegetation has raised the land surface temperature of the city slightly. This on the other hand has influenced the propagation of the GNSS signal in the lower part of the atmosphere.
- The UP direction of the GPS signal at the IGS station ADIS was also showing subsidence, without a definable cause. This study showed that the station might not be fully physically subsiding, but the processing of data is influenced by changes in the lower atmosphere, that on the other hand is caused by urbanization. The strong correlation between built-up cover, vegetation cover, and LST on hand and the UP direction of the daily solutions on the other hand showed that urbanization is affects the UP direction GNSS position of ADIS.

Finally as a result of this study, one can conclude that urbanization and associated climate change have an effect on the propagation GNSS signal. Thus, when processing GNSS data one should consider the influence and effect of urbanization and urban climate change on the GNSS signal before using the locations derived from the stations for other purposes to the effect should be modeled and remove from the processed result.

6.2 Recommendation

Any work which needs precise and accurate positioning such as geodetic work, meteorology, deformation analysis and etc. should seriously consider the effect of urbanization on observed GNSS signal.

From the results achieved in this study the following recommendations are made:

- It is necessary to carry out similar research in other major cities that are growing very fast to ascertain results that are found in this research work.
- To further study urban climate change using other parameters and identify, which change has affected the GNSS signal.
- The issue of urbanization in this study is only addressed by urban physical expansion. Other urbanization measuring parameters are recommended to be analyzed in order to ascertain the results found in this study.
- Further study is needed to find out the cause and effect relationship through quantitative approaches.
- As the subsidence is substantial (1cm) and the behavior of the curves to some extent differs, it is necessary to check if the whole subsidence is caused due to the effect of urbanization or if there is any other additional effect, during the same period of time.

REFERENCE

Abtew, W., & Melesse, A. M. (2016). Landscape Changes Impact on Regional Hydrology and Climate Wossenu. In *Landscape Dynamics, Soils and Hydrological Processes in Varied Climates* (pp. 31–50).

Adeyeri, O. E., Akinsanola, A. A., & Ishola, K. A. (2017). Investigating surface urban heat island characteristics over Abuja , Nigeria : Relationship between land surface temperature and multiple vegetation indices. *Remote Sensing Applications: Society and Environment*, *7*(June), 57–68. https://doi.org/10.1016/j.rsase.2017.06.005

Agnihotri, A. K., Ohri, A., & Mishra, S. (2018). Impact of Green Spaces on the Urban Microclimate through Landsat 8 and TIRS Data , in Varanasi , India.

Ali, S. B., Patnaik, S., & Madguni, O. (2017). Microclimate land surface temperatures across urban land use / land cover forms, *3*(3), 231–242. https://doi.org/10.22034/gjesm.2017.03.03.001

Alshawaf, F., Fuhrmann, T., Knöpfler, A., Luo, X., Mayer, M., Hinz, S., & Heck, B. (2015). Accurate Estimation of Atmospheric Water Vapor Using GNSS Observations and Surface Meteorological Data. *IEEE Transactions on Geoscience and Remote Sensing*, *53*(7), 3764–3771. https://doi.org/10.1109/TGRS.2014.2382713

Arora VK, Montenegro A (2011) Small temperature benefits provided by realistic afforestation efforts. Nat Geosci 4(8):514–518

Assiri, M. E. (2017). Assessing MODIS land surface temperature (LST) over Jeddah. *Polish Journal of Environmental Studies*, *26*(4), 1461–1470. https://doi.org/10.15244/pjoes/68960

Awange, J. (2018). *GNSS Environmental Sensing Revolutionizing Environmental Monitoring* (2nd ed.).

Berry, B. J. L. (2008). Urbanization. In J. M. Marzluff, E. Shulenberger, W. Endlicher, W. Endlicher, G. Bradley, C. Ryan, … U. Simon (Eds.), *Urban Ecology* (pp. 25–48). Springer Science+Business Media, LLC.

Betts AK, Ball JH, Beljaars A, Miller MJ, Viterbo PA (1996) The land surface-atmosphere interaction: A review based on observational and global modeling perspectives. J Geophys Res Atmos (1984–2012) 101(D3):7209–7225

Bhagat RB, Mohanty S (2009) Emerging pattern of urbanization and the contribution of migration in urban growth in India. Asian Popul Stud 5(1):5–20

Bhatti, S. S., & Tripathi, N. K. (2014). Built-up area extraction using Landsat 8 OLI imagery, *51*(June), 445–467. https://doi.org/10.1080/15481603.2014.939539

Böhm, J., & Schuh, H. (2013). *Atmospheric Effects in Space Geodesy*. New York Dordrecht London: Springer-Verlag Berlin Heidelberg.

Brovkin V, Ganopolski A, Claussen M, Kubatzki C, Petoukhov V (1999) Modelling climate response to historical land cover change. Glob Ecol Biogeogr 8(6):509–517

Cao, R., Li, F., & Feng, P. (2020). Impact of urbanization on precipitation in North Haihe Basin, China. *Atmosphere*, *11*(1). https://doi.org/10.3390/ATMOS11010016

Carlson, T. N., & Arthur, S. T. (2000). The impact of land use — land cover changes due to urbanization on surface microclimate and hydrology : a satellite perspective, 49–65.

Central Statistical Agency of Ethiopia (CSA). (2013) Population and Housing Report of Ethiopia, CSA, Addis Ababa, Ethiopia.

CERUZZI, P. E. (2018). *GPS*. Cambridge, Massachusetts: Massachusetts Institute of Technology.

Choudhary, B. K., & Tripathi, A. K. (2018). Failing Cityscape : Urbanization and Urban Climate, *64*(1), 174–184.

Cohen, B. (2006). Urbanization in developing countries : Current trends , future projections , and key challenges for sustainability, *28*, 63–80. https://doi.org/10.1016/j.techsoc.2005.10.005

Cooperation, S. A. for D. and. (2017). *Urban and Peri- Urban Development Dynamics in Ethiopia*.

Cracknell, A.P., 2001. The exciting and totally unanticipated success of the AVHRR in applications for which it was never intended. Advanced Space Research, 28(1): 233–240.

Cui, L., & Shi, J. (2012). Urbanization and its environmental effects in Shanghai , China. *Urban Climate*, *2*, 1–15. https://doi.org/10.1016/j.uclim.2012.10.008

Curran P (1980) Multispectral remote sensing of vegetation amount. Progr Phys Geogr 4:315–341

Da Silva, Á. A., Yamaguti, W., Kuga, H. K., & Celestino, C. C. (2012). Assessment of the ionospheric and tropospheric effects in location errors of data collection platforms in equatorial region during high and low solar activity periods. *Mathematical Problems in Engineering*, *2012*. https://doi.org/10.1155/2012/734280

Delucchi, L. (2017). pyModis Documentation.

Deng, X., Güneralp, B., & Su, H. (2014). Systematic Modeling of Land Use Impacts on Surface Climate. In X. Deng, B. Güneralp, J. Zhan, & H. Su (Eds.), *Land Use Impacts on Climate* (pp. 1–18). Springer-Verlag Berlin Heidelberg.

Deng, Y., Wang, S., Bai, X., Tian, Y., & Wu, L. (2018). Relationship among land surface temperature and LUCC , NDVI in typical karst area. *Scientific Reports*, (December 2017), 1–12. https://doi.org/10.1038/s41598-017-19088-x

Dirmeyer PA, Shukla J (1994) Albedo as a modulator of climate response to tropical

deforestation. J Geophys Res 99(D10):20863–20877

Doberstein, D. (2012). *Fundamentals of GPS Receivers A Hardware Approach*. New York, USA: Springer Science+Business Media.

Dow, J., & Neilan, R. (1994). International GPS Service. *Eos, Transactions American Geophysical Union*, *75*(44), 514–514. https://doi.org/10.1029/EO075i044p00514-03

Dutta D, Kundu A, Patel NR (2013) Predicting agricul- tural drought in eastern Rajasthan of India using NDVI and standardized precipitation index. Geocarto Int 28(3):192–209. doi:10.1080/10106049.2012. 679975

El-Rabbany, A. (2002). *Introduction to GPS The Global Positioning System*. Boston, London: Artech House.

Emlen, J. T. 1974. An urban bird community in Tucson, Arizona: derivation, structure, regulation. Condor 76:184–197.

Fang, W., & Quansheng, G. E. (2012). Estimation of urbanization bias in observed surface temperature change in China from 1980 to 2009 using satellite land-use data, *57*(14), 1708–1715. https://doi.org/10.1007/s11434-012-4999-0

Gallo, K. P., Easterling, D. R., & Peterson, T. C. (1996). The Influence of Land Use/Land Cover on Climatological Values of the Diurnal Temperature Range.

GALLO, K. P., OWEN, T. W., EASTERLING, D. R., & JAMASON, P. F. (1999). Temperature Trends of the U . S . Historical Climatology Network Based on Satellite-Designated Land Use / Land Cover, 1344–1348.

Gao, J. (2009). *Digital Analysis of Remotely Sensed Imagery*. McGraw-Hill.

Ghosh, S., & Siddique, P. G. (2018). Change Detection of Built-Up Areas Applying Built-Up Index for Chandannagar Change Detection of Built-Up Areas Applying Built-Up Index for Chandannagar City, (April).

Gregorio, A. Di, & Jansen, L. J. M. (1998). A new concept for a land cover classification system, *2*(1), 1–9.

Greiser, C., Meineri, E., Luoto, M., Ehrlén, J., & Hylander, K. (2018). Monthly microclimate models in a managed boreal forest landscape. *Agricultural and Forest Meteorology*, *250–251*(December 2017), 147–158. https://doi.org/10.1016/j.agrformet.2017.12.252

Grimm, N. B., Grove, J. M., Pickett, S. T. A., & Redman, C. L. (2008). Integrated Approaches to Long-Term Studies of Urban Ecological Systems. In J. M. Marzluff, E. Shulenberger, W. Endlicher, W. Endlicher, G. Bradley, C. Ryan, … U. Simon (Eds.), *Urban Ecology* (pp. 123–143). Springer Science+Business Media, LLC.

Haishan, C., & Ye, Z. (2013). Sensitivity experiments of impacts of large-scale urbanization in

East China on East Asian winter monsoon, *58*(7), 809–815. https://doi.org/10.1007/s11434-012-5579-z

Han, J., Baik, J., & Lee, H. (2013). Urban Impacts on Precipitation. https://doi.org/10.1007/s13143-014-0016-7

Hern´andez-Pajares, M., Zornoza, J. M. J., & Subirana, J. S. (2005). *GPS data processing : code and phase Algorithms , Techniques and Recipes*.

Herring, T. A., Floyd, M. A., King, R. W., & Mc Clusky, S. C. (2015). GLOBK Reference Manual, (June), 1–95. Retrieved from http://geoweb.mit.edu/gg/GLOBK_Ref.pdf

Herzog T (2009) World greenhouse gas emissions in 2005. World Resources Institute

Herring, T., King, R. W., & McClusky, S. C. (2010). Introduction to GAMIT/GLOBK. *Mass. Inst. of Technol., Cambridge, Mass*, (October 2010), 1–48.

Hibbard K, Janetos A, Van Vuuren DP, Pongratz J, Rose SK, Betts R, et al (2010) Research priorities in land use and land-cover change for the Earth system and integrated assessment modelling. Int J Climatol 30(13):2118–2128

Hoang, N., Linh, K., & Chuong, H. Van. (2015). ASSESSING THE IMPACT OF URBANIZATION ON URBAN CLIMATE BY REMOTE SENSING PERSPECTIVE : A CASE STUDY IN DANANG CITY , VIETNAM, *XL-7/W3*(May 11-15), 207–212. https://doi.org/10.5194/isprsarchives-XL-7-W3-207-2015

Hofmann-Wellenhof, B., Lichtenegger, H., & Wasle, E. (2008). *GNSS – Global Navigation Satellite Systems GPS, GLONASS, Galileo, and more*. Austria: Springer-Verlag Wien.

Hordyniec, P., Kapłon, J., & Rohm, W. (2018). Residuals of Tropospheric Delays from GNSS Data and Ray-Tracing as a Potential Indicator of Rain and Clouds. https://doi.org/10.3390/rs10121917

Hulme M, Doherty R, Ngara T, New M, Lister D (2001) African climate change: 1900–2100. Clim Res 17:145–168

Hung T, Uchihama D, Ochi S, Yasuoka Y (2006) Assessment with satellite data of the urban heat island effects in Asian mega cities. Int J Appl Earth Obs Geoinf 8:34–48

International Organization for Migration (IOM). (2015). *WORLD MIGRATION REPORT 2015*. London.

Jamei, Y., Rajagopalan, P., & Chayn, Q. (2019). Time-series dataset on land surface temperature , vegetation , built up areas and other climatic factors in top 20 global cities (2000 e 2018). *Data in Brief*, *23*, 103803. https://doi.org/10.1016/j.dib.2019.103803

Jansen, J. C. and Paelinck, J. H. P. (1981). The urbanization of phenomenon in the process of development: some statistical evidence. In The Dynamic of Urban Development. Klaasen,

L. H., Molle, W. T. M. and Paelinck, J. H. P. (Eds.). Proceeding. St. martin's Press New York, N. Y., United States. pp. 31-46.

Jiao, L. (2015). Landscape and Urban Planning Urban land density function : A new method to characterize urban expansion. *Landscape and Urban Planning*, *139*, 26–39. https://doi.org/10.1016/j.landurbplan.2015.02.017

Jin, S. (2012). *GLOBAL NAVIGATION SATELLITE SYSTEMS – SIGNAL, THEORY AND APPLICATIONS*. Rijeka, Croatia: InTech.

Jin, S., Cardellach, E., & Xie, F. (2014). *GNSS Remote Sensing Theory, Methods and Applications*.

Jin, S., & Gleason, O. F. L. S. (2009). Characterization of diurnal cycles in ZTD from a decade of global GPS observations, 537–545. https://doi.org/10.1007/s00190-008-0264-3

Jin, S., & Luo, O. F. (2009). Variability and Climatology of PWV From Global 13-Year GPS Observations, *47*(7), 1918–1924.

Jin, S., Park, J., Cho, J., & Park, P. (2007). Seasonal variability of GPS-derived zenith tropospheric delay (1994 – 2006) and climate implications, *112*(November 2006), 1–11. https://doi.org/10.1029/2006JD007772

Jingyong, Z., Peiyan, C., & Lee, D. (2005). Impact of Land Use Changes on Surface Warming in China, *22*(3), 343–344.

Johnston, G., Riddell, A., & Hausler, G. (2017). The International GNSS Service. *Springer Handbooks*, 967–982. https://doi.org/10.1007/978-3-319-42928-1_33

Kaida, Y. (1992). Integrated rural development and land use. In Proceeding of International Symposium: Rural Land Use in Asian Countries, October 7-8, 1992, Japan National Committee for Rural Planning, pp. 220-221.

Kaplan, E. D., & Hegarty, C. J. (2017). *Understanding GPS / GNSS Principles and Applications*. (E. D. Kaplan & C. J. Hegarty, Eds.) (3rd ed.). Boston, London: Artech House.

Karanam, H. K., & Babuneela, V. (2017). Study of normalized difference built-up (NDBI) index in automatically mapping urban areas from Landsat TM, *6*(8), 239–248.

Kasa, L., Zeleke, G., Alemu, D., & Hagos, F. G. (2011). IMPACT OF URBANIZATION OF ADDIS ABEBA CITY ON PERI-URBAN, (February).

Ke, X., Zhan, J., Ma, E., & Huang, J. (2014). Regional Climate Impacts of Future Urbanization in China. In X. Deng, B. Güneralp, J. Zhan, & H. Su (Eds.), *Land Use Impacts on Climate* (pp. 167–206). Springer-Verlag Berlin Heidelberg.

Kleusberg, A., & Teunissen, P. J. G. (1996). *GPS for Geodesy*. Germany.

Kumar, S., Agrawal, S., & Krishnaveni, M. (2014). Time-Series analysis of MODIS NDVI data along with ancillary data for Land use / Land cover mapping of Uttarakhand, *XL*(December), 9–

12. https://doi.org/10.5194/isprsarchives-XL-8-1491-2014

Kundu A, Dwivedi S, Dutta D (2016) Monitoring the vegetation health over India during contrasting mon- soon years using satellite remote sensing indices. Arab

Kundu, A., Denis, D. M., Patel, N. R., & Dutta, D. (2018). Long-Term Trend of Vegetation in Bundelkhand Region (India): An Assessment Through SPOT-VGT NDVI Datasets. In *Climate Change, Extreme Events and Disaster Risk Reduction* (pp. 89–100). Springer International Publishing.

Kuttler, W. (2008). The Urban Climate – Basic and Applied Aspects. In J. M. Marzluff, E. Shulenberger, W. Endlicher, W. Endlicher, G. Bradley, C. Ryan, … U. Simon (Eds.), *Urban Ecology* (pp. 233–248). Springer Science+Business Media, LLC.

Laat, A. T. J. D. E., & Maurellis, A. N. (2006). EVIDENCE FOR INFLUENCE OF ANTHROPOGENIC SURFACE PROCESSES. *INTERNATIONAL JOURNAL OF CLIMATOLOGY*, *913*(March), 897–913. https://doi.org/10.1002/joc.1292

LEICK, A., RAPOPORT, L., & TATARNIKOV, D. (2015). *GPS SATELLITE SURVEYING* (4th ed.). Canada: John Wiley & Sons.

Li, J., Song, C., Cao, L., Zhu, F., Meng, X., & Wu, J. (2011). Impacts of landscape structure on surface urban heat islands: A case study of Shanghai, China. *Remote Sensing of Environment*, *115*(12), 3249–3263. https://doi.org/10.1016/j.rse.2011.07.008

Li, X. X., Koh, T. Y., Panda, J., & Norford, L. K. (2016). Impact of urbanization patterns on the local climate of a tropical city, Singapore: An ensemble study. *Journal of Geophysical Research*, *121*(9), 4386–4403. https://doi.org/10.1002/2015JD024452

Lim, Y., Cai, M., Kalnay, E., & Zhou, L. (2005). Observational evidence of sensitivity of surface climate changes to land types and urbanization, *32*(October), 40–43. https://doi.org/10.1029/2005GL024267

Liu, S., R., J. ·, & X., J. ·. (2019). *GNSS Atmospheric Seismology Theory, Observations and Modeling*. Gateway East, Singapore: Springer Nature Singapore Pte Ltd.

Lo CP, Quattrochi DA (2003) Land-use and land-cover change, urban heat island phenomenon, and health implications: A remote sensing approach. Photogramm Eng Rem Sens 69(9):1053–1063

Lowry, W. P. (1977) – Empirical estimation of Urban effects on climate: A problem Analysis. Journal of Applied Meteorology, 16 (2): 129–135.

Luo, H., Wang, L., Fang, J., Li, Y., Li, H., & Dai, S. (2015). NDVI, Temperature and Precipitation Variables and Their Relationships in Hainan Island from 2001 to 2014 Based on MODIS NDVI. In *Geo-Informatics in Resource Management and Sustainable Ecosystem* (pp. 336–344).

Madry, S. (2015). *Global Navigation Satellite Systems and Their Applications*.

Makinde, O. O. (2012). Urbanization, housing, and environment: Megacities of Africa. International Journal of Development and Sustainability. Vol. 1 No.3. ISSN: 2168-8662.

Malik, M. S., Shukla, J. P., & Mishra, S. (2019). Relationship of LST , NDBI and NDVI using Landsat-8 data in Kandaihimmat, *48*(January), 25–31.

Maselli F, Chiesi M, Barbati A, Chirici G, Corona P (2006) Use of remotely sensed and ancillary data for estimating forest gross primary productivity in Italy. Remote Sens Environ 100(4):563–575. doi:10.1016/j. rse.2005.11.010

Mccarthy, M. P., Best, M. J., & Betts, R. A. (2010). Climate change in cities due to global warming and urban effects, *37*, 1–5. https://doi.org/10.1029/2010GL042845

MCINTYRE, N. E., ANEZ, K. K.-Y., & HOPE, D. (2001). Urban ecology as an interdisciplinary field : differences in the use of " urban " between the social and natural sciences, (1997), 5–24.

Meiyappan P, Jain AK (2012) Three distinct global estimates of historical land-cover change and land-use conversions for over 200 years. Front Earth Sci 6(2):122–139.

Misra, P., & Enge, P. (2006). *GLOBAL POSITIONING SYSTEM Signals, Measurements, and Performance* (2nd ed.). USA.

MOLDERS, N., & OLSON, M. A. (2004). Impact of Urban Effects on Precipitation in High Latitudes, (1980), 409–429.

Möller, G., & Landskron, D. (2019). Atmospheric bending effects in GNSS tomography. *Atmospheric Measurement Techniques*, *12*(1), 23–34. https://doi.org/10.5194/amt-12-23-2019

Molly E.B. (2008). *Early, Famine Systems, Warning Data, Remote Sensing*.

Muttttanon W, Tripathi NK (2005) Land use/land cover changes in the coastal zone of Ban Don Bay, Thailand using Landsat 5 TM data. Int J Rem Sens 26(1):2311–2323

Myneni, R.B., Hall, F.G., Sellers, P.J. and Marshak, A.L., 1995. The interpretation of spectral vegetation indexes. IEEE Transactions Geoscience and Remote Sensing, 33(2): 481–486.

Myneni RB, Keeling CD, Tucker CJ, Asrar G, Nemani RR (1997) Increased plant growth in the northern high latitudes from 1981 to 1991. Nature 386:698–702. doi:10.1038/386698a0

Naserikia, M., Shamsabadi, E. A., Rafieian, M., & Filho, W. L. (2019). The Urban Heat Island in an Urban Context : A Case Study of Mashhad , Iran. https://doi.org/10.3390/ijerph16030313

Nemani RR, Keeling CD, Hashimoto H, Jolly WM, Piper SC, Tucker CJ (2003) Climate-driven increases in global terrestrial net primary production from 1982 to 1999. Science 300(5625):1560–1563. doi:10.1126/ science.1082750

Odindi, J. O., Bangamwabo, V., & Mutanga, O. (2015). Assessing the value of urban green spaces in mitigating multi-seasonal urban heat using MODIS land surface temperature (LST) and landsat 8 data. *International Journal of Environmental Research*, *9*(1), 9–18. https://doi.org/10.22059/ijer.2015.868

Odum, E.P. (1997) Ecology: A Bridge Between Science and Society. Sinauer, Sunderland, MA, USA.

OKE, T. R. (1995). THE HEAT ISLAND OF URBAN BOUNDARY LAYER: CHARACTERISTICS, CAUSES AND EFFECTS.

Oliveira, D., Souza, D., Célia, R., & Guedes, M. (2016). Urbanization effects on the microclimate of Manaus : A modeling study. *Atmospheric Research*, *167*, 237–248. https://doi.org/10.1016/j.atmosres.2015.08.016

Palmate, S. S., Pandey, A., Kumar, D., Pandey, R. P., & Mishra, S. K. (2017). Climate change impact on forest cover and vegetation in Betwa Basin , India. *Applied Water Science*, 103–114. https://doi.org/10.1007/s13201-014-0222-6

Parkinson, B. W., Jr., J. J. S., Axelrad, P., & Enge, P. (1996). *Global Positioning System: Theory and Applications Volume I* (3rd ed.). Washington, DC: American Institute of Aeronautics and Astronautics.

Pathirana, A., Denekew, H. B., Veerbeek, W., Zevenbergen, C., & Banda, A. T. (2014). Impact of urban growth-driven landuse change on microclimate and extreme precipitation — A sensitivity study. *Atmospheric Research*, *138*, 59–72. https://doi.org/10.1016/j.atmosres.2013.10.005

Phillips OL, Aragão LE, Lewis SL, Fisher JB, Lloyd J, López-González G, Malhi Y, Monteagudo A, Peacock J, Quesada CA (2009) Drought sensitivity of the Amazon rainforest. Science 323(5919):1344–1347

Pickett, S. T. A., Cadenasso, M. L., J.M. Grove, C. H. N., Pouyat, R. V., Zipperer, W. C., & Costanza, R. (2008). Urban Ecological Systems: Linking Terrestrial Ecological, Physical, and Socioeconomic Components of Metropolitan Areas. In J. M. Marzluff, E. Shulenberger, W. Endlicher, W. Endlicher, G. Bradley, C. Ryan, … U. Simon (Eds.), *Urban Ecology* (pp. 99–122). Springer Science+Business Media, LLC.

Pielke R, Adegoke J, Beltran-Przekurat A, Hiemstra C, Lin J, Nair U, Niyogi D, Nobis T (2007) An overview of regional land-use and land-cover impacts on rainfall. Tellus B 59(3):587–601

Pielke, R. A., Marland, G., Betts, R. A., Thomas, N., Eastman, J. L., Niles, J. O., … Lond, R. S.

(2002). The influence of land-use change and landscape dynamics on the climate system : relevance to climate-change policy beyond the radiative effect of greenhouse gases, 1705–1719. https://doi.org/10.1098/rsta.2002.1027

Potter, C. (2019). Shifts in Vegetation Cover of Southern California Deserts in Response to Recent Climate Variations, 1999–2002.

Pravitasari, A. E. (2015). *STUDY ON IMPACT OF URBANIZATION AND RAPID URBAN EXPANSION IN JAVA AND JABODETABEK MEGACITY, INDONESIA(Dissertation_全文)*. Kyoto University. Retrieved from https://doi.org/10.14989/doctor.k19347

Qu, J. J., Gao, W., Kafatos, M., Murphy, R. E., & Salomonson, V. V. (2006). *Earth Science Satellite Remote Sensing Vol. 1: Science and Instruments*.

Rasul, G., & Ibrahim, F. (2017). Urban Land Use Land Cover Changes and Their Effect on Land Surface Temperature : Case Study Using Dohuk City in the Kurdistan Region of Iraq. https://doi.org/10.3390/cli5010013

Rees, W., & Wackernagel, M. (2008). Urban ecological footprints: Why cities cannot be sustainable-and why they are a key to sustainability. In J. M. Marzluff, E. Shulenberger, W. Endlicher, W. Endlicher, G. Bradley, C. Ryan, … U. Simon (Eds.), *Urban Ecology: An International Perspective on the Interaction Between Humans and Nature* (pp. 537–555). Springer Science+Business Media, LLC. https://doi.org/10.1007/978-0-387-73412-5_35

Ruocco, A. Di, Gasparini, P., & Weets, G. (2015). Urbanisation and Climate Change in Africa: Setting the Scene. In S. Pauleit, A. Coly, S. Fohlmeister, P. Gasparini, G. Jørgensen, S. Kabisch, … K. Yeshitela (Eds.), *Urban Vulnerability and Climate Change in Africa* (pp. 1–36). Switzerland: Springer International Publishing Switzerland.

Seeber, G. (2003). *Satellite Geodesy* (2nd ed.). Berlin, New York: Walter de Gruyter.

Sharma, R., & Joshi, P. K. (2015). The Changing Urban Landscape and Its Impact on Local Environment in an Indian Megacity: The Case of Delhi. In R. B. Singh (Ed.), *Urban Development Challenges, Risks and Resilience in Asian Mega Cities* (pp. 61–83). Springer Japan.

Sickle, J. Van. (2015). *GPS for Land Surveyors* (4th ed.). Boca Raton: Taylor & Francis Group.

Singh, R.B., and Aakriti Grover. 2015. “Spatial Correlations of Changing Land Use, Surface Temperature (UHI) and NDVI in Delhi Using Landsat Satellite Images.” In *Urban Development Challenges, Risks and Resilience in Asian Mega Cities*, ed. R.B. Singh. Springer Japan, 83–98.

Solano, R., Didan, K., Jacobson, A., & Huete, A. (2010). MODIS Vegetation Index User ’ s Guide (MOD13 Series), *2010*(May).

Spangmyr M (2010) Global effects of albedo change due to urbanization. In: Seminar series no. 180. Department of Earth and Ecosystem Sciences, Lund University

Strang, G., & Borre, K. A. I. (1997). *Linear Algrbra, Geodesy, and GPS*. United States of America: Wellesley-Cambridge Press.

Stone Jr B (2009) Land use as climate change mitigation. Environ Sci Technol 43(24):9052–9056

Study for Swiss Agency for Development and Cooperation (2017). *Urban and Peri- Urban Development Dynamics in Ethiopia*.

Subirana, J. S., Zornoza, J. M. J., & Hernández-Pajares, M. (2013). *GNSS DATA PROCESSING Volume I: Fundamentals and Algorithms*. (K. Fletcher, Ed.) (Vol. I). ESA Communications.

Sun, Q., Wu, Z., & Tan, J. (2012). The relationship between land surface temperature and land use / land cover in Guangzhou , China, (March). https://doi.org/10.1007/s12665-011-1145-2

Tahir, A. A., Muhammad, A., Mahmood, Q., Ahmad, S. S., & Ullah, Z. (2014). Impact of rapid urbanization on microclimate of urban areas of Pakistan. https://doi.org/10.1007/s11869-014-0288-1

Tavernia, B. G., & Reed, J. M. (2009). Spatial extent and habitat context influence the nature and strength of relationships between urbanization measures. Landscape and Urban Planning, 92(1), 47–52.

Torres-Vera MA, Prol-Ledesma RM, Garcia-Lopez D (2009) Three decades of land use variations in Mexico city. Int J Rem Sens 30(1):117–138

Trenberth, K. E. (2011). Changes in precipitation with climate change. *Climate Research*, *47*(1–2), 123–138. https://doi.org/10.3354/cr00953

Tsoka, S., Tsikaloudaki, K., & Theodosiou, T. (2020). Investigation Methods and Mitigation.

Tucker, C.J., 1979. Red and photographic infrared linear combinations for monitoring vegetation. Remote Sensing of Environment, 8: 127–150.

Tucker CJ, Fung IY, Keeling CD, Gammon RH (1986) Relationship between atmospheric CO2 variations and a satellite-derived vegetation index. Nature 319:195– 199. doi:10.1038/319195a0

UN-Habitat. (2017). *THE STATE OF ADDIS ABABA 2017*. Nairobi, Kenya.

United Nations. (1968) Demographic Handbook for Africa. United Nations Economic Commission for Africa, Addis Ababa, Ethiopia.

United Nations. (2019). *World Urbanization Prospects 2018*. New York.

USGS. (2019a). Landsat 7 (L7) Data Users Handbook, *7*(November).

USGS. (2019b). *Landsat 8 (L8) Data Users Handbook* (Vol. 8).

Uttara, S., Bhuvandas, N., & Aggarwal, V. (2012). IMPACTS OF URBANIZATION ON ENVIRONMENT. *IJREAS*, *2*(2), 1637–1645.

Wang, K., Wang, J., Wang, P., Sparrow, M., Yang, J., & Chen, H. (2007). Influences of urbanization on surface characteristics as derived from the Moderate-Resolution Imaging Spectroradiometer : A case study for the Beijing metropolitan area. *JOURNAL OF GEOPHYSICAL RESEARCH*, *112*, 1–12. https://doi.org/10.1029/2006JD007997

Wang, Y., Bakker, F., de Groot, R., Wortche, H., & Leemans, R. (2015). Effects of urban trees on local outdoor microclimate: synthesizing field measurements by numerical modelling. *Urban Ecosystems*, *18*(4), 1305–1331. https://doi.org/10.1007/s11252-015-0447-7

Wilson, E. H., Hurd, J. D., Civco, D. L., Prisloe, M. P., & Arnold, C. (2003). Development of a geospatial model to quantify, describe and map urban growth. Remote Sensing of Environment, 86(3), 275–285.

Woldemichael AT, Hossain F, Pielke Sr R, Beltrán-Przekurat A (2012) Understanding the impact of dam-triggered land use/land cover change on the modification of extreme precipitation. Water Resour Res 48(9):W09547

World Bank Group. 2015. Ethiopia Poverty Assessment 2014. Washington, DC. © World Bank. Retrieved in https://openknowledge.worldbank.org/handle/10986/21323 License: CC BY 3.0 IGO."

Weng, Q. (2011). *Advances in Environmental Remote Sensing*. Taylor and Francis Group.

Xu, G., & Xu, Y. (2016). *GPS Theory, Algorithms and Applications* (3rd ed.). Springer-Verlag GmbH Berlin Heidelberg.

Zha, Y. (2003). Use of normalized di ff erence built-up index in automatically mapping urban areas from TM imagery, 583–594.

Zhan, J., Liu, J., Lin, Y., Wu, F., & Ma, E. (2014). Land Use Change Dynamics Model Compatible with Climate Models. In X. Deng, B. Güneralp, J. Zhan, & H. Su (Eds.), *Land Use Impacts on Climate* (pp. 19–48). Springer-Verlag Berlin Heidelberg.

Zhang, W., Zhu, Y., & Jiang, J. (2016). Effect of the Urbanization of Wetlands on Microclimate : A Case Study of Xixi Wetland ,. https://doi.org/10.3390/su8090885

ANNEX

The daily solution graph of IGS stations which are used in this study to process ADIS IGS station in GAMIT/GLOBK.

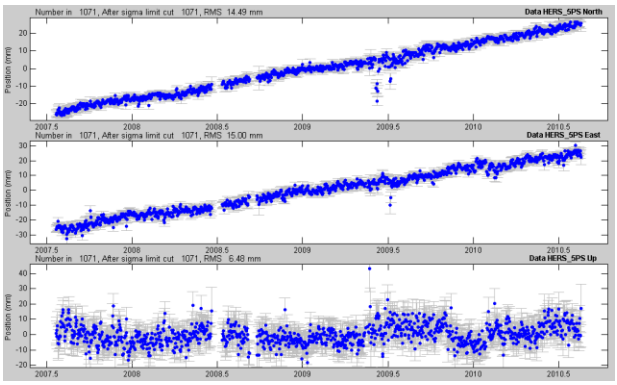

Daily GPS solution of HERS

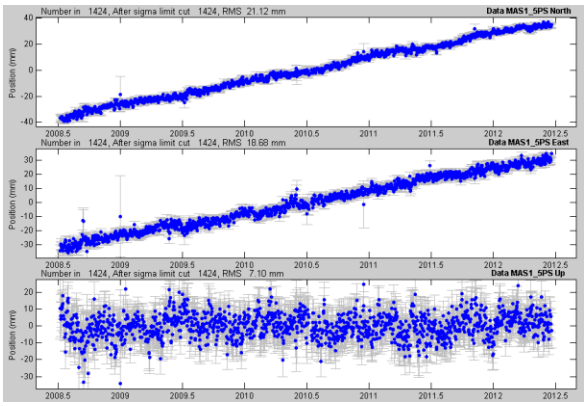

Daily solution of MAS1

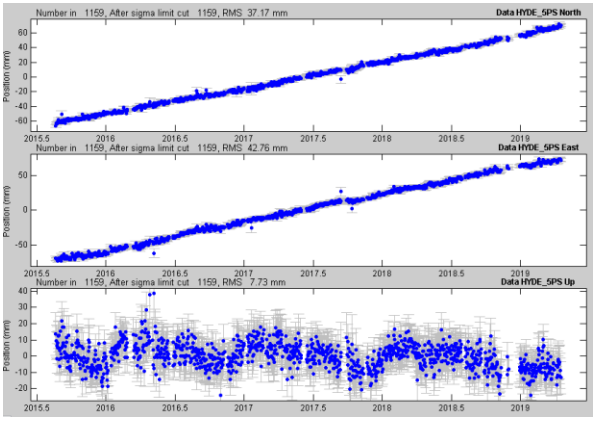

Daily GPS solution of HYDE

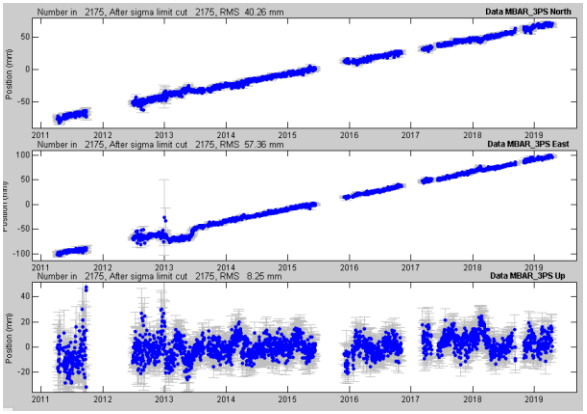

Daily GPS solution of MBAR

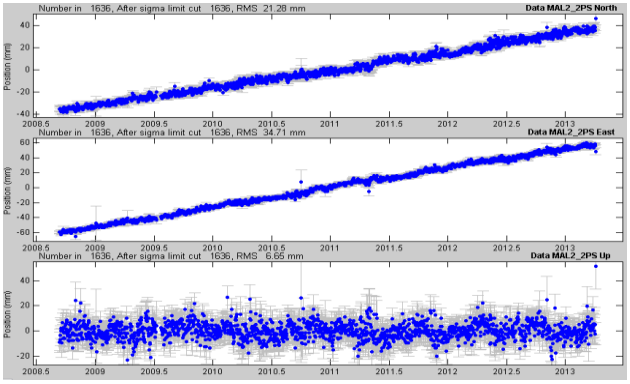

Daily GPS solution of MAL2

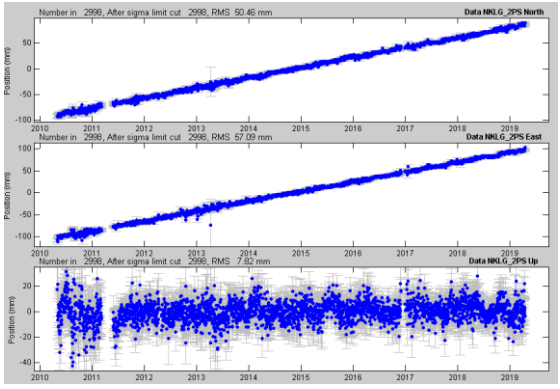

Daily GPS Solution OF NKLG

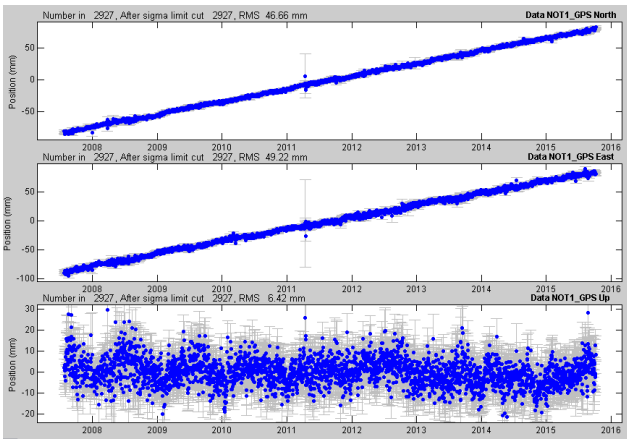

Daily GPS solution of NOT1

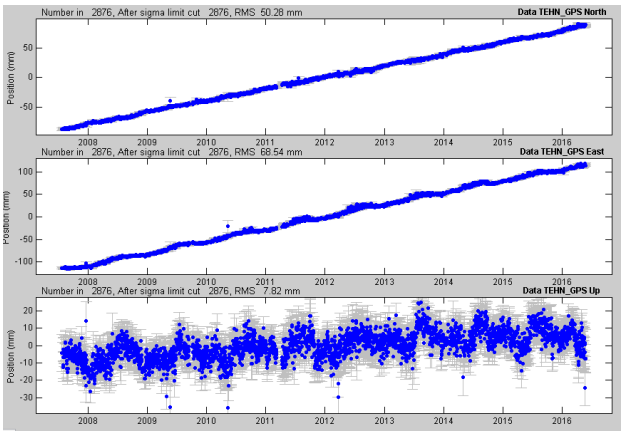

Daily GPS solution of TEHN

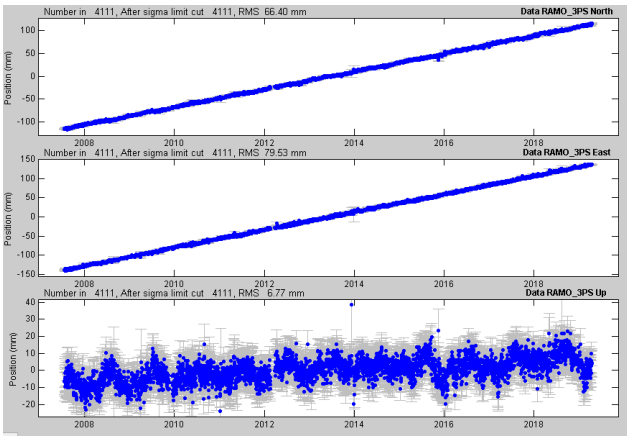

Daily GPS solution of RAMO

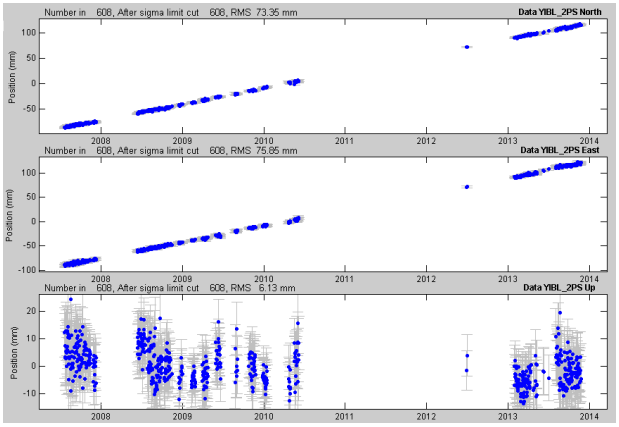

Daily GPS solution of YIBL

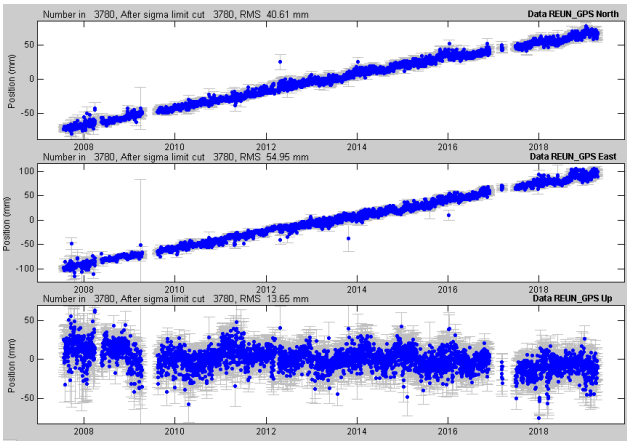

Daily GPS Solution of REUN